# Hydrogen Metabolism in *Synechocystis* sp. PCC 6803: Insight into the Light-Dependent and Light-Independent Hydrogenase Activities

by

Ipsita Dutta

A Dissertation Presented in Partial Fulfillment
of the Requirements for the Degree
Doctor of Philosophy

Approved July 2015 by the
Graduate Supervisory Committee:

Willem F. J. Vermaas, Chair
Ferran Garcia-Pichel
Bruce Rittmann
Anne K. Jones

ARIZONA STATE UNIVERSITY

August 2015

ABSTRACT

The unicellular cyanobacterium *Synechocystis* sp. PCC 6803 contains a NiFe-type bidirectional hydrogenase that is capable of using reducing equivalents to reduce protons and generate $H_2$. In order to achieve sustained $H_2$ production using this cyanobacterium many challenges need to be overcome. Reported $H_2$ production from *Synechocystis* is of low rate and often transient. Results described in this dissertation show that the hydrogenase activity in *Synechocystis* is quite different during periods of darkness and light. In darkness, the hydrogenase enzyme acts in a truly bidirectional way and a particular $H_2$ concentration is reached that depends upon the amount of biomass involved in $H_2$ production. On the other hand, in the presence of light the enzyme shows only transient $H_2$ production followed by a rapid and constitutive $H_2$ oxidation. $H_2$ oxidation and production were measured from a variety of *Synechocystis* strains in which components of the photosynthetic or respiratory electron transport chain were either deleted or inhibited. It was shown that the light-induced $H_2$ oxidation is dependent on the activity of cytochrome $b_6f$ and photosystem I but not on the activity of photosystem II, indicating a channeling of electrons through cytochrome $b_6f$ and photosystem I. Because of the sequence similarities between subunits of NADH dehydrogenase I in *E. coli* and subunits of hydrogenase in *Synechocystis*, NADH dehydrogenase I was considered as the most likely candidate to mediate the electron transfer from hydrogenase to the membrane electron carrier plastoquinone, and a three-dimensional homology model with the associated subunits shows that structurally it is possible for the subunits of the two complexes to assemble. Finally, with the aim of improving the rate of $H_2$ production in *Synechocystis* by using a powerful hydrogenase enzyme, a mutant strain of *Synechocystis*

was created in which the native hydrogenase was replaced with the hydrogenase from *Lyngbya aestuarii* BL J, a strain with higher capacity for $H_2$ production. $H_2$ production was detected in this *Synechocystis* mutant strain, but only in the presence of external reductants. Overall, this study emphasizes the importance of redox partners in determining the direction of $H_2$ flux in *Synechocystis*.

# DEDICATION

This dissertation is dedicated to the memory of my father Malay Kumar Dutta, whose support and motivation have always been my greatest asset. Since my childhood my father had encouraged me to pursue higher education and had made great sacrifices so that I can follow my dreams. His faith provided strength to me during the ups and downs of my career and life.

I also dedicate this dissertation to my mother Krishna Dutta for her loving support and blessings.

ACKNOWLEDGMENTS

First and foremost I thank my advisor Dr. Wim Vermaas for his immense support, guidance, ideas and inspirations throughout my PhD. I also thank my Committee Members, Dr. Ferran Garcia-Pichel, Dr. Bruce Rittmann and Dr. Anne Jones for their guidance and valuable feedback. I would specifically like to thank Dr. Garcia-Pichel for allowing me to use the $H_2$ electrode in his laboratory.

I thank Michael Vaughn for his guidance in protein homology modeling, Dr. Daniel Brune and Dr. Xuan Wang for their guidance, and Dr. Hongliang Wang for his plasmid vectors that have made cloning a lot easier for every member in our laboratory.

I thank Dr. Gaozhang Shen for the Δ*psaAB* strain, Dr. Julian J. Eaton-Rye for the Δ*psbB* strain and Dr. Crispin Howitt for the Δ*ox* and *hoxEF*$^-$ strains. I also thank Dr. Laurent Cournac for the HoxH antibodies.

I thank my friends and colleagues Shuqin, Raul, Otilia and Vicki for providing guidance in experimental setups, Wesley for helping me with writing, and also Lisa, Angela, Anna, Danny, Heather, Lucas, Luke for their support. I would like to thank my friend Ankita Kothari who has been a part of the Biohydrogen project, and an extremely helpful fellow graduate student throughout the project.

I am grateful to Brian Swette and his family for supporting this research through the ASU President's Fusion Fund. I would also like to thank Dr. Vermaas, Dr. Rittmann and the School of Life Sciences for financial support.

TABLE OF CONTENTS

Page

CHAPTER Page

CHAPTER Page

CHAPTER Page

LIST OF TABLES

Table Page

LIST OF FIGURES

Figure Page

Figure Page

Figure Page

# ABBREVIATIONS

BLAST Basic Local Alignment Search Tool

CCM Carbon Concentrating Mechanism

Chl Chlorophyll

DBMIB 2,5-Dibromo-3-Methyl-6-Isopropylbenzoquinone

MV Methyl Viologen

NAD(P) Nicotinamide Adenine Dinucleotide (Phosphate)

NCBI National Center for Biotechnology Information

PAGE Polyacrylamide Gel Electrophoresis

PCC Pasteur Culture Collection

PDB Protein Data Bank

PQ Plastoquinone

PS I Photosystem I

PS II Photosystem II

PVDF Polyvinylidene Difluoride

SD Sodium Dithionite

SDS Sodium Dodecyl Sulfate

# CHAPTER 1

# LITERATURE REVIEW: ENZYMES RELATED TO MICROBIAL $H_2$ PRODUCTION

## 1.1 Role of $H_2$ as an Energy Carrier

Hydrogen ($H_2$) is a versatile energy carrier and a viable alternative to the conventional carbon-based fossil fuels. Upon combustion, $H_2$ (specific energy 142 MJ/kg) releases energy with only water as a byproduct and therefore is regarded as a clean, non-polluting fuel. It can also be potentially used in chemical fuel cells to generate electricity (Dincer, 2007).

Hydrogen is distributed abundantly in nature, especially as a component of water and organic compounds. However, only a small portion of it is present as molecular hydrogen gas, $H_2$. Thus, $H_2$ must be manufactured from feedstocks before it can be either stored or used to produce electricity in fuel cells or heat upon combustion (Ogden, 1999).

Currently, most of the commercially produced $H_2$ is formed by steam reforming of natural gas or by the gasification of coal (He and Li, 2014), represented by the equations below:

$$CH_4 + H_2O \text{ (+ heat)} \rightarrow CO + 3H_2$$

$$3C \text{ (coal)} + O_2 + H_2O \rightarrow H_2 + 3CO$$

Both processes have the advantage of fast supply of large amounts of hydrogen gas to

refineries and chemical plants. However, they also require extremely high temperature and generate CO as a byproduct, making them environmentally unfriendly. Another currently used method that produces a relatively small portion of hydrogen is electrolysis, in which electricity is used to split water into $H_2$ and $O_2$.

$$2H_2O \rightarrow O_2 + 2H_2$$

In this process, the economic viability of $H_2$ production depends on the source of the electricity used - its cost, efficiency and possible emissions during its generation (Onda et al., 2004).

### 1.2 Biological $H_2$ Production

Biological $H_2$ production is a relatively new and yet-to-be-fully-explored approach that has long-term potential for sustainable $H_2$ production with low environmental impact. Biological $H_2$ production involves certain microbes that can produce $H_2$ as part of their metabolic processes by using the enzymes nitrogenase and/or hydrogenase. Nitrogenases are found in selected phototrophic bacteria such as in some cyanobacteria, purple non-sulfur and green sulfur bacteria as well as in some heterotrophic bacteria including in some Clostridia and Rhizobia (Weber et al., 2014; Basak and Das, 2007; Tourova et al., 2014; Kasap and Chen, 2005), where they catalyze $N_2$ fixation and produce $H_2$ as a byproduct, as per the reaction:

$$N_2 + 8H^+ + 8e^- + 16ATP \rightarrow 2NH_3 + H_2 + 16ADP + 16P_i$$

This mode of $H_2$ production requires a large amount of energy in the form of ATP (two

ATPs per electron) making it an energetically expensive process.

The second $H_2$ producing enzyme, hydrogenase, is found in a variety of bacteria, including cyanobacteria, archaea and algae (Tamagnini et al., 2002 and 2007; Weber et al., 2014). Hydrogenase can catalyze the reversible formation of $H_2$ by obtaining electrons from a variety of electron donors. The net reaction catalyzed by the enzyme can be represented as:

$$2e^- + 2H^+ \leftrightarrows H_2$$

The electrons in this reaction are provided by redox partners such as NADPH, NADH, ferredoxin/flavodoxin, coenzyme $F_{420}$, cytochrome $c_3$ and menaquinone (a comprehensive list ofaredox partners is provided by Fontecilla-Camps et al. (2007)). While no ATP is required for $H_2$ production with this enzyme, the direction of the reaction is determined by the concentrations as well as the redox potentials of the reactants and products.

Hydrogenases are classified into two major categories according the metal content of their active site: NiFe-type and FeFe-type (Vignais et al., 2001). Both hydrogenases contain several [Fe-S] clusters (Lyon et al., 2004; Nicolet et al., 1999; Peters et al., 1998). A third type of hydrogenase (Fe-only hydrogenase), without any Fe-S cluster, is also found in some methanogenic archaea (Lyon et al., 2004). These three types of hydrogenases form phylogenetically distinct classes of proteins based on the amino acid sequences of their catalytic subunits (Vignais et al., 2001, Vignais, 2008). A brief description of the three types of hydrogenases is given below.

**a) NiFe-Hydrogenase**

NiFe-hydrogenases are a common class of hydrogenases, found mainly in bacteria and archaea. The first crystal structure of a NiFe hydrogenase (from *Desulfovibrio gigas*) was published in 1995 and was followed by several others in later years (Volbeda et al., 1995; Frielingsdorf et al., 2014; Fritsch et al., 2011; Ogata et al., 2002 and 2005; Rousset et al., 1998). The core enzyme consists of a large subunit of ~60 kDa, and a small subunit of ~30 kDa (Figure 1.1). The bimetallic NiFe active site is deeply buried in the large subunit, where the nickel is coordinated by four cysteine residues and the iron is coordinated by one CO and two CN ligands, and two of the Ni-binding cysteine residues.

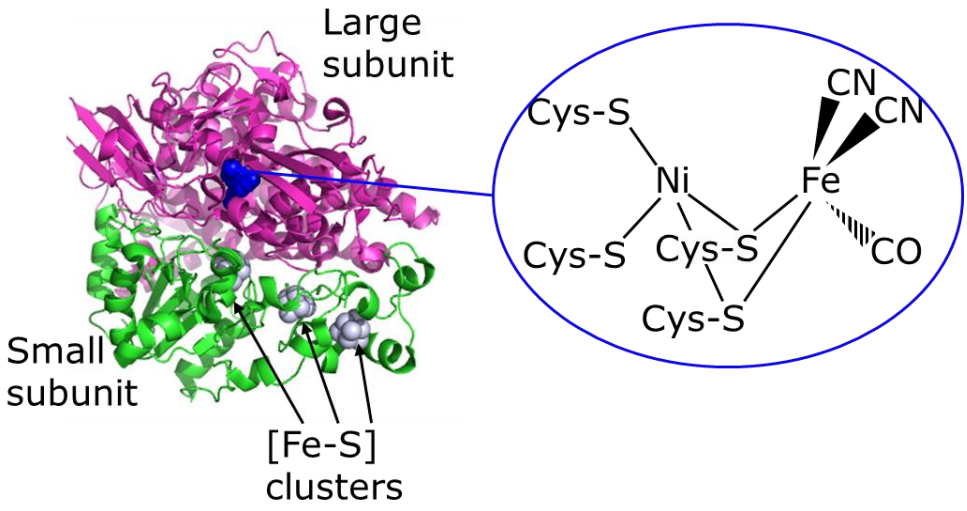


Figure 1.1
Representation of a NiFe-hydrogenase from *D. fructosovorans* (PDB ID: 1YQ9). The NiFe active site and the [Fe-S] clusters are represented by blue and silver spheres, respectively.

The small subunit usually hosts three [Fe-S] clusters. These [Fe-S] clusters conduct electrons between the active site and the physiological electron donor/acceptor of hydrogenase. On the other hand, gas access to the active site is mediated by hydrophobic channels connecting the active site in the large subunit to the surface of the molecule (Cano et al., 2014; Wang et al., 2011; Bleijlevens et al., 2001). NiFe-hydrogenases are reversibly inactivated by oxygen and usually have low turnover numbers (e.g., 98 $s^{-1}$ in *D. fructosovorans*) (Hallenbeck and Benemann, 2002).

**b) <u>FeFe-Hydrogenase</u>**

FeFe-hydrogenases are mostly found in anaerobic prokaryotes and eukaryotes, located exclusively in organelles such as chloroplasts or hydrogenosomes (Peters et al., 2015; Tamagnini et al., 2007; Vignais et al., 2001). The catalytic unit contains the active site domain (also called the H-cluster) where a binuclear FeFe center is coordinated by CO and CN ligands, and also to a [4Fe-4S] cluster by a bridging cysteine residue (Figure 1.2) (Vignais and Billoud, 2007). Reduced ferredoxins usually serve as electron donors for this class of hydrogenases (Peters et al., 2015). Among different types of hydrogenases, FeFe-hydrogenases usually have higher turnover numbers (e.g., 9000 $s^{-1}$ for *Desulfovibrio* sp. and 6000 $s^{-1}$ for *Clostridium pasteurianum*) compared to the NiFe-hydrogenases (Hallenbeck and Benemann, 2002). However, in the presence of $O_2$ they get rapidly and irreversibly inactivated.

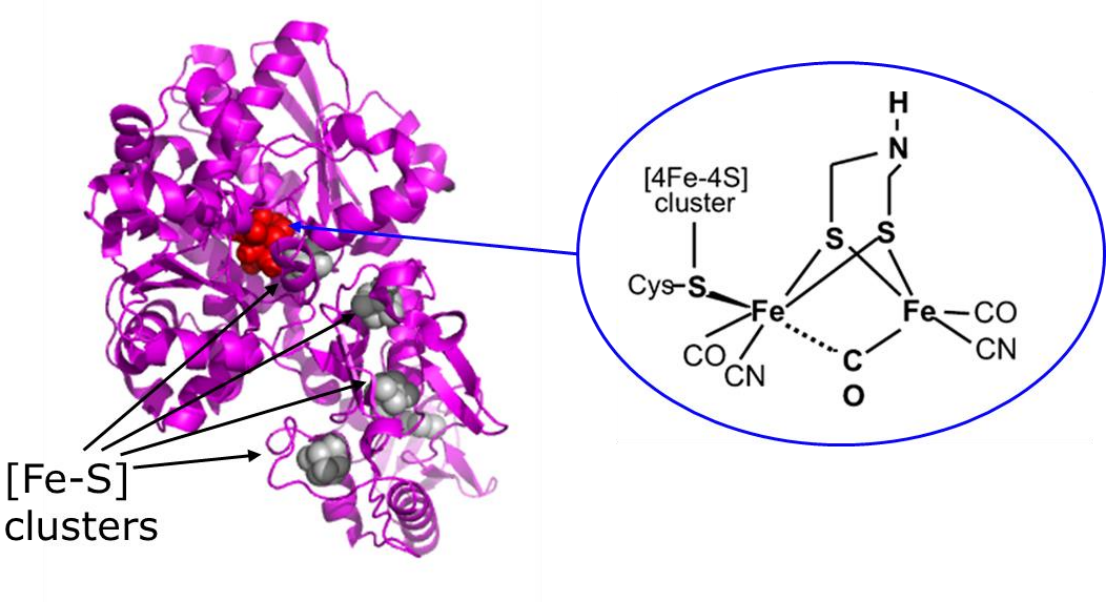


Figure 1.2
Representation of a FeFe-hydrogenase from *Clostridium pasteurianum* (PDB ID: 3C8Y). The FeFe active site and the [Fe-S] clusters are represented by blue and silver spheres, respectively.

**c) <u>Fe-Only Hydrogenase</u>**

Fe-only hydrogenases (also called Hmd) are found in some methanogenic archaea such as *Methanothermobacter marburgensis*. Unlike the other two classes of hydrogenases, they do not catalyze the reversible reaction between protons and electrons to form $H_2$. Instead, they catalyze the reversible reduction of methenyltetrahydromethanopterin with $H_2$ to form methylenetetrahydromethanopterin (Vignais and Billoud, 2007; Peters et al., 2015) and function only under growth conditions of nickel limitation. Fe-only hydrogenases are composed of two identical subunits, with two Fe per homodimer. However, these irons may not be catalytically active and the enzymes do not contain any [Fe-S] cluster (Vignais and Billoud, 2007).

Biological $H_2$ production can be broadly classified into the following categories:

### 1.2.1 Direct Photolysis

Direct photolysis is mainly observed in certain species of algae and cyanobacteria. In direct photolysis, photosynthesis converts solar energy into chemical energy in the form of $H_2$, following the general reaction:

$$2H_2O \text{ (+ light energy)} \rightarrow 2H_2 + O_2$$

The process usually takes place in two steps: first, photosynthesis splits water at photosystem II (PS II) evolving $O_2$, protons ($H^+$) and electrons ($e^-$). The electrons are subsequently transferred to photosystem I (PS I), ferredoxin and $NADP^+$ to produce NADPH. In algae and cyanobacteria cytoplasmic protons are reduced by ferredoxin and NADPH, respectively, to form $H_2$, a reaction mediated by hydrogenase (Das and Veziroglu, 2008; Benemann, 2000; Tamagnini et al., 2002; Zhang et al., 2010). The electron transfer pathway can be described as:

$$H_2O \rightarrow \text{PS II} \rightarrow \text{PS I} \rightarrow \text{Ferredoxin} \rightarrow (\text{NADPH} \rightarrow) \text{Hydrogenase} \rightarrow H_2$$

The biotechnological advantages of producing $H_2$ in this mode are that a) it couples photosynthesis directly with $H_2$ production without involving carbon fixation, and b) it does not involve any greenhouse gas emission. In cyanobacteria the reaction is mediated by a NiFe-hydrogenase. $H_2$ production with this enzyme in the presence of light is transient (~30 s), and is followed by $H_2$ uptake, resulting no net production of $H_2$ (Cournac et al., 2004).

Green algae possess FeFe-hydrogenases with high turnover numbers, but these enzymes are irreversibly inactivated in the presence of $O_2$ and in certain cases are also light

sensitive (Chen et al., 2002; Hallenbeck and Benemann, 2002; Volgusheva et al., 2015). Since PS II produces $O_2$ by water photolysis, the oxygen sensitivity of the hydrogenase enzyme poses a significant challenge for continuous $H_2$ production using algal hydrogenases.

Because of the $O_2$ sensitivity of algal hydrogenases, photosynthetic $O_2$ and $H_2$ evolution must be temporarily and/or spatially separated in order to obtain sustained $H_2$ production in the presence of light (Levin et al., 2004). Such sustained $H_2$ production was demonstrated in *Chlamydomonas reinhardtii* by temporally separating photosynthetic $O_2$ evolution and carbon fixation (stage 1) from concomitant $H_2$ production using the cell's stored metabolites (stage 2). During the transition from stage 1 to stage 2, the culture medium was deprived of various inorganic nutrients such as S, P or Mg that are required for the synthesis of components of the photosynthetic apparatus or intermediates of the reductive pentose phosphate cycle (Volgusheva et al., 2015; Antal et al., 2014; Williams and Bees, 2014; Batyrova et al., 2012). When cultures were incubated in such media, the rates of $O_2$ evolution and $CO_2$ fixation declined significantly and the media became $O_2$-deprived within 22-35 hours due to respiration. Within a few hours of the onset of anaerobiosis, C. *reinhardtii* started producing $H_2$ in the presence of light. Studies show that $H_2$ evolution in the absence of sulfur depends upon electron supply from endogenous substrates (Kosourov et al., 2003; Melis et al., 2000) as well as residual PS II activity and non-photochemical plastoquinone reduction (Hemschemeier et al., 2008). The $H_2$ production could be sustained, on average, for 4-5 days (Zhang et al., 2002).

### 1.2.2 Indirect Photolysis

In indirect photolysis, $O_2$ evolution and $H_2$ production are temporarily separated, thus offering a convenient solution for the $O_2$ sensitivity problem of hydrogenase (Manish and Banerjee, 2007). In the presence of light, the light and dark reactions of photosynthesis fix carbon into organic compounds with simultaneous $O_2$ evolution. Later, in the absence of light, fermentative degradation of stored organic compounds (e.g., glycogen in certain cyanobacteria) results in $H_2$ production. Both algae and cyanobacteria can produce $H_2$ in this mode (Stal and Moezelaar, 1997; Melis and Melnicki, 2006). In certain cyanobacteria $H_2$ production in the dark by fermentation showed considerably high rates such as of 5.3 $\pm$ 2.7 µmol (mg chl *a*)$^{-1}$ h$^{-1}$ in *Lyngbya aestuarii* BL J (Kothari et al., 2014). The overall reactions of photosynthesis and $H_2$ production can be described by the equations:

$$12H_2O + 6CO_2 \text{ (+ light energy)} \rightarrow C_6H_{12}O_6 + 6O_2$$

$$C_6H_{12}O_6 \rightarrow\rightarrow NAD(P)H \rightarrow H_2$$

### 1.2.3 Photo-Fermentation

Photo-fermentation is the conversion of organic compounds to $H_2$ by a series of biochemical reactions observed in photosynthetic non-sulfur bacteria (Azwar et al., 2014). Attempts were made to produce $H_2$ in this way using certain purple non-sulfur bacteria such as *Rhodospirillium rubrum*, *Rhodobacter capsulatus* and *Rhodopseudomonas palustris* (Basak and Das, 2007). Nitrogenase is the main enzyme that participates in $H_2$ production in these organisms. These bacteria were shown to

produce $H_2$ from various organic acids and agricultural wastes in the presence of light (Hallenbeck and Benemann 2002; Basak et al., 2014).

The photo-fermentation process has several drawbacks such as the high energy demand of the nitrogenase enzyme, requirements of strict control of environmental conditions (e.g., optimal pH and temperature range between 6.8 and 7.5, and 31 and 36 °C, respectively), low solar conversion efficiency in ideal (low) light conditions, and metabolic shift from $H_2$ production to polyhydroxybutyrate synthesis (Cai and Wang, 2014; Basak and Das, 2007; Hallenbeck and Benemann 2002; Koku et al., 2002).

### 1.2.4 Dark Fermentation

A wide variety of anaerobic heterotrophic bacteria such as *Clostridium, Enterobacter* and *Bacillus* produce $H_2$ in darkness using carbohydrate-rich substrates (Kapdan and Kargi, 2006; Levin et al., 2004). Pyruvate is often the preferred substrate for $H_2$ production, which takes place in one of the two routes: a) via pyruvate formate lyase (PFL) or b) via pyruvate ferredoxin oxidoreductase (PFOR) (Hallenbeck, 2009*)*. In the former route, pyruvate is first converted to formic acid by PFL, and then to $H_2$ and $CO_2$ by a second enzyme, formate hydrogen lyase (FHL).

$$\text{Pyruvate} + \text{CoA} \rightarrow \text{Acetyl-CoA} + \text{Formate}$$

$$\text{Formic acid} \rightarrow CO_2 + H_2$$

In the second route, pyruvate is converted to acetyl-CoA by the enzyme PFOR, producing $CO_2$ and reduced ferredoxin in the process. Reduced ferredoxin, in turn, supplies the electrons to reduce protons to produce $H_2$ via a FeFe-hydrogenase.

$$\text{Pyruvate} + \text{CoA} + 2\text{Fd (ox)} \rightarrow \text{Acetyl-CoA} + CO_2 + 2\text{Fd (red)}$$

$$2\text{Fd (red)} + 2H^+ \rightarrow 2\text{Fd (ox)} + H_2$$

While direct and indirect photolysis produce pure $H_2$, dark fermentation produces a mixed biogas, containing mainly $H_2$ and $CO_2$ and occasionally small amount of methane, CO and $H_2S$ (Levin et al., 2004). In many organisms the actual yield of $H_2$ is further reduced by $H_2$ recycling by one or more uptake hydrogenases (Hallenbeck and Benemann, 2002).

### 1.3 Cyanobacterial $H_2$ Metabolism

Cyanobacteria are a large group of photoautotrophic microorganisms found in almost all ecological niches including aquatic (saltwater and freshwater), terrestrial and even extreme environments (such as frigid lakes of the Antarctic or hot springs) (Tamagnini et al., 2002). They can be either unicellular or filamentous. Certain strains of cyanobacteria can fix atmospheric $N_2$ as well. Cyanobacteria are sometimes referred as blue-green algae, mainly because they display a variety of colors due to the presence of different photosynthetic pigments such as chlorophylls, carotenoids and phycobiliproteins. What separates this group from some other groups of photosynthetic bacteria is the presence of chlorophyll *a* (chl *a*) and the complete machinery for oxygenic photosynthesis. They can use the energy from sunlight to split water during photosynthesis and trap atmospheric $CO_2$ by carbon fixation. Certain cyanobacteria (e.g., *Oscillatoria* sp.) can also perform anoxygenic photosynthesis using an alternate electron donor such as $H_2S$ and As (III) (Kulp et al., 2008).

Cyanobacteria may possess three different types of enzymes that are involved in hydrogen metabolism: nitrogenase, which catalyzes the production of $H_2$ as a byproduct; uptake hydrogenase, which consumes $H_2$ produced by the nitrogenase; and bidirectional hydrogenase, which can catalyze both $H_2$ production and consumption. A basic description of the three enzymes is provided below.

### 1.3.1 Nitrogenase

As stated earlier, nitrogenases are the primary enzymes for $N_2$ fixation, a process where atmospheric $N_2$ is converted to ammonia ($NH_3$), which can then be used in biological processes. $H_2$ is produced as a byproduct of this reaction. The reaction of $N_2$ fixation requires 2 molecules of ATP per electron, making the process of $H_2$ production energetically expensive.

Nitrogenases are sensitive to $O_2$. In heterocyst-containing filamentous strains, $N_2$ fixation occurs in the anaerobic environment of the heterocyst, where PS II stays inactive. The active site of the nitrogenase contains a molybdenum (Mo) and an iron (Fe). When Mo is unavailable it can be replaced by a vanadium (V). When both metals are unavailable, some cyanobacterial strains can synthesizes an alternate Fe-only nitrogenase (Hodkinson et al., 2014; Glass et al., 2010; Angermayr et al., 2009; Tamagnini et al., 2007).

Depending on the metal content of the nitrogenase, different amounts of reducing equivalents are assigned for $N_2$ fixation and $H_2$ production (described in detail by Rees et al., 2005). For example, while Mo nitrogenase follows the equation:

$$N_2 + 8H^+ + 8e^- + 16ATP \rightarrow 2NH_3 + H_2 + 16ADP + 16Pi$$

With V nitrogenase, the reaction of $N_2$ fixation follows the equation:

$$N_2 + 12H^+ + 12e^- + 24ATP \rightarrow 2NH_3 + 3H_2 + 24ADP + 24Pi$$

### 1.3.2 Uptake Hydrogenase

Cyanobacterial uptake hydrogenases are found exclusively in $N_2$-fixing strains, where they rapidly consume the $H_2$ produced during $N_2$ fixation. Uptake hydrogenases are generally suggested to be localized on the cytoplasmic side of either the cytoplasmic or the thylakoid membrane (Vignais and Billoud, 2007). Immunolocalization studies have indicated the presence of uptake hydrogenases in both vegetative cells and in heterocysts in several *Nostoc* strains and in *Lyngbya majuscula* (Seabra et al., 2009; Tamagnini et al., 2007; Houchins and Burris, 1981).

The main physiological function of uptake hydrogenase is to regain the electrons produced by $H_2$ evolution through nitrogenase. This recycling has been suggested to benefit the organism in several ways. For example, it protects nitrogenase by removing low concentrations of $O_2$ (in a Knallgas-type reaction) and supplies reducing equivalents to various cellular functions (Tamagnini et al., 2007; Smith and Gianinazzi-Pearson, 1990).

### 1.3.3. Bidirectional Hydrogenase

The soluble or membrane-associated bidirectional hydrogenases are found in both $N_2$-fixing and non-$N_2$-fixing cyanobacterial strains (reviewed in detail by Tamagnini et al., 2002, 2007) and are the principal enzymes of interest for cyanobacterial biohydrogen

production. In cyanobacteria bidirectional hydrogenases are known to produce $H_2$ using electrons from their redox partners, NADH and/or NADPH (Tamagnini et al., 2007; Tiwari and Pandey, 2012; Vignais and Billoud, 2007; Cassier-Chauvat et al., 2014). The enzyme catalyzes two reversible half-reactions:

$$NAD(P)H + H^+ \leftrightarrows NAD(P)^+ + 2H^+ + 2e^-$$

and

$$2H^+ + 2e^- \leftrightarrows H_2$$

Therefore, the net reaction catalyzed by the enzyme is:

$$NAD(P)H + H^+ \leftrightarrows H_2 + NAD(P)^+$$

Recently, reduced ferredoxin (Fd)/flavodoxin (Flv) were also suggested as redox partners of these enzymes (Gutekunst et al., 2014).

#### 1.3.3.1 Physiological Role of Bidirectional Hydrogenase

The physiological role of the cyanobacterial bidirectional hydrogenase is not entirely clear. It has been suggested that the enzyme acts as an electron relief valve to get rid of excess reducing equivalents (NADH/NADPH/reduced Fd) produced by the light reactions of photosynthesis in *Synechocystis* sp. PCC 6803 (Appel et al., 2000). Although Flv1 and Flv3 proteins (Allahverdiyeva et al., 2011), which also accept electrons from photosynthetically produced NADH and NADPH to reduce $O_2$ and produce water, are likely to be more suitable choices for electron acceptors. Hydrogenase is also known to take part in fermentation by disposing electrons and regenerating $NAD(P)^+$ from

NAD(P)H, thus participating in the maintenance of redox balance of the cell during fermentation (Barz et al., 2010; Carrieri et al., 2011; Stal and Moezelaar, 1997).

#### 1.3.3.2 Localization of the Bidirectional Hydrogenase

Like their physiological function, the subcellular localization of cyanobacterial bidirectional hydrogenase too is controversial. In $N_2$-fixing strains the bidirectional enzymes can be found in both vegetative cells and heterocysts (Houchins and Burris, 1981). Cyanobacterial bidirectional hydrogenases are generally classified as soluble enzymes (Vignais and Billoud, 2007). However, several studies have suggested an association of the enzymes in *Synechocystis* and *Anabaena variabilis* with their thylakoid membrane (Burroughs et al., 2014; Serebrikova et al., 1994; Appel et al., 2000)

## 1.4 Bidirectional Hydrogenase in *Synechocystis*

The cyanobacterial bidirectional hydrogenase is most studied in the freshwater cyanobacterium *Synechocystis* sp. PCC 6803 (hereafter *Synechocystis*), where they show $H_2$ production in darkness and under anaerobic conditions. Also, transient $H_2$ production is observed during the transition from darkness to the light (Cournac et al., 2004, 2002; Appel et al., 2000). $H_2$ production in the later mode quickly reverses its direction and changes to $H_2$ consumption. A satisfactory explanation for such reversal of direction is not available so far.

Hydrogenase in *Synechocystis* is a pentameric NiFe-type enzyme, consisting of five protein subunits: HoxE, HoxF, HoxU, HoxY and HoxH. HoxH (also called the large subunit) is the main catalytic subunit, and along with HoxY (also called the small

subunit) it forms the hydrogenase moiety of the enzyme. While the large subunit catalyzes the $H_2/H^+$ oxidation/reduction reaction in its NiFe active site, a putative [Fe-S] cluster in the small subunit likely functions in transferring electrons from/to the large subunit. HoxE, HoxF and HoxU comprise the diaphorase moiety with a NAD(P)H binding site in HoxF. All subunits in the diaphorase moiety contain putative sites for binding [Fe-S] clusters (Appel and Schulz, 1996).The diaphorase moiety is unique for cyanobacterial bidirectional hydrogenases and is likely to participate in electron transfer between the redox partner of the enzyme and the hydrogenase moiety.

### 1.4.1 Hydrogenase Genes in *Synechocystis*

The five hydrogenase subunits are encoded by five *hox* (hydrogen oxidation) genes, *hoxE, hoxF, hoxU, hoxY* and *hoxH.* The five genes are located in one operon, with three open reading frames (ORFs) with unknown functions (Figure 1.3). These ORFs are *sll1222*, located in the downstream region of *hoxF,* and *ssl2420* and *sll1225*, both located in the downstream region of *hoxY.*

The five *hox* genes are known to be expressed as a single transcript and their transcription is regulated by a relatively weak promoter, located in the upstream region of *hoxE* (Dutheil et al., 2012; Gutekunst et al., 2005). The transcription start point of the operon is

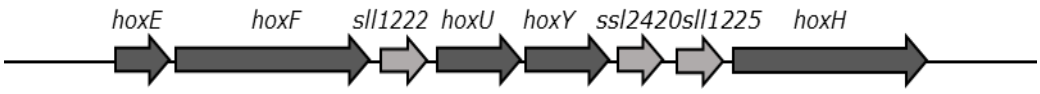


Figure 1.3
Schematic representation of the *hox* operon in *Synechocystis*, with five *hox* genes and three ORFs.

located 168 nucleotides upstream of the start codon of *hoxE*. The transcription of the *hox* operon is regulated by several factors such as environmental conditions (e.g., $H_2$, light, nickel, nitrate and sulfur availabilities) as well as transcription regulators and repressors. *Hox* genes are expressed both in the presence and absence of $O_2$. However, the transcript levels are increased (five- to six-fold) under microaerobic conditions ($O_2$ concentration below 1 µM) with an additional induction of *hoxE* and *hoxF* in darkness (Kiss et al., 2009; Summerfield et al., 2008; Oliveira and Lindblad, 2005). The expression of the *hox* operon is controlled by three transcription factors, LexA and AbrB1 acting as positive regulators, and AbrB2 acting as a repressor (Cassier-Chauvat et al., 2014).

### 1.4.2 Hydrogenase Maturation

The assembly of the NiFe-hydrogenase enzyme is a complex process involving at least seven proteins, known as maturase proteins (Peters et al., 2015; Eckert et al., 2012; Hoffmann et al., 2006). Six of these proteins are encoded by six *hyp* genes (hydrogen pleiotropic) and take part in various stages of the active site assembly including the incorporations of the metal ions and ligands in the active site and probably in the orientation of the [Fe-S] clusters in the small subunit as well. Homologs of the *hyp* genes are present in all organisms containing NiFe-hydrogenases. The maturation process involves the incorporation of CN ligands from carbamoyl phosphate aided by HypE and HypF, the incorporation of iron by HypC and HypD, and the incorporation of nickel by HypA and HypB in the large subunit of hydrogenase. The exact processes involved in the incorporation of the CO ligand in the large subunit and the [Fe-S] clusters in the diaphorase subunits are not known. The seventh protein, HoxW, is an endoprotease that

cleaves the C-terminus of the HoxH subunit as a final step of HoxH maturation during the assembly of HoxYH (Eckert et al., 2012). The knowledge on the maturation of the small subunit is scarce but the process is likely to occur at the same time as the large subunit maturation. A summary of the maturation process is depicted in Figure 1.4.

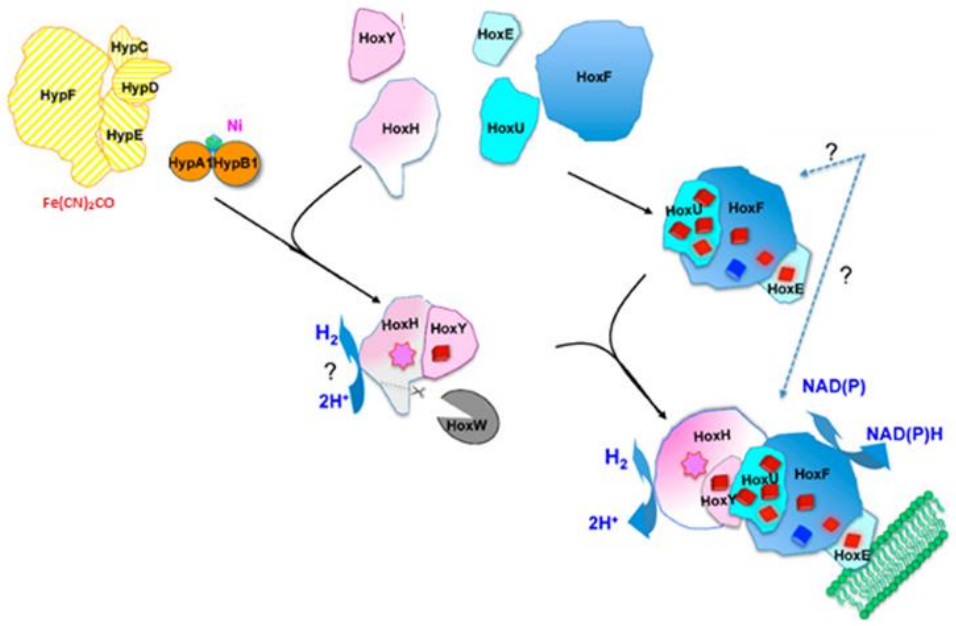


Figure 1.4
Schematic representation of the hydrogenase protein assembly adapted from Cassier-Chauvat et al. (2014).

### 1.4.3. Factors Controlling the Direction of $H_2$ Flux in *Synechocystis*

The active site of NiFe-hydrogenase catalyzes the reversible reaction between protons and electrons to form $H_2$. *In vitro*, as one would normally expect, the enzyme showed a

higher rate of $H^+$ reduction at low pH (McIntosh et al., 2011). However, *in vivo* an improvement of $H_2$ production was observed by increasing the pH of the culture medium from 6.5 to 7.5 (Baebprasert et al., 2010).

On the other hand, $H_2$ production showed improvement by the inhibition of nitrate assimilation, a process which uses reduced ferredoxin for the supply of electrons, and in the absence of NDH-1 that resulted in a very reduced NAD(P) pool (Gutthann et al., 2007; Cournac et al., 2004; Cooley and Vermaas, 2001). Therefore, the direction of the $H_2$ flux was suggested to rely mainly on the redox status of the NAD(P) and/or the ferredoxin/flavodoxin pool in the cell (Gutekunst et al., 2014; Chongsukantikul et al., 2014; Appel et al., 2000).

### 1.4.4 Factors Controlling the Redox Status of NAD(P) and Fd/Flv in *Synechocystis*

The ratios of NADPH and $NADP^+$, NADH and $NAD^+$, and reduced and oxidized form of Fd/Flv in *Synechocystis* are controlled by a great number of cellular processes. NADP and NAD are coenzymes, whose production and utilization differ significantly between periods of light and darkness. During the day, NADPH is primarily produced by the photosynthetic light reaction, and is utilized by the Calvin cycle (Knoop et al., 2013; Young et al., 2011; Yang et al., 2002). A portion of the photosynthetically generated NADPH is also used to reduce $O_2$ to $H_2O$ by Flv1 and Flv3 proteins (Allahverdiyeva et al., 2011). At night, cells use endogenous storage compounds (mainly glycogen) to maintain cellular processes (Grundel et al., 2012). Glycogen breaks down to glucose, which is used primarily by the oxidative pentose phosphate pathway, producing NADPH, and to a lesser extent by glycolysis producing both NADPH and NADH (Yang et al.,

2002). The reduced coenzymes are then reoxidized at night during respiration, where they are both utilized as substrates of the respiratory Complex I or NDH-1, although the NDH-1 in *Synechocystis* is known to prefer NADPH over NADH (Ma et al., 2006; Shastri and Morgan, 2005). Other than the central carbon metabolism, several other cellular processes (e.g., lipid synthesis and nucleotide synthesis) participate in the redox reactions of NADPH and/or NADH. While some of them are mainly active during the day, others are active both during day and night (Knoop et al., 2013; Yang et al., 2002), thus maintaining the balance between oxidized and reduced forms of NADP and NADH.

Fd and Flv are soluble proteins that are the final electron acceptors of the photosynthetic electron transfer chain. *Synechocystis* contains at least eight different ferredoxins (plant-type as well as bacterial-type, usually found in chloroplasts and bacteria, respectively); five of them are plant-type and three of them are bacterial-type ferredoxin (Mustila et al., 2014). The distinct functions of bacterial-type ferredoxins are poorly understood. The most abundant type, plant-type ferredoxin 1 (Fd1) is reduced by PS I, and then reoxidized by donating its electrons to Fd:$NADP^+$ oxidoreductase (FNR, EC 1.18.1.2). Fd1 acts as the redox partner of a variety of other enzymes as well. Examples of Fd1-binding enzymes include Fd:thioredoxin reductase (EC 1.8.7.2), nitrate reductase (EC 1.7.7.2) and nitrite reductase (EC 1.7.7.1). A comprehensive list of all possible ferredoxin-binding proteins in *Synechocystis* can be found in Hanke et al. (2011). *Synechocystis* also contains a pyruvate-ferredoxin oxidoreductase (PFOR, EC 1.2.7.1) that reduces ferredoxin during the conversion of pyruvate to acetyl-CoA (Schmitz et al., 2001). Flv, on the other hand, contains FMN as a cofactor and can substitute for Fd under conditions of iron deprivation (Goñi et al., 2009).

## 1.5 NAD(P)H Dehydrogenase (NDH-1)

The energy-converting NADH-ubiquinone oxidoreductase is the first enzyme of the respiratory electron transport chain in bacteria and mitochondria. The mitochondrial enzyme is referred as Complex I, whereas the bacterial enzyme is often referred as NADH-dehydrogenase or NDH-1. The general functions of this enzyme are to transfer electrons to the quinone pool of the respiratory electron transport chain (ETC) and to transport protons across the cytoplasmic membrane (Efremov et al., 2010). Even though these enzymes are found in all subdivisions of bacteria, archaea and eukarya, they differ significantly in their subunit compositions among various classes. The number of the protein subunits in Complex I generally increases with the complexity of the organism. For example, the bovine mitochondrial Complex I contains 46 different subunits (Hirst, 2013; Carroll et al., 2003), whereas most bacterial species, except cyanobacteria, contain at least 14 subunits, all of which have homologs in the bovine enzyme (Vignais and Billoud, 2007). The 14 subunits found in *E. coli* are considered to comprise a minimal set of proteins capable to perform all bioenergetic functions (Brandt, 2006).

The enzyme is L-shaped, with a hydrophobic membrane-embedded domain and a hydrophilic peripheral domain that extends to the cytosol (Friedrich and Scheide, 2000). The hydrophilic, peripheral arm consists of two distinct units. One, which is furthest from the membrane-embedded domain, contains three subunits with a NADH-binding and a FMN-binding domain and several Fe-S clusters. The other hydrophilic unit consists of four subunits and connects the NADH-oxidizing subunits to the membrane-embedded hydrophobic domain.

### 1.5.1 Cyanobacterial NDH-1

The NDH-1 complex in cyanobacteria is a membrane-embedded complex, but its precise location is debated. Cyanobacteria contain extensive thylakoid membranes that host components of their photosynthetic as well as respiratory electron transport chain. NDH-1 subunits were found in both cytoplasmic and thylakoid membranes in *Synechocystis* and *Synechococcus elongatus* (Berger et al, 1993; Pieulle et al., 2000; Ohkawa et al., 2002; Ogawa, 1992).

NDH-1 in all cyanobacteria has a unique subunit composition. Homologs of only 11 *nuo* genes of the minimal complex of *E. coli* have been found in the cyanobacterial genome (*ndhA-K* in *Synechocystis*) (Zhao et al., 2014a; Yagi et al., 1998; Battchikova and Aro, 2007; Kaneko et al., 2003 and 1996). This is puzzling because the three subunits that are present in the *E. coli* minimal complex but missing from cyanobacteria, include the NADH- and FMN-binding domain and several Fe-S clusters necessary for the catalytic activity of the enzyme. Without the knowledge of these crucial sites, the identity and the mechanism of catalysis at the active site of the enzyme have always been unclear.

Other than the 11 essential subunits, seven additional subunits (NdhL-NdhQ and NdhS), also called the oxygenic photosynthesis specific (OPS) subunits have been discovered recently in cyanobacteria (Zhang et al., 2014; Zhao et al., 2014b; Nowaczyk et al., 2011). Except for NdhQ, the six other subunits are unrelated to any eubacterial NDH-1 but have homologs in chloroplast NDH complex (Ma and Ogawa, 2015; Prommeenate et al., 2004). The suggested functions of these subunits are listed in Table 1.1.

Among the OPS subunits, NdhS is especially interesting because it has a SH3-like domain, which has the potential to bind proline-rich sequences that can mediate protein-protein interaction. The homolog of NdhS in chloroplasts is CRR31. CRR31, along with two other subunits, NdhT (CRRJ) and NdhU (CRRL), in *Arabidopsis thaliana* was suggested to form a catalytic domain that connects NDH-1 with Fd (Yamamoto et al., 2011). No homolog of NdhT or NdhU is present in the cyanobacterial genome (Yamamoto et al., 2011; Ma and Ogawa, 2015). The discovery of NdhS in *Synechocystis* and the co-elution of Fd and Fd-$NADP^+$ oxidoreductase with NDH-1 from *T. elongatus* recently raised the question on whether Fd can donate electrons to the bacterial NDH-1 as well (Ma and Ogawa, 2015).

Table 1.1.
Comparison of localization and function of the OPS NDH-1 subunits in cyanobacteria. Table was reproduced from Ma and Ogawa (2015).

| **OPS Subunit** | **Localization** | **Function in assembly** | **Function in cyclic electron flow** | **Function in $CO_2$ uptake** | **Function in respiration** |
|---|---|---|---|---|---|
| NdhL | MA | - | + | + | + |
| NdhM | MA | n.a. | n.a. | n.a. | n.a. |
| NdhN | MA | n.a. | n.a. | n.a. | n.a. |
| NdhO | HA | + | + | + | - |
| NdhP | MA | + | + | - | + |
| NdhQ | MA | + | + | - | + |
| NdhS | HA | - | + | - | - |

+, affected; -, unaffected; n.a., not analyzed; MA, membrane arm; HA, hydrophilic arm.

The localization of NdhS is controversial. Ma and Ogawa (2015) have placed this subunit far from the membrane-embedded domain and close to the missing NAD(P)H-binding unit (Figure 1.5). On the other hand, Battchikova et al. (2011b) have localized this subunit near the thylakoid membrane, along with other OPS subunits.

It should be noted, as Ma and Ogawa (2015) have pointed out, that even though the OPS subunits are common in the bacterial and the chloroplast NDH-1 complexes, there may be some functional differences between the two. For example, the absence of NdhL in cyanobacteria showed no effect in the stability and assembly of the complex, but in higher plant *ndhL* knockout resulted in a complete collapse of the hydrophilic arm of NDH-1 (Shimizu et al., 2008). Similarly, the deletion of *ndhO* stabilized the cyanobacterial complex and increased NDH-1 mediated cyclic electron transport (CET) around PS I, while in plants, *ndhO* deletion resulted in complete impairment of the NDH-

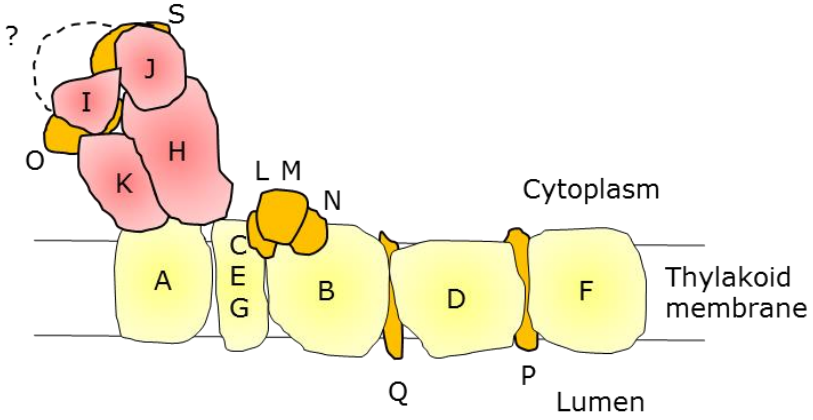


Figure 1.5

Hypothetical model of cyanobacterial NDH-1 with suggested locations of the newly discovered subunits. The unknown NADH-accepting subunit is shown with a question mark. Figure adapted from Ma and Ogawa (2015).

CET function and in a collapse of the hydrophilic arm (Rumeau et al., 2005). Based on these differences, Ma and Ogawa (2015) suggested a "divergent enzymatic activity" of cyanobacterial and chloroplast NDH-1.

### 1.5.2 NDH-1 Subcomplexes

NDH-1 in *Synechocystis* is known to exist as several subcomplexes with varying functions. Proteomic studies first revealed the presence of such functionally distinct complexes (Herranen et al., 2004). NDH-1M, comprising hydrophilic (NdhH-K, NdhM-O and NdhS) and hydrophobic (NdhA-C, NdhE, NdhG and NdhL) subunits, seems to be a common unit in all variants of cyanobacterial NDH-1 complexes (Battchikova et al., 2011a, 2005). Specific NdhD/NdhF membrane modules combine with this unit to form diverse subcomplexes (Figure 1.6), such as NDH-1L with NdhD1/NdhF1, NDH-1L' with NdhD2/NdhF1 and NDH-1MS with NdhD3/NdhF3. The NDH-1L (Large) subcomplex contains subunits NdhA–K, homologous to the subunits of the Complex I from *E. coli*, and OPS subunits NdhL–NdhO and NdhS (but not NdhP/NdhQ) (Ma and Ogawa, 2015; Zhao et al., 2014b; Battchikova et al., 2005 and 2011b; Zhang et al., 2005; Prommeenate et al., 2004; Herranen et al., 2004).

NDH-1S is small subcomplex that comprises of only NdhD3, NdhF3, CupA and CupS proteins (Ogawa and Mi, 2007). CupA and CupS are both novel proteins of cyanobacterial NDH-1, participating in $CO_2$ uptake (Korste et al., 2015; Folea et al., 2008). Another variation of the complex, NDH-1MS', comprises the NdhD4/NdhF4 and CupB proteins (Xu et al., 2008; Shibata et al., 2002).

It is important to note that no protein subunit homologous to the *E. coli* NuoE, F and G subunits, essential for their NADPH/NADH dehydrogenase activity, has been found in any of the NDH-1 subcomplexes detected so far.

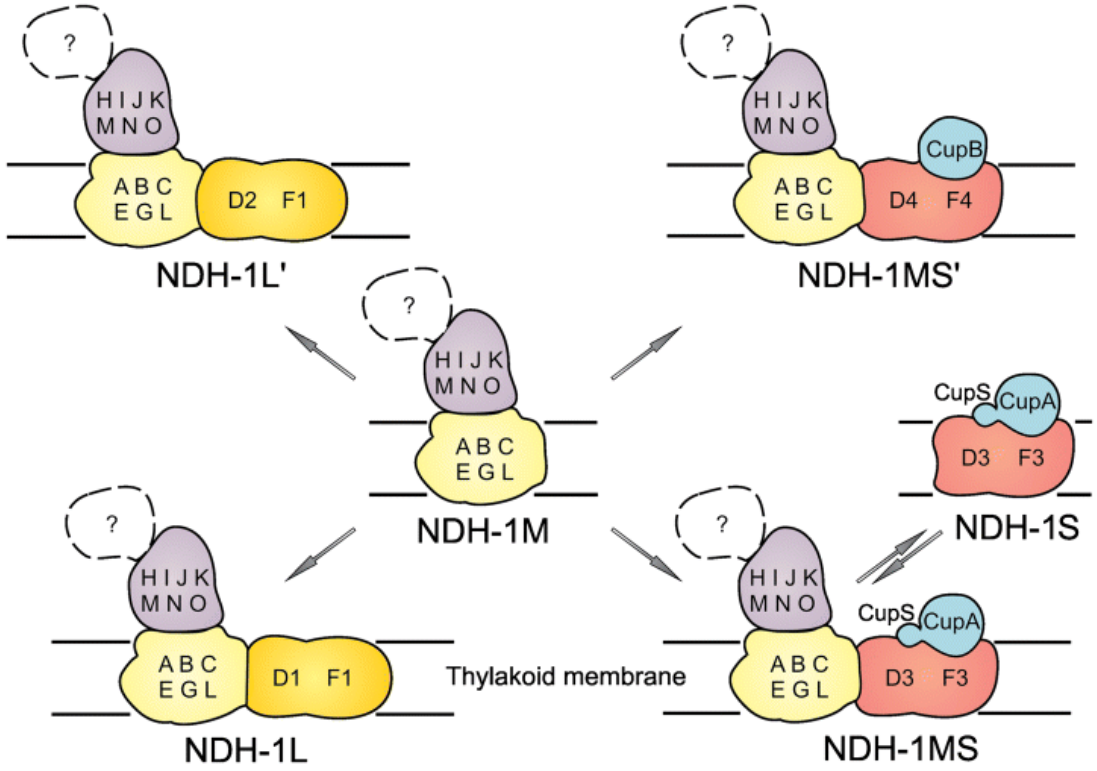


Figure 1.6
Variations of cyanobacterial NDH-1 complexes. The hypothetical domain responsible for the dehydrogenase activity is indicated by a question mark. Figure from Battchikova and Aro (2007).

### 1.5.3 Function of NDH-1 in Cyanobacteria

NDH-1 in cyanobacteria is known to be involved in a wide variety of cellular functions such as respiration, $CO_2$ uptake and cyclic electron transport around PS I.

#### a) Respiration:

The role of NDH-1 in cyanobacterial respiration is debated. The *ndhB*-insertion mutant strain of *Synechocystis* (M55) as well as *ndhD1/ndhD2* mutants showed lower rates of respiration and inability to grow under photoheterotrophic conditions (Ohkawa et al., 2000). On the other hand, *ndhD3/ndhD4* and *ndhD5/ndhD6* mutants showed respiration rates similar to the wild-type strain. However, according to Cooley and Vermaas (2001), in *Synechocystis* another enzyme, succinate dehydrogenase, and not NDH-1 plays a major role in electron donation to the plastoquinone (PQ) pool during respiration in darkness. They argued that the decreased respiratory electron flow in the *ndhB* mutant (and possibly in the other *ndh* mutants as well), may be a consequence of low succinate levels in this strain rather than the primary lack of NDH-1 activity.

#### b) Cyclic Electron Flow:

Aside from the linear flow of electrons from PS II to cytochrome $b_6f$, PS I and ferredoxin, in cyanobacteria and plant photosynthetic systems cyclic electron flow around PS I is observed that helps to increase the ATP/NADPH ratio without any net NADPH production. The NdhB-deficient mutant M55 was shown to be severely impaired in cyclic electron flow around PS I. Similar to respiration, NdhD1 or NdhD2, but not NdhD3 or NdhD4 seem to be involved in the cyclic electron flow (Ohkawa et al., 2000).

### c) $CO_2$ uptake:

Cyanobacteria have a well-established system of concentrating inorganic carbon ($C_i$) in order to cope with the low affinity of their central enzyme ribulose 1,5-bisphosphate carboxylase/oxygenase or Rubisco (reviewed in detail by Price et al., 2008). Similar to the previous functions, some, but not all, NDH-1 subunits participate in $CO_2$ uptake most likely by creating an alkaline pocket where $CO_2$ can be converted by carbonic anhydrase to $HOC_3^-$ (Kaplan and Reinhold, 1999). Reverse genetics studies showed that the operons containing *ndhF3-ndhD3-cupA1-chpY*, and *ndhF4-ndhD4-cupB1-chpX* are required for $CO_2$ uptake (Ohkawa et al., 2000; Shibata et al., 2001). On the other hand, *ndhD1/ndhD2* mutants showed normal growth under photoautotrophic conditions indicating that the products of these two genes did not participate in $CO_2$ uptake (Ohkawa et al., 2000).

### d) Function in Driving the $H_2$ flux:

Sustained photo-$H_2$ production for at least 10 min was observed in the *ndhB* mutant of *Synechocystis* (M55) upon illumination (Cournac et al., 2004). As mentioned earlier, $H_2$ production in cyanobacteria upon illumination is transient, lasting only for ~30 s, and is immediately followed by $H_2$ oxidation. In M55 the light-induced $H_2$ uptake was negligible (Cournac et al., 2004). Also, the NAD(P)H pool in M55 was almost entirely in reduced state (Cooley and Vermaas, 2001), allowing several minutes of sustained $H_2$ photoevolution. The role of NDH-1 in cyanobacterial $H_2$ metabolism is discussed in more detail in the next few chapters.

### 1.5.4 NDH-1 and Hydrogenase

Sequence homologies between subunits of hydrogenase and NDH-1 have been observed for a long time (Böhm et al., 1990; Sauter et al., 1992; Friedrich, 1998; Appel and Schulz, 1996). NuoB and NuoD subunits of *E. coli* NDH-1 show similarities with the small and large subunits, respectively, of NiFe-hydrogenases. The similarities between NuoD and the large subunit are mostly centered near the NiFe active site region. However, the counterparts of the cysteine ligands of the nickel in the large subunit are missing in NuoD (Vignais et al., 2001). The NiFe binding site in the large subunit has been hypothesized to have converted to the quinone binding site in NuoD (Dupuis et al., 2001).

Striking similarities have been observed between HoxE, HoxF and HoxU subunits of cyanobacterial NiFe-hydrogenases and NuoE, NuoF and the N-terminal region of NuoG subunits, respectively, of *E. coli* NDH-1. This is particularly interesting because homologs of these *E. coli* subunits are otherwise missing in cyanobacteria. Based on the sequence similarities, a common use of the diaphorase subunits between NDH-1 and hydrogenase was suggested in cyanobacteria (Appel and Schulz, 1996; Schmitz and Bothe, 1996). Later it was argued that several cyanobacterial strains lack a bidirectional hydrogenase (Tamagnini et al., 2002). Even in the strains with a bidirectional hydrogenase, the deletion of the *hox* genes did not show any noticeable difference in their growth rates (Appel et al., 2000), and the rates of $O_2$ uptake due to respiration in *Synechocystis* strains with and without the diaphorase subunits were found to be nearly identical (Howitt and Vermaas, 1999).

However, it should be noted that the cyanobacterial NDH-1 complex is quite unique in subunit composition as well as function. Succinate dehydrogenase, and not NDH-1, is now known as the main electron supplier to the PQ pool for the reduction of $O_2$ in *Synechocystis* during respiration (Cooley and Vermaas, 2001). Therefore, a significant change in the respiratory $O_2$ uptake rate could not be expected in the diaphorase-deletion strain anyway. As for the lack of hydrogenase in various cyanobacterial strains, NDH-1 in cyanobacteria is known to exist as several subcomplexes in the cell with different subunit compositions and functions and not all of these subcomplexes participate in respiratory electron flow. In fact one of such subcomplexes has been suggested to accept electrons from Fd with the mysterious NdhS subunit (Ma and Ogawa, 2015). The possibility of another of these subcomplexes accepting electrons from the diaphorase subunits under optimal conditions can not be ruled out either.

# CHAPTER 2

# $H_2$ OXIDATION AND PRODUCTION PROFILE IN *SYNECHOCYSTIS* SP. PCC 6803 AND HETEROLOGOUS EXPRESSION OF THE HYDROGENASE FROM *LYNGBYA AESTUARII* BL J IN THE *SYNECHOCYSTIS* Δ*HOX* STRAIN


## Summary

The unicellular model cyanobacterium *Synechocystis* contains a NiFe-bidirectional hydrogenase capable of producing or oxidizing $H_2$ in anaerobic conditions both in darkness and in the presence of light. In darkness, the direction of $H_2$ flux depends upon the initial concentration of $H_2$ in the culture medium and continues to either produce or oxidize $H_2$ until a particular concentration of $H_2$ is reached. This particular $H_2$ concentration depends upon the amount of biomass used during measurements. In the presence of light, the enzyme shows only transient $H_2$ production and rapid $H_2$ oxidation at a rate that is an order of magnitude higher than the rate of $H_2$ oxidation observed in darkness and that continues until $H_2$ is exhausted. Aside from *Synechocystis*, *Lyngbya aestuarii* BL J, a marine microbial strain showing high $H_2$-producing capacity in darkness, also shows similar light-induced rapid $H_2$ uptake. The hydrogenase from *Lyngbya* BL J, when expressed heterologously in *Synechocystis* Δ*hox* strain, shows $H_2$ evolution, but only in the presence of reduced methyl viologen.

## 2.1 Introduction

The cyanobacterial bidirectional hydrogenase has been most studied in the unicellular fresh-water strain *Synechocystis* sp. PCC 6803. The absence of a nitrogenase or an uptake hydrogenase makes the bidirectional enzyme the only one in the cell that can catalyze $H_2$ production or oxidation (Appel et al., 2000; Kaneko et al., 1996). $H_2$ production in *Synechocystis* is controlled by two main factors: the absence of $O_2$ and the availability of electron donors such as NADH, NADPH or, as recently suggested, reduced Fd/ Flv (Cournac et al., 2004; Gutekunst et al., 2014).

The maximal $H_2$ production rates in *Synechocystis* and in many other strains that can be easily grown in bioreactors are quite low, typically ranging between 0.02 µmoles $H_2$ (mg chl *a*)$^{-1}$ h$^{-1}$ (Baebprasert et al., 2010) and 0.3 µmoles $H_2$ (mg chl *a*)$^{-1}$ h$^{-1}$ (Kothari et al., 2014), and the production period is often transient and dominated by $H_2$ uptake, although few data are available on $H_2$ uptake (Carrieri et al., 2008; Antal and Lindblad, 2005). Some improvements in $H_2$ production were achieved by optimizing the growth conditions (e.g., saturating nickel concentration (Carrieri et al., 2008), sulfur deprivation (Burrows et al., 2008), optimum pH maintenance (Burrows et al., 2009), and inhibition of respiration and nitrate assimilation in the cells (Gutthann et al., 2007)). However, a comprehensive understanding of all the important factors controlling the $H_2$ flux is still lacking.

$H_2$ photoevolution, which is in theory a preferred method of $H_2$ production since it does not use a carbohydrate intermediate, does not last for more than 30 s in *Synechocystis*. Reports of $H_2$ photoevolution from *Synechocystis* wild-type strain show a transient $H_2$ production upon illumination, which quickly reverts its direction to $H_2$ uptake until the

hydrogenase enzyme is inactivated by photosynthetically produced $O_2$ (Cournac et al., 2002 and 2004; Gutthann et al., 2007). While no satisfactory explanation is available for this change of direction of the $H_2$ flux, the uptake activity in the light has not been researched in detail either. Recently a marine cyanobacterial strain, *Lyngbya aestuarii* BL J (hereafter, *Lyngbya* BL J), was shown to produce $H_2$ for a prolonged period of time (more than 24 h) in darkness, either naturally or in the presence of external reductants (Kothari et al., 2012 and 2014). This filamentous, non-heterocystous strain showed a 20-fold faster $H_2$ production rate and a 45-fold higher maximum concentration of produced $H_2$ by fermentation, compared to *Synechocystis*. Thus, the hydrogenase enzyme in this strain offers a great potential for fermentative $H_2$ production. The presence or absence of $H_2$ production in the light was not reported in those studies, but the maximal $H_2$-producing capacity of the NiFe hydrogenase (measured in terms of $H_2$ production with excess reductants) in *Lyngbya* BL J was 16-fold higher compared to the maximum $H_2$ producing capacity observed in *Synechocystis* under identical conditions.

With the aim of gaining a better understanding of the hydrogenase activity in *Synechocystis* under physiological conditions, this chapter presents a complete hydrogenase-activity profile for in the light and in darkness. Also, *Lyngbya* BL J was assayed for $H_2$ production and uptake activity in the presence of light. Finally, a *Synechocystis hox*-deletion mutant strain was created and the NiFe hydrogenase from *Lyngbya* BL J was heterologously expressed in this strain.

## 2.2 Materials and Methods

### 2.2.1 Cyanobacterial Growth Conditions

*Synechocystis* cultures were grown in standard BG-11 media (Rippka et al., 1979) at 30 °C, in 200-ml culture flasks, illuminated at a light intensity between 50 and 55 µmol photons $m^{-2}$ $s^{-1}$ and bubbled with air. For the *Lyngbya* BL J strain, IMR medium, set at 3% (w/v) salinity (named as such by Eppley et al. (1968)) was used. *Lyngbya* cultures were grown in 200-ml culture flasks, at 30 to 35 µmol photons $m^{-2}$ $s^{-1}$ light intensity, without additional bubbling.

### 2.2.2 Assay for $H_2$ Production and Uptake

**a) Electrode Setup:**

A modified Clark-type electrode ($H_2$ microsensor, Unisense, Aarhus, Denmark) was used to monitor the partial pressures of $H_2$ in sealed culture media. The electrode setup included a microrespiration chamber (Unisense) of 4.5 ml inner volume. During measurements, the chamber was completely filled with cultures and tightly sealed with a lid, which allowed the insertion of the electrode through a thin capillary. The concentration of $H_2$ in the culture medium was recorded with the electrode, which was connected to a picoammeter (PA2000, Unisense) that polarized the electrode at a voltage of +1000 mV (the Clark-type electrode traditionally measures $O_2$ at a polarizing voltage of -800 to -1000 mV) and measured the current signal in pA. The picoammeter was connected to an A/D converter, which converted the output analog signal to a digital one, which could be read on a computer with the Sensor Trace Basic software (Unisense).

Calibration of the electrode was done as recommended by the company, using a two-point calibration in water bubbled with either air (considered to be 0% of $H_2$) or with 5% $H_2$ in $N_2$.

**b) Culture Setup:**

For measurements of $H_2$ production or uptake, *Synechocystis* cultures were grown to mid- to late-exponential phase ($OD_{730}$ between 0.8 and 1, determined by a Shimadzu UV-1800 UV-VIS dual beam spectrophotometer). Cells were harvested by centrifugation and then resuspended in fresh BG-11 medium to a final cell density of 11 µg chl *a* $ml^{-1}$. *Lyngbya* BL J, on the other hand, grew as clumps. These clumps of biomass were collected after 3-4 days of growth and resuspended in IMR medium (3% (w/v) salinity) for hydrogenase activity assays. The total chl *a* content of the cell suspensions (usually between 2 and 3 µg chl *a* $ml)^{-1}$) was measured after the completion of the measurement assays. To measure the chlorophyll content, the absorbance of methanol extract of a culture was measured at 665 nm with a spectrophotometer and the chlorophyll concentration was calculated using an extinction coefficient at that wavelength of 82.0 L $g^{-1}$ $cm^{-1}$ (Porra et al., 1989).

The resuspended cultures were loaded into the microrespiration chamber, as described above. Before sealing the chamber, a mixture of glucose (10 mM), glucose oxidase (40 U $ml^{-1}$) and catalase (50 U $ml^{-1}$) was added to make the culture completely anaerobic (Appel et al., 2000). When monitoring $H_2$ uptake, 2 ml of BG-11 medium saturated with 5% $H_2$ was added to the mixture. During measurements, cultures were either kept in

darkness, or were illuminated at an intensity between 800 and 1000 µmol photons $m^{-2}$ $s^{-1}$ using a Fiber Optic Illuminator (Fiber-Lite, model 190).

While measuring $H_2$ production with excess external reductants, measurements were carried out in darkness and after the addition of 5 mM methyl viologen and 10 mM sodium dithionite to the cell suspension (Appel et al., 2000). Sodium dithionite removes $O_2$ from the medium and reduces methyl viologen, which in turn supplies electrons to the bidirectional hydrogenase for $H_2$ production.

### 2.2.3 Construction of the *hox*-Deletion Mutant

Primers used for the construction of the *hox*-deletion mutant (Δ*hox*) are listed in Table 2.1. PCR was used to amplify portions of the *Synechocystis* genome containing the flanking regions of the *hox* operon on both ends (1679265-1678582 and 1672239-1671416, Figure 2.1) and also a 1024 bp DNA fragment containing the chloramphenicol resistance cassette, from an existing plasmid vector, Vector-V (constructed in our laboratory by Dr. Hongliang Wang). The sequence locations in the *Synechocystis* genome are stated according to CyanoBase.

To delete the *hox* operon, a pUC19-based plasmid (pΔ*hox*) was constructed with the 684-bp upstream and 824-bp downstream flanking regions of the *Synechocystis hox* operon, with the chloramphenicol-resistance cassette in between (Figure 2.1), fused together by the extension PCR method (Pogulis et al., 1996). A wild-type *Synechocystis* culture was transformed with this pΔ*hox* following the procedure as described by Vermaas et al. (1987).

Table 2.1.
Primers used in the construction of the Δ*hox* mutant strain. In the primer sequences, letters in bold indicate restriction sites used for digestion and the lower case letters indicate 5' nucleotides that were added.

| **Primer** | **Sequence** | **Description** |
|---|---|---|
| Δ*hox*1-F | aatt**GAGCTC**ATCACTTCCAAACAACACCCAGAAC | Region upstream of *hoxE* |
| Δ*hox*-1-R | AGGAGCAATACAGCAGATAAAAG | |
| Δ*hox*-3-F | agacgaaagggcctcgtgatacCATTCGCAATCATGATGTGCAAG | Region downstream of *hoxH* |
| Δ*hox*-3-R | aatt**GCATGC**CACTCCATCGTAGTACTCCTGC | |
| Δ*hox*-2-F | cttttatctgctgtattgctcctTATTTAACGACCCTGCCCTGAAC | Chloram-phenicol resistance cassette |
| Δ*hox*-2-R | GTATCACGAGGCCCTTTCGTCTTC | |
| Δ*hox*-Seg-F | GCTACCGTTTGGCTCGCTGGTTG | DNA segment inside the *hox* operon |
| Δ*hox*-Seg-R | GCGATTGGTTTCAATTTTCCCCA | |

Transformants were subcultured in the presence of increasing concentrations of chloramphenicol to aid in segregation of the wild-type and mutant genome copies. Segregation analysis was performed by PCR using primers Δ*hox*-Seg-F and Δ*hox*-Seg-R, which amplifies a DNA fragment inside the *hox* operon. The resultant fully segregated mutant colonies were obtained on BG-11 plates with 100 µg $ml^{-1}$ chloramphenicol.

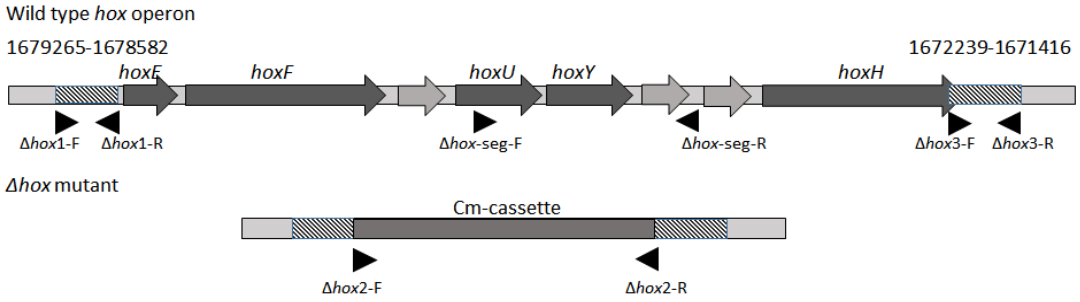


Figure 2.1

Schematic representation of the *hox*-deletion construct and the positions of the primers used.

### 2.2.4 Construction of the *Synechocystis* Δ*hox*$_{6803}$/*hox*$_{BL\ J}$ Mutant Strain

Primers used for the construction of the Δ*hox*$_{6803}$/*hox*$_{BL\ J}$ strain are listed in Table 2.2. The *hox* operon (including the five *hox* genes, *hcp* (located in between *hoxF* and *hoxU*), two ORFs downstream of *hoxH*, and *hoxW*) was amplified from the *Lyngbya* BL J strain by PCR, using the LongAmp Taq DNA polymerase (purchased from NEB) with primers BL J-*hox*-F and BL J-*hox*-R (Table 2.2), with unique restriction sites (BamHI and NotI)

engineered into them. The nucleotide sequence of the *hox* operon of *Lyngbya* BL J was obtained from NCBI (Ref Seq number NZ_AUZM00000000.1). The PCR amplicon was subsequently cloned into a cloning vector, Vector-1 (constructed by Dr. Hongliang Wang). This vector had a pUC19 backbone, into which a Ni-inducible promoter 2676566 and 2676567 (numbered according to CyanoBase) to direct homologous recombination. The amplified *hox* operon was cloned into Vector-I, in between a BamHI site at the 3' end of the promoter sequence and a NotI site at the 5' of the terminator sequence (Figure 2.2). The *Synechocystis* Δ*hox* mutant strain was transformed with the resulting plasmid p$hox_{\text{BL J}}$, following the procedure as previously reported (Vermaas et al., 1987). Transformants were grown on BG-11 plates with kanamycin and the

Table 2.2.
Primers used for the construction of the Δ$hox_{6803}$/$hox_{\text{BL J}}$ strain. In the primer sequences, letters in bold indicate the restriction sites used for digestion and the lower case letters indicate 5' nucleotides that were added.

| **Primer** | **Sequence** |
|---|---|
| BL J-*hox*-F | aatt**GGATCC**ATGCAATCTTCGACAAAAAAAC |
| BL J-*hox*-R | aatt**GCGGCCGC**GCCGTTCGAGAGTTTAGACTGTG |
| BL J-seg-F | CGCTTGGCATTCAAACAAAGATAAG |
| BL J-seg-R | CATTAGTTAACCCATGGCCATTATC |
| BL J-ins-F | GGATCGCAGTGTGCTTGAAAGTG |
| BL J-ins-R | CGACAAGGAATACATTTTCCAC |

concentration of kanamycin was increased gradually with each subculture, starting from 10 µg $ml^{-1}$. Segregation and the presence of the BL J *hox*-insert were checked periodically by PCR using primers BL J-seg-F (location in CyanoBase: 2676211-2676235) and BL J-seg-R (location in CyanoBase: 2676799-2676755), and BL J-ins-F and BL J-ins-R, respectively, with genomic DNA isolated from the wild-type and the transformed strains.

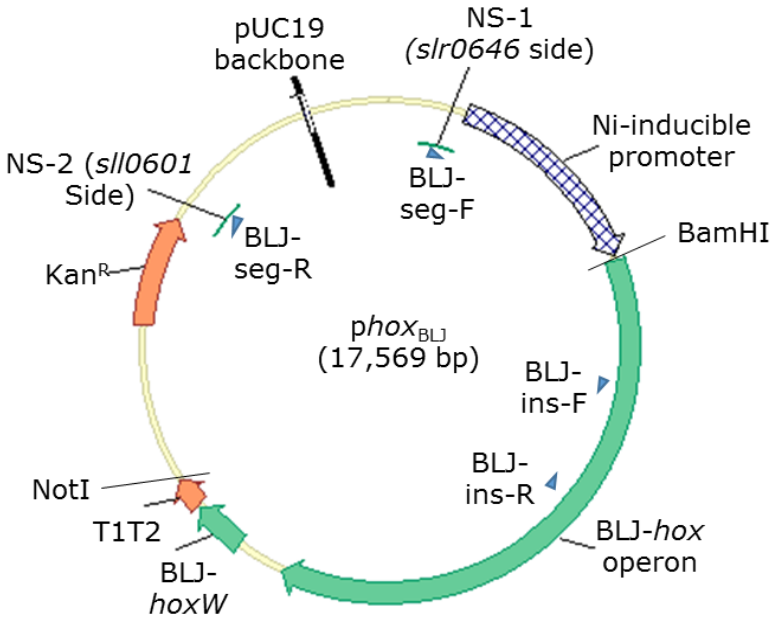


Figure 2.2
Plasmid p*hox*$_{BL\ J}$ containing the *hox* operon from *Lyngbya* BL J under the expression of the Ni-inducible promoter ($P_{nrsBACD}$). The triangles labelled BL J-seg-F and BL J-seg-R represent the positions of the primers used to check the segregation, and the triangles labelled BL J-ins-F and BL J-ins-R represent the positions of the primers used to check the presence of the insert in *Synechocystis* transformants.

### 2.2.5 RT-PCR

RNA was extracted from cultures of *Synechocystis Δhox* and *Δhox/hox*$_{BL\ J}$ mutant strains using Trizol reagent (Life Technologies) following the manufacturer's protocol. DNAse treatment was done by Turbo DNA-free$^{TM}$ DNAse (Life Technologies), followed by cDNA synthesis using the iScript Select cDNA Synthesis Kit (Bio-Rad), following the manufacturer's protocols in both cases. For RT-PCR, iTaq SYBR Green Supermix with ROX (Bio-Rad) was used with primers listed in Table 2.3 and reactions were performed using the manufacturer's protocol. An ABI Prism 7900HT Sequence Detector System was used for measuring fluorescence of SYBR green/double-stranded DNA and analysis was done using the $2^{-\Delta Ct}$ method (Schmittgen and Livak, 2008).

Table 2.3.

Primer sequences used for RT-PCR of cDNA from the *Synechocystis Δhox* and *Δhox/hox*$_{BL\ J}$ mutant strains.

| **Primer** | **Sequence** | **Amplicon Size in bp** |
|---|---|---|
| BL J-*hoxE*-F | CATGAAACGCAGCCAATATC | 105 |
| BL J-*hoxE*-R | CGGGCGATGTACATTAACAC | |
| BL J-*hoxF*-F | CAAGAACGTCAATCCCTCAA | 128 |
| BL J-*hoxF*-R | TTATCTTGGAGTCCGGCTTT | |
| BL J-*hoxU*-F | CTCGCTGTGTTCGAGTCTGT | 105 |
| BL J-*hoxU*-R | CAAGGTTGATTTAACCCGGTA | |
| BL J-*hoxY*-F | ATTTGGTTAGCGGGTTGTTC | 102 |
| BL J-*hoxY*-R | CACCGGACTGAAGACAACAT | |
| BL J-*hoxH*-F | GTTAGGATATCCGCAGGGAA | 111 |
| BL J-*hoxH*-R | CGATCGCGAAATTCTTGTAA | |
| *atpA*-F | TCCCCGGCCCCTGGAATTATT | 100 |
| *atpA*-R | GCTGACCCCGACCAATGGGA | |

## 2.3 Results

### 2.3.1 Hydrogenase Activity in *Synechocystis* sp. PCC 6803

#### a) $H_2$ Production in Darkness

When *Synechocystis* cultures (11 µg chl *a* $ml^{-1}$) were incubated under anaerobic conditions in darkness without added $H_2$, $H_2$ production (also known as fermentative $H_2$ production) started within ~two minutes of incubation (Figure 2.3 (A)) and a maximum net production rate of 2.31 ± 0.50 µmoles (mg chl *a*)$^{-1}$ $h^{-1}$ (average of three independent measurements) was observed between 3 and 6 minutes of incubation. The maximum rate of $H_2$ evolution observed in this study was similar to the rates previously reported in the literature, typically ranging between 0.3 and 2.7 µmoles of $H_2$ (mg chl *a*)$^{-1}$ $h^{-1}$ (Kothari et al., 2014; Cournac et al., 2004; Gutthann et al., 2007; Schütz et al., 2004). The production continued for 5-10 minutes, after which the rate began to decrease, eventually reaching a

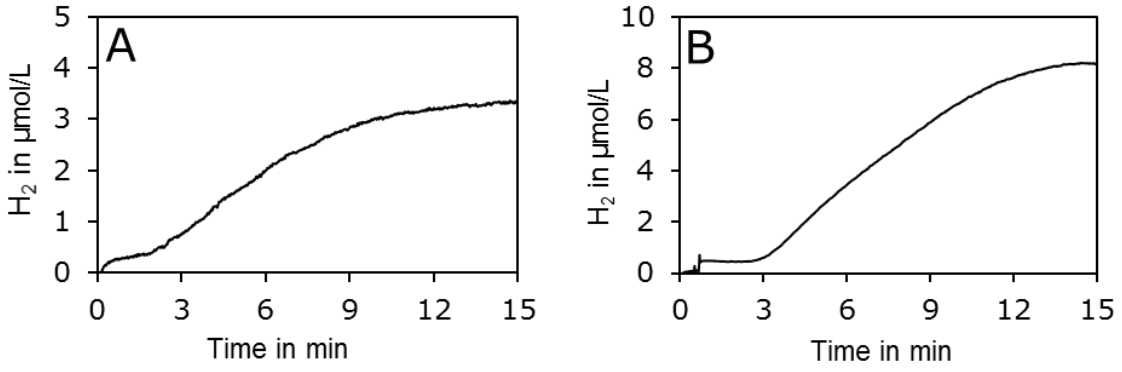


Figure 2.3

$H_2$ production in *Synechocystis* cultures incubated in darkness and under anaerobic conditions. Anaerobiosis was induced by the addition of glucose, glucose oxidase and catalase at time 0. Cell suspensions of 11 µg chl *a* $ml^{-1}$ (A) and 22 µg chl *a* $ml^{-1}$ (B) were used.

final concentration of 4 ± 1 µM. After this point, no further net increase in the concentration of $H_2$ was observed.

To check whether this final concentration depends on the amount of biomass used, the same measurements were taken using cell suspension 22 µg chl *a* $ml^{-1}$ (Figure 2.3 (B)). The final $H_2$ concentration increased to a value of 11 ± 2.9 µM (average from three independent measurements).

### b) $H_2$ Uptake in Darkness

To monitor $H_2$ uptake in darkness and under anaerobic conditions, cultures were incubated in the presence of 18-20 µM $H_2$. $H_2$ uptake began within approximately 10 minutes of incubation and continued until the concentration of $H_2$ in the chamber decreased to 4.1 ± 0.8 µM (average of three independent measurements) (Figure 2.4).

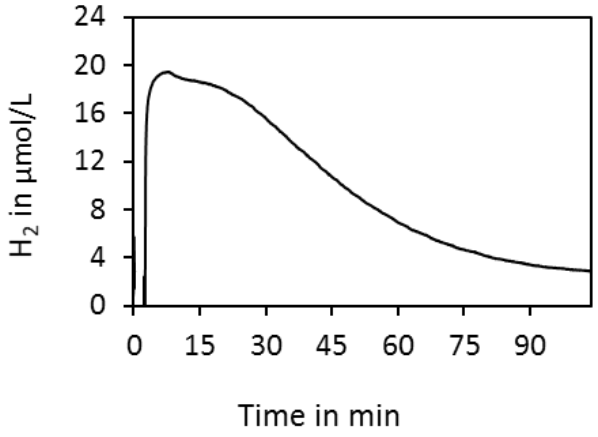


Figure 2.4
$H_2$ uptake in *Synechocystis* culture incubated in darkness and in anaerobic conditions. The initial steep rise of the curve represents the addition of $H_2$-saturated BG-11. A cell suspension of 11 µg chl *a* $ml^{-1}$ was used.

The uptake continued for 60-90 min (depending upon the initial concentration of $H_2$), with a maximum rate of 2.25 $\pm$ 0.84 µmol $H_2$ (mg chl *a*)$^{-1}$ h$^{-1}$.

### c) $H_2$ Production in Light:

Light-induced $H_2$ production was measured during a dark-to-light transition with a cell suspension of *Synechocystis* adapted to anaerobic conditions. After the addition of glucose, glucose oxidase and catalase, the cell suspension was left in darkness in the microrespiration chamber for the fermentative $H_2$ production to stabilize. When the $H_2$ concentration stabilized, cells were illuminated with light at an intensity of 800-1000 µmol photons m$^{-2}$ s$^{-1}$. An initial burst of $H_2$ production was observed that lasted for 20-30 s (Figure 2.5). This burst was followed by $H_2$ uptake of approximately the same initial rate that consumed all the $H_2$ produced earlier. Similar results were obtained when light was switched on at any point during the fermentative $H_2$ production. The rate of $H_2$ photoevolution found in this study was 4.14 $\pm$ 0.15 µmol (mg chl *a*)$^{-1}$ h$^{-1}$, which was slightly higher than the rate reported previously by Cournac et al. (2004).

### d) $H_2$ Uptake In Light

To examine the light-induced $H_2$ uptake in more detail, cell suspension was initially incubated in the measurement chamber with 18 µM $H_2$ along with glucose, glucose oxidase and catalase. The chamber was left in darkness for a few minutes for the glucose and glucose oxidase to consume all the $O_2$ present in the medium, before switching on the light. After an initial $H_2$ photoevolution, $H_2$ uptake started at a rapid rate and continued until all the $H_2$ in the medium was consumed (Figure 2.6). The maximum uptake rate in

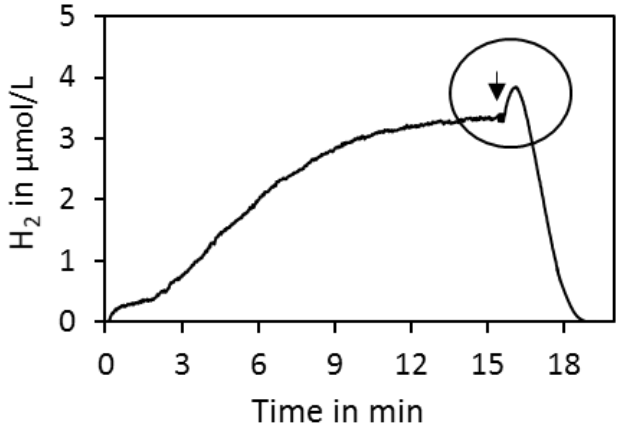


Figure 2.5
$H_2$ photoevolution and subsequent consumption in *Synechocystis.* A cell suspension of 11 µg chl *a* $ml^{-1}$ was initially incubated in darkness and under anaerobic conditions at time 0. After the completion of the fermentative $H_2$ production, light (at an intensity of 800-1000 µmol photons $m^{-2}$ $s^{-1}$) was switched on (as indicated by an arrow) and $H_2$ photoevolution (circled) was observed transiently.

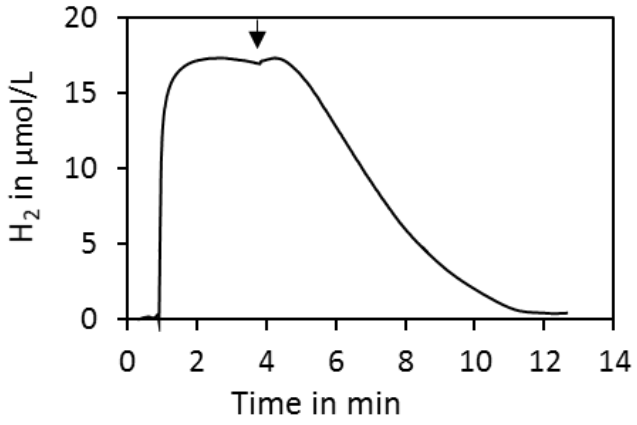


Figure 2.6
Measurement of the light-induced $H_2$ uptake in *Synechocystis* culture (11 µg chl *a* $ml^{-1}$) with 18 µM $H_2$ present initially. The initial steep rise of the curve represents the addition of $H_2$-saturated BG-11. After a few minutes of incubation in darkness, the culture was illuminated with light at an intensity of 800-1000 µmol photons $m^{-2}$ $s^{-1}$ (indicated by an arrow).

light (20.14 $\pm$ 2.53 µmoles of (mg chl *a*)$^{-1}$ h$^{-1}$, average of three independent measurements), achieved within 30 to 60 s of the beginning of $H_2$ consumption, was an order of magnitude higher than the maximum rate observed in darkness. The maximum rates of $H_2$ uptake and production observed in the presence or absence of light are listed in Table 2.4.

Table 2.4.

Maximum $H_2$ production and uptake rates (average of three independent experiments) from wild-type *Synechocystis* cultures. Measurements were taken using 4.6 ml cell suspension containing 50 µg of chl *a*.

| **Hydrogenase activity** | **Maximum rate in µmoles of $H_2$ (mg chl *a*)$^{-1}$ h$^{-1}$** |
|---|---|
| $H_2$ production in dark | 2.31 $\pm$ 0.50 |
| $H_2$ production in light | 4.14 $\pm$ 0.15 |
| $H_2$ uptake in dark | 2.25 $\pm$ 0.84 |
| $H_2$ uptake in light | 20.14 $\pm$ 2.53 |

### 2.3.2 Construction and Characterization of Hydrogenase-Deletion Mutant Strain

A hydrogenase-deletion mutant strain of *Synechocystis* (Δ*hox*) was created by deleting the *hox* operon from the *Synechocystis* genome and replacing it with a chloramphenicol resistance cassette. Growth of the wild-type and the *Δhox* mutant strains, maintained photoautotrophically under 50-55 µmol photons m$^{-2}$ s$^{-1}$ light, was monitored (Figure 2.7). No significant difference was found in the growth characteristics of the two cultures.

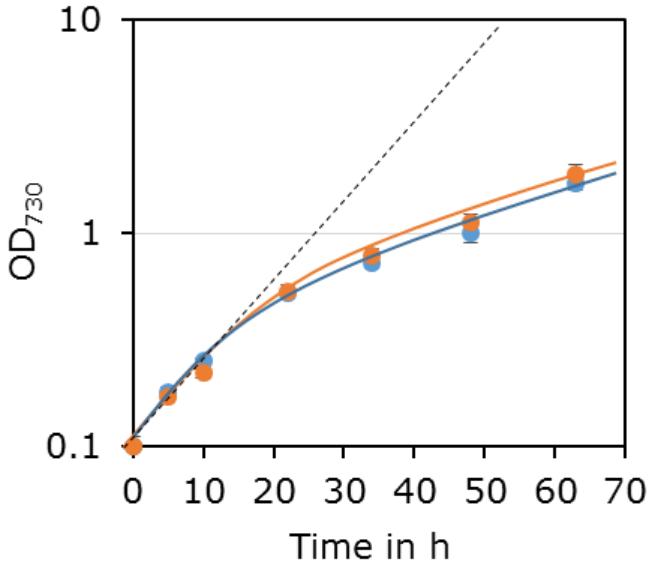


Figure 2.7
Growth curves of wild type (blue) and *Δhox* (orange) cultures. Experiments were carried out in triplicate. Cultures were grown photoautotrophically (bubbled with air), at a light intensity of 50-55 µmol photons $m^{-2}$ $s^{-1}$.

The *hox*-encoded bidirectional hydrogenase is the only known enzyme in *Synechocystis* that is capable of $H_2$ production or oxidation. To confirm this, cell suspension of the Δ*hox* strain was incubated in darkness with glucose, glucose oxidase and catalase. When no fermentative $H_2$ production was observed even after 10 minutes of incubation, the cell suspension was illuminated with light (at an intensity of 800-1000 µmol photons $m^{-2}$ $s^{-1}$) (Figure 2.8 (A)). No $H_2$ photoevolution was observed either. To measure $H_2$ uptake the same experiment was repeated, with added $H_2$ (18-20 µM) at the beginning. The culture was kept in darkness for 15 minutes before switching on the light. No uptake of $H_2$ was observed in either case (Figure 2.8 (B)).

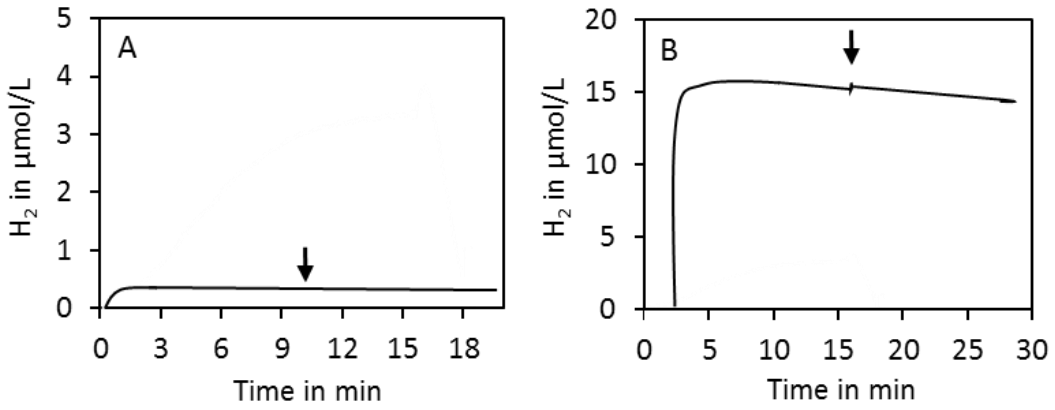


Figure 2.8
$H_2$ production (A) and uptake (B) in the Δ*hox* mutant strain. Cell suspensions of 11 µg chl *a* $ml^{-1}$ were incubated in darkness in presence of glucose, glucose oxidase and catalase without or with $H_2$. The initial steep rise of the curve in graph B represents the addition of $H_2$-saturated BG-11. Positions where the light was switched on are indicated by arrows.

### 2.3.3 Light Dependent Hydrogenase Activity in *Lyngbya aestuarii* BL J

Fermentative $H_2$ production in the *Lyngbya* BL J strain was reported recently by Kothari et al. (2014). While the rate of $H_2$ production observed in the strain in darkness was considerably high, $H_2$ photoevolution was not reported. Therefore, in the current study the light-induced hydrogenase activity of *Lyngbya* BL J was measured. Cell suspensions of *Lyngbya* BL J were incubated in darkness and under anaerobic conditions (anaerobiosis was induced by the addition of glucose, glucose oxidase and catalase) and fermentative $H_2$ production was recorded (Figure 2.9). The overall rate of fermentative $H_2$ production found in this study (5.5 $\pm$ 2.9 µmol (mg chl *a*)$^{-1}$ $h^{-1}$) was two-fold higher than the rate reported previously (2.8 $\pm$ 1.7 µmol (mg chl *a*)$^{-1}$ $h^{-1}$) by Kothari et al.

(2014), even though the differences are not necessarily significant because of the uncertainty in the measurements. To observe $H_2$ photoevolution during the transition from darkness to the light, cultures were illuminated with light (800-1000 µmol photons $m^{-2}$ $s^{-1}$) at various points during fermentative $H_2$ production.

Graphs A, B and C in Figure 2.9 show three representative recordings where the light was switched on after approximately 12 minutes, 40 minutes and 6 hours, respectively, of the beginning of fermentative $H_2$ production. In cases of the measurements shown in graphs A and B, the cultures were illuminated before the fermentative $H_2$ production plateaued at a particular $H_2$ concentration. After illumination $H_2$ production continued for 1 minute and 30 seconds, respectively, before the production stopped and reverted to $H_2$ consumption, which continued until the $H_2$ concentration in the medium became zero. In case of the measurement shown in graph C, the culture was left in darkness and in anaerobic conditions for ~6 h and was illuminated when no further fermentative $H_2$ production was observed. The culture did not show any $H_2$ photoevolution and $H_2$ consumption started in approximately 1 min.

The overall rate of light-induced $H_2$ consumption was 17.01 $\pm$ 4.74 µmol (mg chl *a*)$^{-1}$ $h^{-1}$ (average rate from four different sets of measurements), which was comparable to the rate observed in *Synechocystis*.

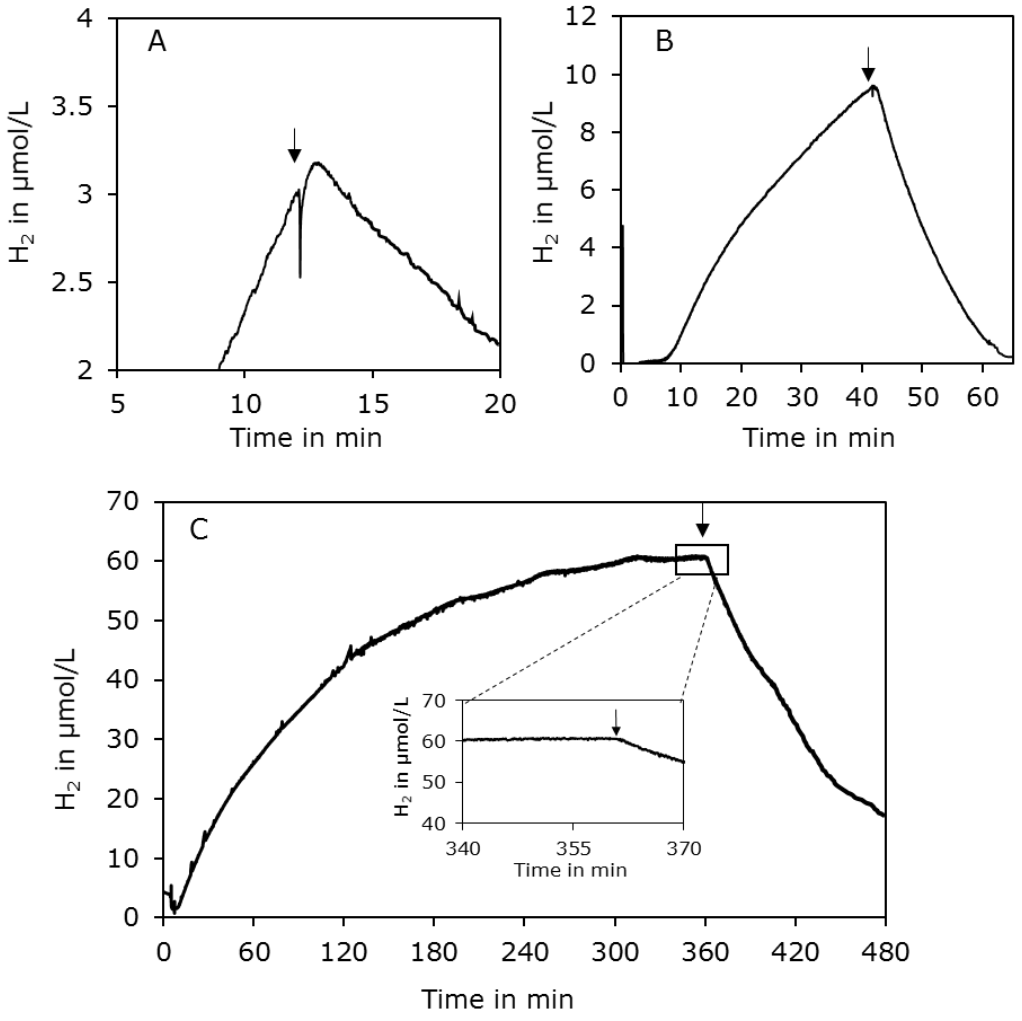


Figure 2.9

Light-induced $H_2$ production and uptake measurements in *Lyngbya* BL J. Cell suspensions were first incubated in darkness and under anaerobic conditions (time 0) and fermentative $H_2$ production was recorded. Cultures were illuminated with light at an intensity of 800-1000 µmol photons $m^{-2}$ $s^{-1}$ (indicated by arrows) after ~12 min (A), ~40 min (B) and ~6 h (C) of incubations. Cell suspensions of 0.5, 1.7 and 2 µg chl *a* $ml^{-1}$ were used for measurements shown in graphs A, B and C, respectively.

### 2.3.4 Heterologous Expression of the Hydrogenase from *Lyngbya* BL J in *Synechocystis*

Heterologous expression of the hydrogenase from *Lyngbya* BL J in *Synechocystis* was achieved by first cloning the *hox* operon of *Lyngbya* BL J into an *E. coli* plasmid vector under the expression of promoter $P_{nrsBACD}$, a Ni-inducible promoter in *Synechocystis* (López-Maury et al., 2002), and subsequently transforming the *Synechocystis* Δ*hox* strain with the resulting plasmid (p$hox_{BL\ J}$). Attempts to express those genes under the expression of the constitutive *psbA2* promoter were also made but remained unsuccessful.

Because of the large size of the insert, the correctness of the resulting plasmid construct was checked by sequencing. A missense mutation was found in the *hoxF* coding sequence (C>T (CTT>TTT) 628 bases from the 5' end of *hoxF*). The *hoxF* sequences from several cyanobacteria were compared and the nucleotide was found not to be strictly conserved; indeed, in at least one strain a TTT is present at that position (Table 2.5). A silent mutation (A>G (GTA>GTG)) was also found at position 1398. Both of these mutations were considered to be minor and insertion of the *hox* operon from *Lyngbya* BL J using this plasmid was continued.

The *Synechocystis* Δ*hox* mutant strain was transformed with the plasmid p$hox_{BL\ J}$, following the procedure as described by Vermaas et al. (1987). Until now, the transformed colonies are not fully segregated (Figure 2.10). Therefore, partially segregated strains (Δ$hox_{6803}$/$hox_{BL\ J}$) were used for all subsequent analysis.

Table 2.5.

Nucleotide sequence corresponding to the codon CTT ($Leu^{210}$) in *Lyngbya* BL J in other cyanobacterial strains

| Strain | Sequence |
|---|---|
| *Lyngbya majuscula* CCAP 1446 | CTT (Leu) |
| *Arthrospira platensis* FACHB 341 | TTA (Leu) |
| *Arthrospira* sp. PCC 8005 | TTA (Leu) |
| *Halothece* sp. PCC 7418 | TTT (Phe) |
| *Synechocystis* sp. PCC 6803 | CTT (Leu) |
| *Cyanothece* sp. PCC 7822 | CCA (Pro) |

### 2.3.5 RT-PCR Analysis

Ni-induced expression of the *hox* genes in the Δ$hox_{6803}$/$hox_{BL\ J}$ strain grown in the presence of 0.5 and 6.0 µM $NiSO_4$ was compared with the expression of these genes in the Δ*hox* mutant strains. Transcripts of all five *hox* genes were detected in the Δ$hox_{6803}$/$hox_{BL\ J}$ strain when grown in the presence of 6 µM $NiSO_4$, but transcript levels were very low when cultures were grown in the presence of 0.5 µM $NiSO_4$ (*hoxH* expression was undetectable) (Figure 2.11). As expected, no transcript of any of the five *hox* genes was detected in the Δ*hox* mutant strain.

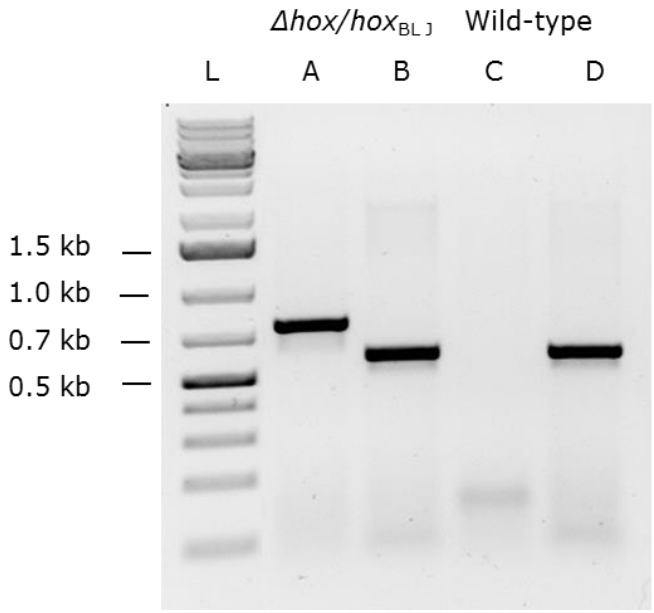


Figure 2.10
DNA gel electrophoresis with genomic DNA from *Synechocystis* wild-type and Δ*hox*$_{6803}$/*hox*$_{BL\ J}$ strain showing incomplete segregation of the *hox*$_{BL\ J}$ in the mutant. Lane L, DNA ladder; Lane A and C, Product of PCR with primer BL J-ins-F+ BL J-ins-R; Lane B and D, Product of PCR with primer BL J-seg-F+ BL J-seg-R.

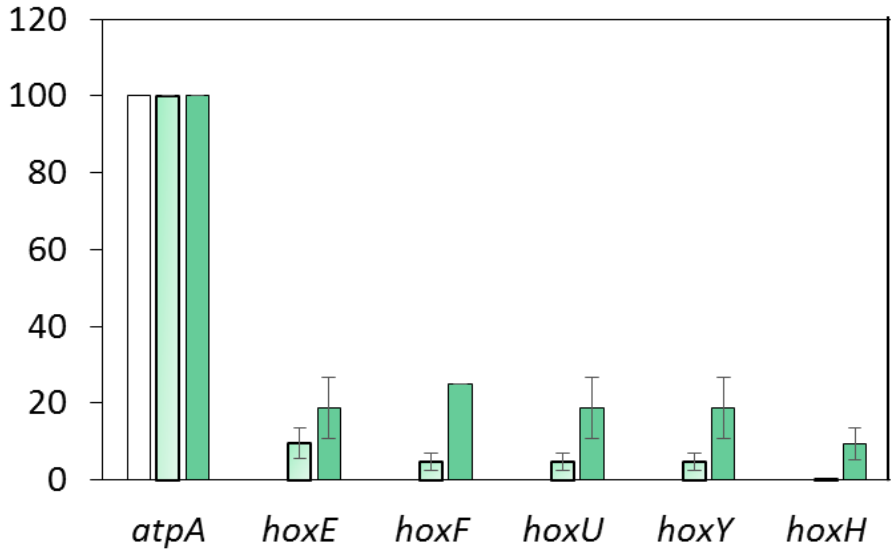


Figure 2.11
Histogram representation of the relative transcript abundances (measured by RT-PCR) of the *hox* genes in the Δ*hox*$_{6803}$/*hox*$_{BL\ J}$ strain grown in the presence of 0.5 µM $NiSO_4$ (light-green) and 6 µM $NiSO_4$ (dark green) and the Δ*hox*$_{6803}$ strain (white). Relative transcript abundances of the *hox* genes were compared to that of *atpA* (set to 100) by using the $2^{\Delta ct}$ method.

### 2.3.6 Hydrogenase Activity in *Synechocystis* Δ*hox*$_{6803}$/*hox*$_{BL\ J}$ Strain

No $H_2$ production or uptake could be detected using the *Synechocystis* Δ*hox*$_{6803}$/*hox*$_{BL\ J}$ strain when the cell suspension was incubated in darkness and under anaerobic conditions in the presence of glucose, glucose oxidase and catalase.

To check whether the hydrogenase enzyme in the mutant strain is catalytically active, a second measurement assay was used, where $H_2$ evolution was measured in the presence of methyl viologen, reduced by sodium dithionite. $H_2$ concentration was recorded over time using the wild-type, Δ*hox* and Δ*hox*$_{6803}$/*hox*$_{BL\ J}$ strains. No $H_2$ evolution was detected in the Δ*hox* mutant. The maximum rate of $H_2$ production found in the Δ*hox*$_{6803}$/*hox*$_{BL\ J}$ strain (19.6 $\pm$ 9.0 µmol (mg chl *a*)$^{-1}$ h$^{-1}$, average rate of three independent measurements) was 2-fold lower than the maximum rate found in the wild-type *Synechocystis* (36.0 $\pm$ 1.2 µmol (mg chl *a*)$^{-1}$ h$^{-1}$, average rate of three independent measurements), but was ~4-fold lower than the maximum rate observed in the wild type *Lyngbya* BL J strain (156 $\pm$ 77 µmol (mg chl *a*)$^{-1}$ h$^{-1}$ (Kothari et al., 2012). The maximum concentration of $H_2$ produced by the Δ*hox*$_{6803}$/*hox*$_{BL\ J}$ strain (31 $\pm$ 10 µM) was lower than the concentration observed both in the wild-type *Synechocystis* strain (79 $\pm$ 16.4 µM) and in wild-type *Lyngbya* BL J strain (487 $\pm$ 12 µM). A representative graph of the $H_2$ evolution from *Synechocystis* wild-type, Δ*hox* and Δ*hox*$_{6803}$/*hox*$_{BL\ J}$ strain is shown in Figure 2.12.

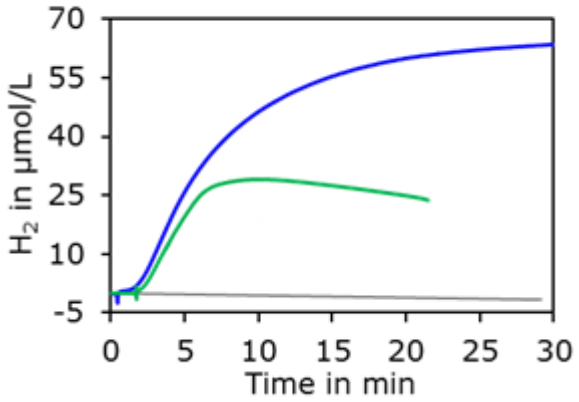


Figure 2.12

Representative recordings of $H_2$ production in *Synechocystis* wild-type (blue), Δ*hox*$_{6803}$/*hox*$_{BL\ J}$ (green) and Δ*hox* (gray) strains in the presence of reduced methyl viologen. Cell suspensions (11 µg chl *a* ml$^{-1}$) were incubated with methyl viologen and sodium dithionite in darkness.

## 2.4 Discussion

In the present chapter it is shown that in *Synechocystis* the hydrogenase activity under physiological conditions differs significantly between periods of light and darkness. The lack of any $H_2$ uptake and production in the Δ*hox* mutant strain confirmed that the activities observed in the wild-type strain were indeed mediated by the bidirectional hydrogenase enzyme. In darkness, the duration of net fermentative $H_2$ production in *Synechocystis* was short (~15 min). As a result, the net yield of $H_2$ from *Synechocystis* was significantly lower compared to *Lyngbya* BL J (13-fold when grown in continuous light and 45-fold when grown in a 12-h light/12-h darkness cycle), where the $H_2$ concentration in the cell suspension increased steadily for about 6 hours before the production rate began to decrease. It was found that doubling the concentration of *Synechocystis* used during the measurements resulted in a $3 \pm 1$ fold increase in net $H_2$

production, but even then the production phase lasted only for 10-15 minutes. One possible reason for why $H_2$ production plateaued after this time is an inhibition of $H^+$ reduction by the produced $H_2$ itself. $H_2$ inhibition of $H^+$ reduction was reported previously by McIntosh et al. (2011) in the purified enzyme from *Synechocystis*. However, it would not explain why increasing the *Synechocystis* cell concentration during the measurement would result in an increase in net $H_2$ production. Also, the possibility of a loss of enzyme activity after ~15 min was ruled out, since the enzyme continued to function for at least 30 minutes in the uptake direction. It was also considered that a system loss of $H_2$ due to a leakage or the reaction at the hydrogen electrode could result in zero net $H_2$ production. However, upon incubation of the Δ*hox* strain with 15 µM $H_2$ (Figure 2.8 (B)) or upon using BG-11 medium with $H_2$ but without any cells present, no significant decrease in the concentration of $H_2$ was observed over a period of 15 min. This indicates that neither a leakage nor the reaction at the electrode could result in the plateau. A fourth possible explanation is that $H_2$ production and uptake use different pathways or redox partners for electron transfer to/from the enzyme and at the plateau concentration the two reactions are continuing at the same rate. Finally, measurements in Figure 2.3 showed that the net reaction during $H_2$ uptake stopped at approximately the same final $H_2$ concentration (~4 µM) as $H_2$ production when cell suspensions of the same cell concentration were used. Therefore, a fifth possible scenario is that at this concentration a steady state involving the reactants and the products was achieved, where neither net $H_2$ formation, nor net NAD(P) (or Fd/Flv) reduction took place. When the concentration of *Synechocystis* cells was increased, the collective $H_2$ production by the cell suspension was increased too as $H_2$ is permeable.

The light-induced hydrogenase activity was analyzed in *Synechocystis* as well as in *Lyngbya* BL J. In *Synechocystis,* illuminating the culture with saturating light intensity resulted in a transient $H_2$ production that was absent in *Lyngbya* BL J. Both strains showed a rapid $H_2$ uptake within 30 seconds to 1 minute of illumination, indicating that hydrogenases in both strains favor $H_2$ uptake over production under physiological conditions in the light. Also, $H_2$ uptake in the light continued until all the remaining $H_2$ in the medium was consumed, as opposed to $H_2$ uptake in darkness, where the uptake stopped when a steady-state $H_2$ concentration was achieved before all of the $H_2$ in the medium was consumed. The maximum rate of light-induced $H_2$ uptake observed in *Synechocystis* was about 10-fold higher than the rate observed in darkness.

Previously, Cournac et al. (2004) reported a rapid drop in the $CO_2$ concentration in *Synechocystis* culture medium upon illumination (without any lag period between the onset of light and the rapid drop in $CO_2$ concentration) that was explained by the light-induced $CO_2$-concentrating mechanisms followed by $CO_2$ fixation by the Calvin cycle. In a proton-deuterium exchange reaction, in the presence of DCMU, net $H_2$ uptake was comparable to the net dissolved carbon that was fixed (Cournac et al., 2004). Therefore, it was suggested that $H_2$ was the main source of electrons for $CO_2$ fixation in such conditions. However, under regular conditions the observed rate of photosynthetic $CO_2$ assimilation in *Synechocystis* is 126 $\pm$ 10 µmol $CO_2$ (mg chl *a*)$^{-1}$ h$^{-1}$ (Tamoi et al., 1998), which should correspond to a NADPH consumption rate of 252 µmol (mg chl *a*)$^{-1}$ h$^{-1}$ by $CO_2$ assimilation. On the other hand, upon illumination with saturating light intensity, the photosynthetic electron transport chain can produce NADPH at a rate between 664 and 700 µmol (mg chl *a*)$^{-1}$ h$^{-1}$, corresponding to the reported maximum rate of photosynthetic

$O_2$ evolution between 332 and 350 µmol of $O_2$ (mg chl *a*) $^{-1}$ $h^{-1}$ (Keilty et al., 2001; Tichy and Vermaas, 1999). Thus, the production of NADPH by photosynthesis should suffice (in fact exceed) the requirement of NADPH for the Calvin cycle. This is also reflected in the observed intracellular NADPH:$NADP^+$ ratio of 3:1 in *Synechocystis* measured in the presence of light (Cooley and Vermaas, 2001). Therefore, an increased NADPH demand for light-induced $CO_2$ fixation cannot account for the rapid consumption of $H_2$ in light.

Therefore, currently available interpretations do not adequately explain the data. Instead, as will be argued in Chapter 3 an alternate interpretation is that during $H_2$ oxidation electrons are feeding a different substrate than where electrons originated from upon $H_2$ production. In this interpretation, electrons from $H_2$ are donated to the mobile electron carrier PQ in the thylakoid membrane that transfers electrons between PS II, cytochrome $b_6f$ and ultimately to PS I (via the lumen electron carrier, plastocyanin) in the presence of light (Figure 2.13). Examples of electron transfer from hydrogenase to the quinone pool of the respiratory electron transport chain are found in many uptake hydrogenases (Vignais et al., 2001; Vignais and Billoud, 2007). The redox potential of PQ is sufficiently high (midpoint potential +80 mV, at pH 7) for a continuous acceptance of electrons from $H_2$ (midpoint potential -0.414, at pH 7) as long as electrons can be released at the acceptor side of PS I. Evidence supporting this speculation will be provided in Chapter 3.

The hydrogenase enzyme from *Lyngbya* BL J was expressed in a *Synechocystis* Δ*hox* strain in an attempt to improve the fermentative $H_2$ production rate in *Synechocystis*. Results from the RT-PCR showed that the *hox* genes from *Lyngbya* BL J are being

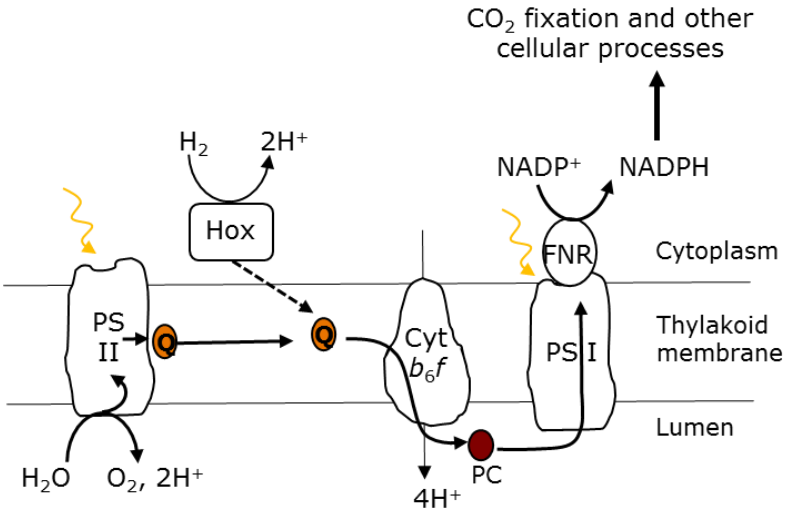


Figure 2.13
Proposed electron transfer from hydrogenase to the PQ pool in the thylakoid membrane (dotted arrow). The regular photosynthetic electron transfer pathway is shown too (solid arrow). Hox, hydrogenase; Q, plastoquinone; PC, plastocyanin; FNR, ferredoxin:NADPH reductase.

expressed in the *Synechocystis* Δ*hox*$_{6803}$/*hox*$_{BL\ J}$ strain. The mutant strain also showed $H_2$ evolution in the presence of reduced methyl viologen, indicating that the heterologously expressed enzyme is catalytically active.

However, the lack of hydrogenase activity under physiological conditions suggested that the enzyme may not be fully assembled in *Synechocystis*. This may have been caused by the absence of the maturase proteins from *Lyngbya* BL J. *Synechocystis* contains at least seven different maturase proteins for the assembly of the NiFe active site and the [Fe-S] clusters in its native hydrogenase, but the *Lyngbya*-hydrogenase may require additional maturation proteins that are not present in *Synechocystis*. Also, the *Lyngbya*-hydrogenase may use a different protein or cofactor as the electron donor that is absent in *Synechocystis*. Either way, further study is required to optimize the non-native enzyme in *Synechocystis* for $H_2$ production without the supply of external electron donors.

# CHAPTER 3

## THE ELECTRON TRANSFER PATHWAY FROM/TO THE NIFE-HYDROGENASE IN *SYNECHOCYSTIS* SP. PCC 6803


### Summary

When a *Synechocystis* culture is illuminated with a saturating intensity of light, a rapid $H_2$ uptake is observed that lasts as long as there is any $H_2$ present in the culture medium. This light-induced rapid $H_2$ uptake was not observed in a photosystem I deletion mutant strain Δ*psaAB* or in wild-type *Synechocystis* that has been treated with the cytochrome $b_6f$ inhibitor DBMIB. On the other hand, a photosystem II deletion mutant strain Δ*psbB* or a terminal oxidase deletion mutant strain Δ*ox* shows the same light-induced $H_2$ uptake profile as the wild-type strain. This indicates a direct electron channeling from $H_2$ to cytochrome $b_6f$ and PS I in the thylakoid membrane in the presence of light. Also, a cell-free extract prepared from wild-type *Synechocystis* showed spontaneous $H_2$ oxidation without the addition of any external oxidant, while $H_2$ production from the same extract required an external supply of NADH or NADPH.


### 3.1 Introduction

Hydrogenase catalyzes the reduction of protons to form $H_2$, as well as the oxidation of $H_2$ to form protons. During $H_2$ formation protons are delivered directly from the cytoplasm of the cell to the active site of the enzyme (Fontecilla-Camps et al., 2007). On the other hand, the delivery of electrons to the active site occurs from one or more redox partner(s) of the enzyme, via several [Fe-S] clusters located within its various subunits. The cyanobacterial bidirectional hydrogenases have long been recognized as NAD(P)-

reducing hydrogenases, based on their sequence homologies to other NAD(P)-binding proteins found in various organisms (Vignais et al., 2001). When the derived amino acid sequences of hydrogenase in *Synechocystis* were analyzed (Appel and Schulz, 1996), a Gly-rich $NAD(P)^+$ binding site was identified between amino acid residues 167 and 206 in the HoxF subunit. Indeed, NADH and NADPH were found to act as electron donors inducing $H_2$ production in cell-free extracts of *Synechocystis* (Cournac et al., 2004; Gutekunst et al., 2014; Aubert-Jousset et al., 2011) and *S. elongatus* (Schmitz et al., 1995) and in purified proteins from *Synechocystis* (Schmitz et al., 2002) and *Gloeocapsa alpicola* CALU 743 (Serebryakova and Sheremetieva, 2006).

Recently, electron transfer from reduced Fd and Flv to hydrogenase was suggested in *Synechocystis* based on the facts that a) $H_2$ production could be observed when reduced Fd or Flv was added to cell-free extracts, b) a merodiploid (partially segregated) ferredoxin-NADP reductase (FNR) mutant with reduced expression of FNR produced more photohydrogen (photo $H_2$) than the wild type, and c) a reduced rate of fermentative $H_2$ production was observed in a pyruvate:flavodoxin/ferredoxin oxidoreductase mutant (Gutekunst et al., 2014). Ferredoxin-dependent hydrogenase activity is observed with the $H_2$-producing cytoplasmic FeFe-hydrogenases in algae and certain clostridial species, and with the membrane-bound, energy converting NiFe-hydrogenases in some archaea and extremophiles (Peters et al., 2015; Meyer, 2007; Hedderich, 2004). In the latter type of hydrogenase, ferredoxin acts as both electron donor and acceptor of the enzyme. Thermodynamically it is more favorable to transfer electrons from reduced Fd/Flv (midpoint potential -440 mV at pH 7) to protons (midpoint potential -414 mV at pH 7) than to transfer them from NAD(P)H (midpoint potential -320 mV at pH 7) to protons.

On the other hand, during $H_2$ oxidation, electron transfer from $H_2$ to $NAD(P)^+$ is more favorable than from $H_2$ to Fd/Flv. In *Synechocystis* or any other cyanobacteria, no evidence of electron transfer to Fd during $H_2$ oxidation is available so far.

In *Synechocystis*, hydrogenase catalyzes net $H_2$ oxidation in the presence of light (Chapter 2, Section 2.3.1). After a period of darkness, when a cell suspension of *Synechocystis* is illuminated with a saturating intensity of light, a rapid $H_2$ uptake completely masks the photo $H_2$ production. The same phenomenon is observed in *Lyngbya* BL J (Chapter 2, Section 2.3.2) as well as in *Oscillatoria chalybea* (Abdel-Basset and Bader, 1998). The identity of the electron sink during this light-induced $H_2$ oxidation has not been confirmed yet. $CO_2$ assimilation, which stays inactive during periods of darkness or even during the early phases (few seconds) of illumination after a period of prolonged darkness but eventually becomes active upon illumination, has been tentatively suggested to use $H_2$ as the source of electrons (Cournac et al., 2004; Greenbaum et al., 1995). However, the uptake of $H_2$ was independent of $CO_2$ assimilation: the light-induced $H_2$ uptake profile was found to be unchanged upon flushing the thylakoids with pure $N_2$ (i.e. no $CO_2$ present, therefore no $CO_2$ assimilation possible) vs. 99% $N_2$-1% $CO_2$ ($CO_2$ assimilation possible) during the measurements (Abdel-Basset and Bader, 1998).

Aside from $CO_2$ assimilation, the major process that is activated upon illumination is the photosynthetic electron transport chain (p-ETC). Several members of the p-ETC are located in the thylakoid membrane, which also hosts several components of the respiratory electron transport chain (r-ETC) in *Synechocystis* (Vermaas, 2001). Members

of the p-ETC, located in the membrane include PS II, the cytochrome $b_6f$ complex and PS I (Mullineaux, 2014). Upon illumination, PS II absorbs photons and generates electrons from water. The mobile electron carrier plastoquinone (PQ) in the membrane carries these electrons to the cytochrome $b_6f$ complex and subsequently to either of the two soluble electron carriers, plastocyanin or cytochrome $c_6$, both located on the luminal side of the thylakoid membrane (Tikhonov, 2014). These soluble electron carriers then transfer their electrons to PS I, which upon illumination reduces ferredoxin and eventually reduces $NADP^+$ to NADPH. NADPH is used as a substrate in various cellular processes, including $CO_2$ assimilation (thermodynamically favorable reaction) and the reductive assimilation of nitrate via FNR and ferredoxin (thermodynamically unfavorable reaction) (Yang et al., 2002). The mobile electron carrier PQ also participates in the r-ETC, whose other components include succinate dehydrogenase (SDH), NDH-1, cytochrome $b_6f$, plastocyanin/cytochrome $c_6$ and terminal oxidases (Lea-Smith et al., 2013).

In this chapter, the effects of various members of the photosynthetic and the respiratory electron transport chains in the thylakoid membrane on $H_2$ uptake and production activities in *Synechocystis* were examined. Our results show that the light-induced rapid $H_2$ uptake is caused by specific components of the p-ETC acting as electron sinks. On the other hand, during $H_2$ production in the presence of light, electrons do not follow the same pathway in reverse direction and rather depend on the traditional redox partners of the hydrogenase, NADPH or NADH.

## 3.2 Materials and Methods

### 3.2.1 Chemicals

NAD, NADP, NADH, NADPH, DBMIB (2,5-dibromo-3-methyl-6-isopropylbenzoquinone) and ferredoxin from spinach were purchased from Sigma-Aldrich.

### 3.2.2 Culture Growth Conditions

Cultures of the *Synechocystis* wild-type and Δ*hox* mutant strains were grown in standard BG-11 medium (supplemented with 5 mM glucose when indicated), as described in Section 2.2.1. Cultures were either bubbled with air or shaken on a New Brunswick Scientific Innova 2300 Platform Shaker (New Brunswick Scientific Co., NJ), when glucose was added to the cultures. A *psaAB*-deletion mutant strain (Δ*psaAB* strain, Shen and Vermaas, 1994), a *psbB*-deletion mutant strain (Δ*psbB* strain, Eaton-Rye and Vermaas, 1991) and a terminal oxidases-deletion mutant strain (*ctaDIEI*$^-$*/ctaDIIEII*$^-$*/cydAB*$^-$, or Δ*ox* strain, Howitt and Vermaas, 1998) were obtained from our laboratory and grown in BG-11 supplemented with 5 mM glucose. The Δ*psaAB* strain was grown under dim light (light intensity between 3 and 5 µmol photons $m^{-2}$ $s^{-1}$). For all other cultures, light intensities between 40 and 55 µmol photons $m^{-2}$ $s^{-1}$ were used.

### 3.2.3 $O_2$ Evolution Measurements

A traditional Clark-type electrode (Hansatech, Cambridge, UK) was used to determine the $O_2$ concentrations in *Synechocystis* cell suspensions, maintained at 30 °C. Cultures were grown to a final $OD_{730}$ between 0.8 and 1.0, harvested and resuspended in fresh BG-11 medium (final concentration 11 µg chl *a* $ml^{-1}$) supplemented with 10 mM sodium bicarbonate ($NaHCO_3$). When indicated, DBMIB (between 0 and 5 µM) was added to the cell suspension 10 minutes before the experiment. To observe photosynthetic $O_2$ evolution, cell suspensions were illuminated with white light at an intensity between 800 and 1000 µmol photons $m^{-2}$ $s^{-1}$.

### 3.2.4 Measurements of Hydrogenase Activity

The wild-type and mutant *Synechocystis* cultures were harvested in their mid- to late-exponential growth phase by centrifugation and were resuspended in fresh BG-11 medium supplemented with 5 mM glucose. When indicated, DBMIB (between 0 and 5 µM) was added to the cell suspension about 10 minutes before the experiments. $H_2$ concentrations were measured using a modified Clark-type electrode, following the same procedure, as described in Section 2.2.2.

### 3.2.5 Preparation of Cell-Free Extract

The wild-type and Δ*hox* mutant strains were harvested in their mid-exponential growth phase by centrifugation and resuspended in 50 mM morpholinoethanesulfonic acid (MES)-KOH buffer (pH 6) supplemented with 2% bovine serum albumin (Cournac et al., 2004). Cells were broken with glass beads (diameter 0.1 mm) in a mini Bead Beater

(BioSpec Products, Bartlesville, OK) by shaking 10 times for 30 seconds each, with two minutes of intermittent cooling on ice. The bead-beating tubes were filled with the cell suspension/beads to prevent foaming during bead-beating. Cell debris was removed by centrifugation at 1300 x g for 10 min, at 4°C.

## 3.3 Results

### 3.3.1 $O_2$ Evolution and $H_2$ Uptake in the Presence of DBMIB

The cytochrome $b_6f$ complex is a key component of the ETC in the thylakoid membrane of *Synechocystis*, participating in both photosynthetic and respiratory electron transport activities. DBMIB, a quinone analog, can bind to the cytochrome $b_6f$ complex in plants and in cyanobacteria and prevent electron transport through this complex (Yamashita et al., 2007). To find the optimum concentration of DBMIB that is sufficient to block the electron transport via cytochrome $b_6f$, $O_2$ evolution rates were measured in *Synechocystis* cell suspensions (11 µg chl *a* $ml^{-1}$) treated with 0, 1, 2.5 or 5 µM DBMIB, and illuminated with light at an intensity between 800 and 1000 µmol photons $m^{-2}$ $s^{-1}$. The rate of $O_2$ evolution decreased with increasing DBMIB concentrations (Figure 3.1 (A)), and $O_2$ evolution was essentially absent when the DBMIB concentration was 5 µM. Therefore, it was concluded that 5 µM was a saturating concentration of DBMIB, sufficient to block electron transfer through the cytochrome $b_6f$ complex.

Next, to test the role of the cytochrome $b_6f$ complex in $H_2$ uptake activity, $H_2$ uptake was measured in *Synechocystis* cultures treated with partially and completely saturating concentrations of DBMIB. Cell suspensions (11 µg chl *a* $ml^{-1}$) were treated with 0, 1, 2.5

or 5 µM DBMIB, and incubated with $H_2$, glucose, glucose oxidase and catalase.

The cultures were first kept in darkness for approximately 10 minutes, during which time $H_2$ uptake continued at a rate of 2.5 ± 1.0 µmol (mg chl *a*)$^{-1}$ h$^{-1}$ (average of total 10 measurements, in two independent sets). The average uptake rate in darkness did not depend on cytochrome $b_6f$-mediated electron transfer.

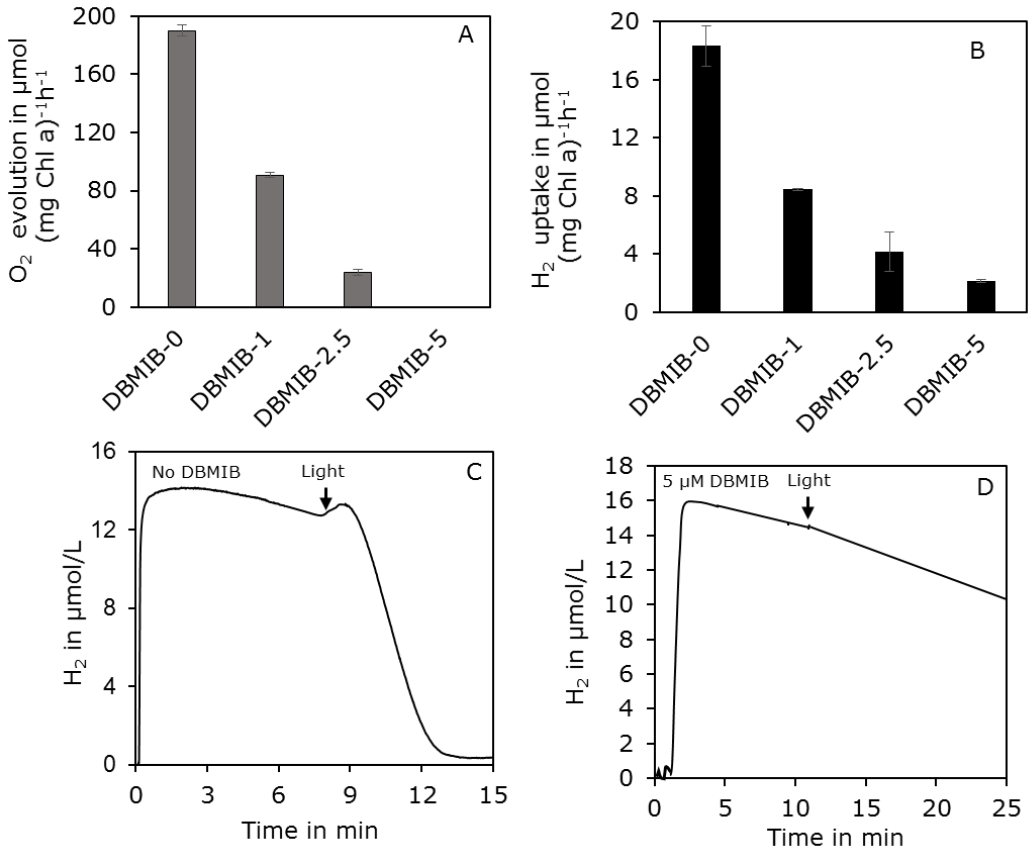


Figure 3.1
$O_2$ evolution (A) and $H_2$ uptake (B) rates in *Synechocystis* cell suspensions (11 µg chl *a* ml$^{-1}$) in the presence of DBMIB. The numbers after the hyphens represent DBMIB concentrations in µM. DBMIB was added 10 minutes prior to a measurement. The average rates of $O_2$ evolution and $H_2$ uptake were calculated from three and two independent sets of measurements, respectively. Representative trace curves of $H_2$ uptake in cell suspensions treated with 0 µM DBMIB (C) and 5 µM DBMIB (D) are also shown. The arrows indicate the positions where the light (800-1000 µmol photons m$^{-2}$ s$^{-1}$) was switched on.

Upon illumination, a higher rate of $H_2$ consumption (18 $\pm$ 1.39 µmol (mg chl *a*)$^{-1}$ h$^{-1}$) was observed in cultures incubated without DBMIB, indicating a light-induced $H_2$ uptake (Figure 3.1 (c)). The uptake rate in light decreased with increasing DBMIB concentrations. At 5 µM DBMIB, the difference in the rates of $H_2$ uptake before and after the cultures were illuminated (1.44 $\pm$ 0.08 µmol (mg chl *a*)$^{-1}$ h$^{-1}$ and 2.08 $\pm$ 0.11 µmol (mg chl *a*)$^{-1}$ h$^{-1}$, respectively) was small (Figure 3.1 (D)), indicating that the light-induced $H_2$ uptake depended heavily on the electron transfer through the cytochrome $b_6f$ complex. The rates of $H_2$ uptake in light with increasing DBMIB concentrations are shown in Figure 3.1 (B).

### 3.3.2 $H_2$ Uptake in the Δ*psbB* and the Δ*psaAB* Mutant Strains

Since light-induced $H_2$ uptake was inhibited with the inhibition of electron transfer through the cytochrome $b_6f$ complex, the uptake activity was further investigated in the *Synechocystis* Δ*psbB* and Δ*psaAB* mutant strains. While consumption of $H_2$ in darkness was found in both mutant strains, the increased rate of $H_2$ consumption upon illumination that was observed earlier in wild-type *Synechocystis* was found to be present in the Δ*psbB* mutant strain (Figure 3.2 (A)) but not in the Δ*psaAB* mutant strain (Figure 3.2 (B)). The average rates of $H_2$ uptake in the Δ*psbB* mutant strain in darkness (2.2 $\pm$ 0.9 µmol (mg chl *a*)$^{-1}$ h$^{-1}$) and in the light (19.4 $\pm$ 4.5 µmol (mg chl *a*)$^{-1}$ h$^{-1}$) were comparable to the corresponding average rates observed earlier in the wild-type strain (Chapter 2, Table 2.4). This indicates that $H_2$ uptake, either in the light or in darkness, was independent of the activity of PS II. However, the average rate of $H_2$ uptake in darkness in the Δ*psaAB* mutant strain was 6.7 $\pm$ 2.1 µmol (mg chl *a*)$^{-1}$ h$^{-1}$ and remained the same

when the light was switched on. The higher rate of $H_2$ uptake in darkness on a per-chlorophyll basis observed in the Δ*psaAB* mutant compared to the wild-type or the Δ*psbB* strain can be attributed to the fact that the Δ*psaAB* mutant lost over 80% of its chlorophyll on a per-cell basis as compared to the wild-type strain while the chlorophyll content in the Δ*psbB* strain was comparable to that of the wild-type (Shen et al., 1993; Shen and Vermaas, 1994; Vavilin et al., 2007). Based on the absence of any light-dependent increase in the $H_2$ uptake rate in the Δ*psaAB* mutant strain, it was concluded that like the cytochrome $b_6f$ complex, the activity of PS I was also required for the light-induced $H_2$ uptake.

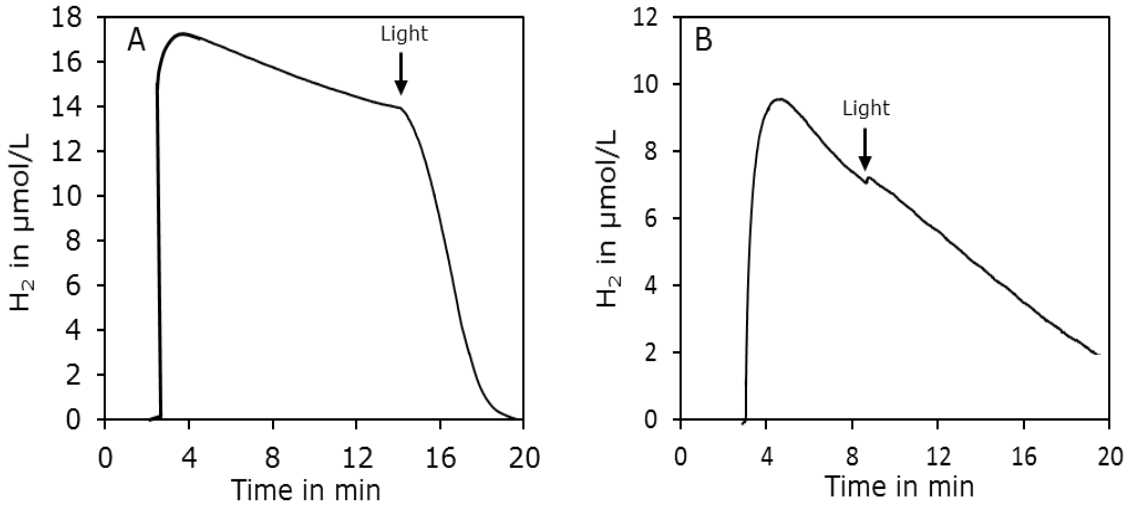


Figure 3.2

$H_2$ uptake profiles in the Δ*psbB* (A) and the Δ*psaAB* (B) mutant strains. Cell suspensions of 11 µg chl *a* $ml^{-1}$ and 4 µg chl *a* $ml^{-1}$ were used for the Δ*psbB* and the Δ*psaAB* mutant strains, respectively. Cultures were first incubated in darkness with $H_2$, glucose, glucose oxidase and catalase. The arrows indicate the positions where light (800-1000 µmol photons $m^{-2}$ $s^{-1}$) was switched on.

### 3.3.3 Effects of the Terminal Oxidases on Light-Independent $H_2$ Uptake

A small amount of light-independent $H_2$ uptake was always present in *Synechocystis* cultures. Since the r-ETC in the thylakoid membrane shares some of its components with the p-ETC, it is plausible that in the absence of light $H_2$ oxidation uses the terminal oxidases as electron sinks via the r-ETC. To test this hypothesis, $H_2$ uptake activity was measured in the *Synechocystis* Δ*ox* mutant strain lacking the three terminal oxidases and therefore lacking any respiratory electron transport activity in darkness.

Because $O_2$ acts as the terminal electron acceptor of respiratory electron flow in *Synechocystis*, the true effect of respiratory electron transport on $H_2$ oxidation can only be seen if there is a small amount of $O_2$ present in the medium. The concentration of $O_2$ should be small enough to maintain the respiratory activity, but not high enough to inactivate the hydrogenase enzyme. Therefore, $H_2$ uptake from the Δ*ox* mutant was measured both in the presence and in the absence of glucose, glucose oxidase and catalase; glucose and glucose oxidase act as an $O_2$-scavenger, thus removing $O_2$ completely from the culture medium. In the latter case, the cell suspension (11 µg chl *a* $ml^{-1}$) was first bubbled with $N_2$ in darkness for 15 minutes for a complete removal of $O_2$ from the medium, followed by the addition of 2 ml of BG-11, saturated with 5% $H_2$/95% $N_2$. Finally, 50 µl of air-bubbled BG-11 was added to the cell suspension before sealing the measurement chamber (total capacity 4.5 ml) to keep the net theoretical $O_2$ concentration at approximately 2.5 µM. No significant difference in the $H_2$ uptake rates was found between the wild-type and the Δ*ox* mutant strain (with or without the addition of glucose, glucose oxidase and catalase). The average $H_2$ uptake rate in darkness

observed in the Δ*ox* strain (2.3 ± 0.2 µmol $H_2$ (mg chl *a*)$^{-1}$ h$^{-1}$, average of total five measurements, three with and two without the addition of glucose, glucose oxidase and catalase) was comparable to the average uptake rate observed before in the wild-type strain. Therefore, it was concluded that the terminal oxidases did not act as the sole electron acceptors during the light-independent $H_2$ uptake. A representative graph of $H_2$ uptake in darkness in the Δ*ox* strain (without glucose, glucose oxidase and catalase) is shown in Figure 3.3.

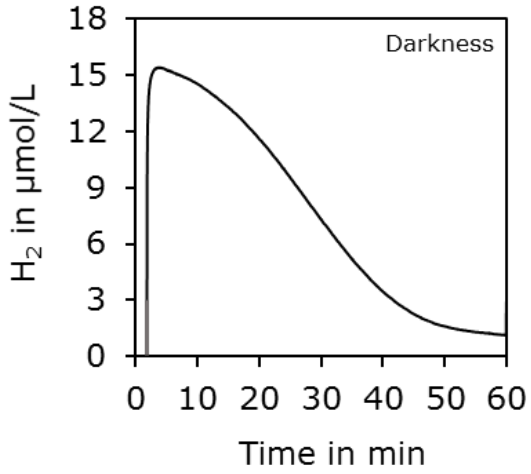


Figure 3.3
$H_2$ uptake activity in the Δ*ox* mutant strain recorded in darkness. Prior to the measurement, the cell suspension (11 µg of chl *a* ml$^{-1}$) was gassed with $N_2$ for 20 min, and then sealed in the measurement chamber with glucose, glucose oxidase and catalase, 2 ml of BG-11 saturated with 5% $H_2$/95% $N_2$ and 50 µl of air-saturated BG-11. The chamber was then sealed quickly to prevent diffusion of $O_2$ from air and $H_2$ uptake was recorded in darkness.

### 3.3.4 Hydrogenase Activity in Cell-Free Extracts

Apart from the *in vivo* measurements, *in vitro* hydrogenase activities were measured in cell-free extracts from the wild-type and Δ*hox* strains of *Synechocystis*. Cell-free extracts were prepared as described by Cournac et al. (2004), except that instead of using a French Press, cells were broken by bead beating.

a) $H_2$ Uptake Activity:

$H_2$ uptake was observed in cell-free extracts from wild-type cultures when incubated in darkness with $H_2$, even before the addition of the oxidized NAD (1.5 mM), NADP (1.5 mM) or Fd (1.5 µM), with an initial uptake rate of $0.41 \pm 0.12$ µmol (mg chl *a*)$^{-1}$ h$^{-1}$ (average of two independent measurements, with two repetitions each). Figure 3.4 (A) shows a trace curve of a $H_2$ uptake measurement using extract from the wild-type

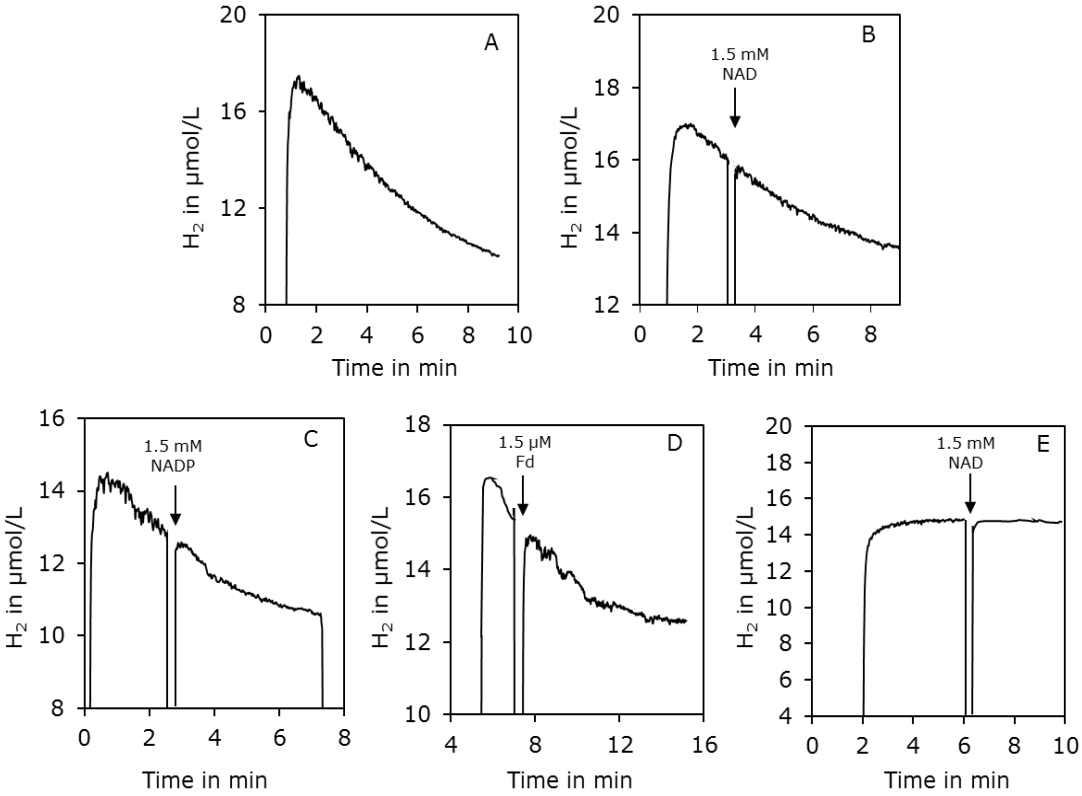


Figure 3.4
$H_2$ uptake in cell-free extracts (90 µg chl *a* ml$^{-1}$) from the *Synechocystis* wild-type (A-D) and Δ*hox* mutant strain (E). Addition of NAD (1.5 mM), NADP (1.5 mM) and Fd (1.5 µM) to the extracts are indicated. All extracts were gassed with $N_2$ for 15 min prior to measurements and then sealed in the measurement chamber with glucose, glucose oxidase and catalase, and BG-11 bubbled with 5% $H_2$/95% $N_2$. The discontinuities in the trace curves were caused by the removal of the electrode from the measurement chamber in order to add oxidants into the medium.

strain (90 µg chl *a* $ml^{-1}$), where uptake activity was measured for approximately 10 min. Interestingly, no significant change in the uptake rates was observed with the addition of any of the three oxidizing compounds (Figure 3.4 (B-D)). No $H_2$ uptake was observed using extracts from the Δ*hox* mutant strain, with or without the addition of the oxidizing agents (Figure 3.4 (E)).

b) $H_2$ Production Activity:

To induce $H_2$ production, cell-free extracts were incubated in darkness with glucose, glucose oxidase and catalase. No $H_2$ production was observed unless NADH, NADPH or reduced Fd was added to the extract. Addition of 1.5 mM NADH or NADPH induced $H_2$ evolution (Figure 3.5), although NADH-induced $H_2$ evolution appeared to be more reproducible. The average $H_2$ evolution rate was $0.08 \pm 0.02$ µmol (mg chl *a*)$^{-1}$ $h^{-1}$ (average was calculated from three separate measurements) when NADH was added as the reducing agent. On the other hand, when NADPH was used as the reducing agent, $H_2$ evolution could be detected in only two out of four measurements, with an average rate of $0.23 \pm 0.10$ µmol (mg chl *a*)$^{-1}$ $h^{-1}$ (average was calculated from the two successful runs). No $H_2$ evolution was observed in cell-free extracts from the Δ*hox* mutant strain upon the addition of NADH or NADPH.

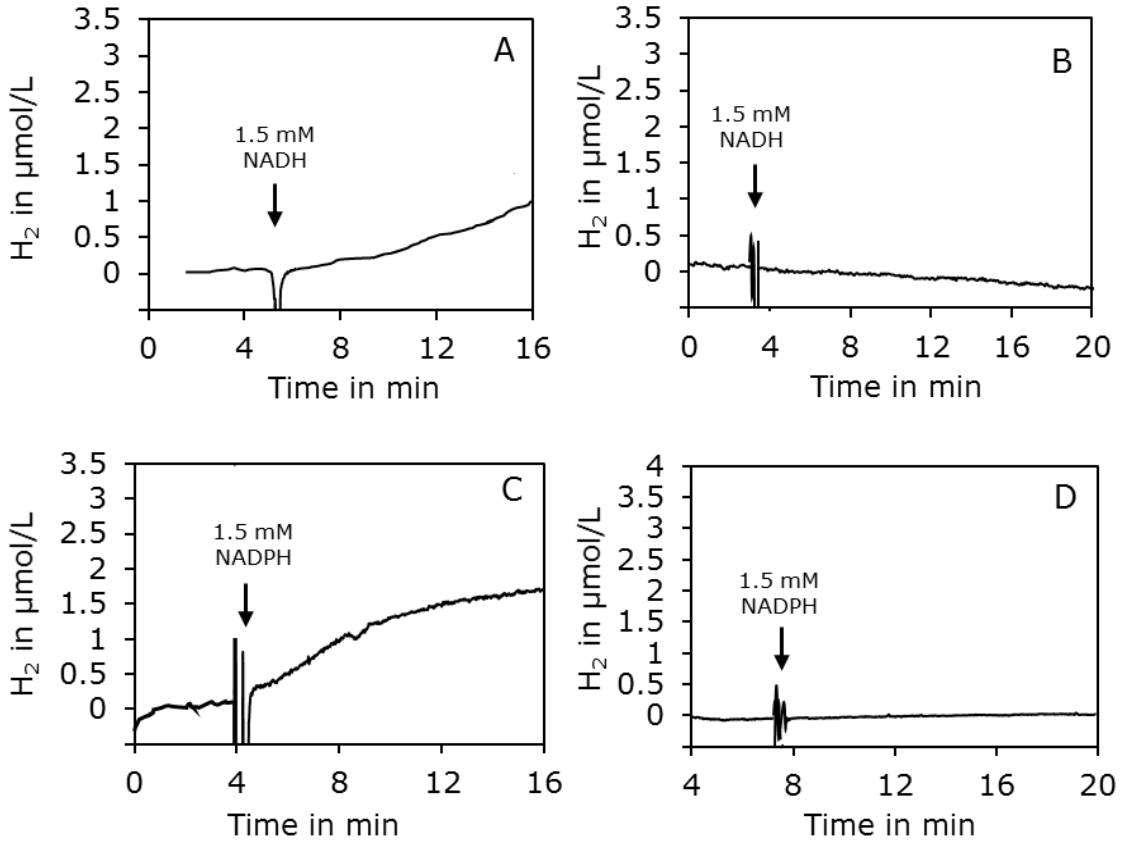


Figure 3.5
Trace curves of $H_2$ production in cell-free extracts from *Synechocystis* wild type upon the addition of NADH (A) and NADPH (C), 1.5 mM each, and extracts from Δ*hox* mutant strain upon the addition of the same concentrations of NADH (B) and NADPH (D). The addition of NADH and NADPH are indicated by the arrows. The discontinuities in the trace curves were caused by the removal of the electrode from the measurement chamber, in order to add NAD/NADPH into the medium. 75 µg chl *a* $ml^{-1}$ was used for each of the measurements.

An assay for $H_2$ production using reduced Fd as the electron donor was performed as described by Gutekunst et al. (2014). Fd from spinach was reduced by 2 mM sodium dithionite prior to the experiment. Extracts were first incubated with sodium dithionite (2 mM) alone that showed $H_2$ production at a slow but steady rate of 0.25 $\pm$ 0.20 µmol (mg chl *a*)$^{-1}$ h$^{-1}$ (average calculated from four independent measurements). Dithionite-reduced Fd was then added to the reaction mix. No significant increase in the $H_2$ production rate was observed when 1.5 µM Fd was used (Figure 3.6 (A)). However, increasing the Fd concentration to 3 µM showed a clear difference in the production rate before and after the addition of Fd (Figure 3.6 (B)). Two independent sets of measurements were taken,

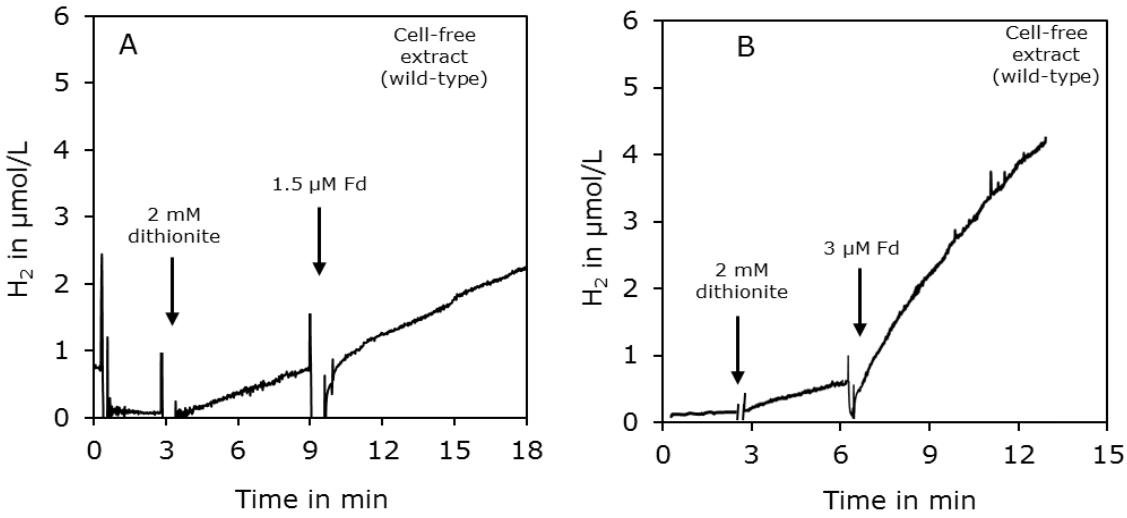


Figure 3.6
Trace curves of $H_2$ evolution in cell-free extracts from the *Synechocystis* wild-type strain upon the addition of Fd, reduced by 2 mM sodium dithionite. The homogenate was used at a final concentration of 100 µg chl *a* ml$^{-1}$. $H_2$ production was first measured with 2 mM dithionite alone, before adding reduced Fd at concentrations of 1.5 µM (A) and 3 µM (B). The discontinuities in the trace curves were caused by the removal of the electrode from the measurement chamber, in order to add dithionite or reduced Fd into the medium.

with two repetitions each time. The average rate of $H_2$ production after the addition of 3 µM Fd was 0.6 ± 0.2 µmol (mg chl *a*)$^{-1}$ h$^{-1}$.

Next, the same experimental procedure was repeated with extract (70 µg chl *a* ml$^{-1}$) prepared from the Δ*hox* mutant strain. Surprisingly, upon the addition of dithionite or dithionite-reduced Fd, $H_2$ production was observed at a comparable rate relative to the wild type (Figure 3.7 (A)). This phenomenon was observed in four out of six measurements (three independent measurements were taken, with two repetitions each time). The average rates of $H_2$ production before and after the addition of reduced Fd (3 µM) in the Δ*hox*-extract were 0.35 ± 0.20 µmol (mg chl *a*)$^{-1}$ h$^{-1}$ and 0.49 ± 0.13 µmol (mg chl *a*)$^{-1}$ h$^{-1}$, respectively. It should be noted that such production of $H_2$ with dithionite or dithionite-reduced Fd in the Δ*hox* mutant was observed only when cell-free extracts were used. When intact cells of the same strain were assayed for $H_2$ production with 2

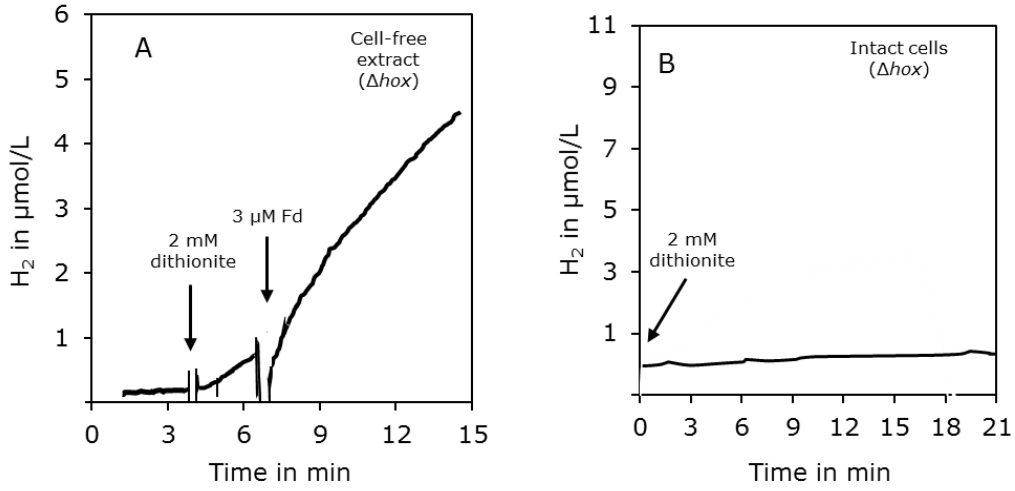


Figure 3.7
Hydrogenase activity in cell-free extracts and intact cells of the Δ*hox* mutant strain. (A) $H_2$ production in cell free extracts (70 µg chl *a* ml$^{-1}$) upon the addition of Fd, reduced by 2 mM sodium dithionite. (B) Hydrogenase activity in intact cells (11 µg chl *a* ml$^{-1}$) of the Δ*hox* mutant strain when incubated with 2 mM sodium dithionite.

mM sodium dithionite, no $H_2$ production was observed (Figure 3.7 (B)). Based on these results, the previous claim of dithionite-reduced ferredoxin acting as an electron donor to the hydrogenase enzyme *in vitro* could not be confirmed.

## 3.4 Discussion

$H_2$ metabolism in *Synechocystis* is dominated by $H_2$ oxidation in the presence of light. In the past, the physiological function of the cyanobacterial bidirectional enzyme was suggested to be the removal of excess reducing power (NAD(P)H or reduced ferredoxin) in the form of $H_2$ (Appel et al., 2000; Carrieri et al., 2011). However, in reality when a dark-adapted culture is illuminated with a saturating intensity of light, $H_2$ production is observed only for 30-45 seconds before the enzyme reverses its direction to $H_2$ uptake, and consumes all the $H_2$ present in the medium. No suitable explanation of this light-induced, rapid $H_2$ uptake was available so far. As indicated in Figure 3.8, in this study a novel electron transfer pathway in *Synechocystis* during $H_2$ oxidation is proposed, based on the occurrence of this rapid $H_2$ uptake in the presence or absence of the activities of various components of the electron transport chain located in its thylakoid membrane. It was shown that the light-induced $H_2$ uptake is dependent on the electron transport activities through the cytochrome $b_6f$ complex and PS I, but is independent of the activity of PS II. In a previous study by Cournac et al. (2004) the absence of the light-induced $H_2$ uptake was observed in the NDH-1 mutant M55 as well. The redox status of the quinone pool under saturating light intensity in these mutant strains vary from being mostly

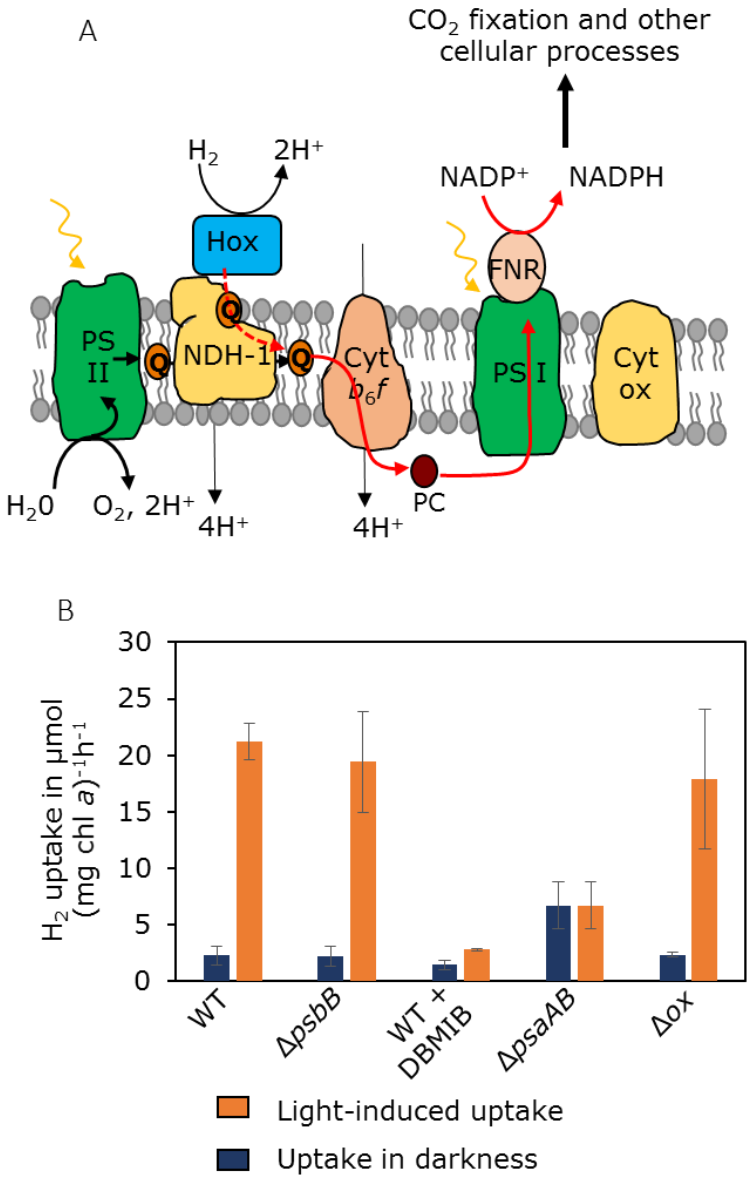


Figure 3.8
Electron transfer pathway through different components of the electron transport chain in the thylakoid membrane of *Synechocystis* and $H_2$ uptake in the presence and absence of light in the absence of one of the electron transport components. (A) Photosynthetic electron transport from PS II to cytochrome $b_6f$ and PS I via plastoquinone (Q) and plastocyanin (PC). The proposed electron transfer pathway from hydrogenase to cytochrome $b_6f$ and PS I is shown with red arrows. A tentative electron transfer from hydrogenase to the plastoquinone pool via NDH-1 is indicated by a dotted arrow. (B) Comparison of the average $H_2$ uptake rates in the presence and absence of light in the wild type and the mutants used in this study.

oxidized in the wild-type, PS II-deficient (Δ*psbB*) and NDH-1-deficient (M55) strains to 50% oxidized in the PS I-deficient (Δ*psaAB*) strain (Cooley and Vermaas, 2001). Therefore, the redox status of the quinone pool is in the thylakoid membrane is not the driving force behind the light-induced $H_2$ uptake. The fact that the uptake is observed in the absence of photosystem II indicates that it is not dependent on the net result of photosynthesis either, but rather on the channeling of electrons from $H_2$ through the cytochrome $b_6f$ complex and PS I.

Since the hydrogenase enzyme in *Synechocystis* does not contain a transmembrane protein subunit, the transfer of electrons from $H_2$ to the cytochrome $b_6f$ complex is likely to be mediated by another protein complex. Electron transfer from $H_2$ to the electron transport chain in the membrane is observed in the membrane-bound respiratory uptake hydrogenases in proteobacteria, some hyperthermophilic bacteria such as *Aquifex aeolicus* and in hydrogenase 2 in *E. coli* (Vignais et al., 2001; Peters et al., 2015; Fontecilla-Camps et al., 2007), where $H_2$ oxidation is coupled with the reduction of the quinone pool. The reduction of the quinone pool through these enzymes is often mediated via a transmembrane *b*-type cytochrome, which acts not only as a redox carrier from $H_2$ to the quinone pool, but also as an anchor, connecting the hydrogenase enzyme to the membrane. The gene encoding this *b*-type cytochrome is usually located in the structural hydrogenase operon. The genome of *Synechocystis* does not contain any homolog of this *b*-type cytochrome, but the genes encoding HoxE, HoxF and HoxU subunits of hydrogenase have significant sequence similarities with the genes encoding NuoE, NuoF and NuoG subunits in *E. coli* NDH-1, part of which is embedded in its cytoplasmic membrane. The physiological function of NDH-1 in many bacteria and mitochondria

(Battchikova et al., 2011a) is to transfer electrons to the quinone pool during respiration and to pump protons across the membrane. *Synechocystis* also contains NDH-1, which is known to be partially embedded in its thylakoid membrane and possibly in the cytoplasmic membrane as well (Pieulle et al., 2000; Howitt et al., 1993; Zhang et al., 2004; Ogawa, 1992) and does not contain any homolog of the three subunits, NuoE, NuoF and NuoG that otherwise form the NAD(P)H-binding module in other bacteria. Therefore, NDH-1 is a likely candidate in *Synechocystis* to mediate the electron transfer from $H_2$ to the PQ pool in its thylakoid membrane.

In all of our measurements a light-independent $H_2$ uptake was also observed in *Synechocystis* and its occurrence and rate were independent of the activity of any of the components of the p-ETC. Due to the fact that the photosynthetic and respiratory electron transport chain in *Synechocystis* co-exist in its thylakoid membrane, with several members (such as the cytochrome $b_6f$ complex and PQ) participating in both of these electron transport chains, the possibility that $O_2$, the final electron acceptor of the r-ETC, may act as the electron sink was considered. However, it was later noted that the light-independent $H_2$ uptake could be observed a) even when $O_2$ was completely removed from the medium by the addition of glucose, glucose oxidase and catalase, b) in the Δ*ox* mutant strain, where the terminal oxidases were deleted, and c) when the electron transport through the cytochrome $b_6f$ complex was blocked. Therefore, it is concluded that the light-independent $H_2$ uptake is not dependent on the terminal electron acceptor of the respiratory electron transport chain.

Even though the light-induced $H_2$ uptake depended upon the activities of specific components of the photosynthetic electron transport chain, $H_2$ photoevolution did not show the same effect. The short burst of $H_2$ photoevolution was absent in both the Δ*psbB* and Δ*psaAB* mutant strains (Figure 3.2) as well as in the wild-type strain, treated with a saturating concentration of DBMIB (Figure 3.1(D)). This indicated that $H_2$ photo-production was dependent on the product(s) of the photosynthetic electron transport chain, NADPH and/or reduced ferredoxin. From a thermodynamic standpoint this makes sense considering the reduction potential of the PQ pool (+80 mV, at pH 7) compared to the same of protons (-414 mV, at pH 7). Therefore, even though the cyanobacterial hydrogenase is a reversible enzyme, during $H_2$ photoevolution electrons do not travel from the PQ pool to the hydrogenase enzyme.

The results from the *in vitro* measurements showed that a) $H_2$ production *in vitro* required the supply of NADH or NADPH (Figure 3.5), and b) $H_2$ uptake could continue without the addition of any oxidizing agent (Figure 3.4). During $H_2$ production, the average production rate was higher with the addition of NADPH as compared to NADH. This was not in agreement with the previous result found by Gutekunst et al. (2014), where $H_2$ production observed with NADPH was negligible, and also with the result found by Cournac et al. (2004), where a similar rate of $H_2$ production was found by the addition of either NADH or NADPH.

The previous claim of *in vitro* $H_2$ production mediated by reduced Fd (Gutekunst et al., 2014) could not be confirmed in this study. Sodium dithionite, required for the reduction of Fd, was shown to induce $H_2$ evolution *in vitro* with cell-free extracts from the wild-

type as well as Δ*hox* mutant strains, when treated with dithionite or dithionite-reduced Fd. Since the Δ*hox* strain did not contain a hydrogenase, this raised doubt on whether $H_2$ production observed in cell-free extracts from the wild-type *Synechocystis* (treated with dithionite) was indeed mediated by hydrogenase. Sodium dithionite is known to be a strong reducing agent (Mayhew, 1978). However, dithionite by itself does not induce $H_2$ production in intact cells. A commonly used method for the measurement of *in vivo* hydrogenase activity involves the incubation of a cell suspension with sodium dithionite and methyl viologen (Appel et al., 2000; Kim et al., 2006; Kothari et al., 2012), where electrons from dithionite are used to reduce methyl viologen. The reduced methyl viologen then supplies electrons to the bidirectional hydrogenase. Currently a good explanation of how dithionite can induce $H_2$ production in a cell-free extract without the presence of hydrogenase is lacking. One possibility is that [Fe-S] clusters in the broken cells may catalyze the reduction of protons using electrons from sodium dithionite or dithionite-reduced Fd. Another possibility is that the signal recorded by the hydrogen electrode, which is known to be affected by the presence of sulfide gas, was in fact due to the production of hydrogen sulfide ($H_2S$) that was induced by the added sodium dithionite to the cell-free extracts.

# CHAPTER 4

# CONSTRUCTION OF A HOMOLOGY MODEL OF THE HYDROPHILIC SUBUNITS OF NDH-1 AND THE DIAPHORASE SUBUNITS OF HYDROGENASE IN *SYNECHOCYSTIS* SP. PCC 6803


## Summary

The three diaphorase subunits of hydrogenase (HoxE, HoxF and HoxU) are structurally modeled and assembled with the cytosolic subunits of NDH-1 (NdhI, NdhJ, NdhK and NdhH) to form a Ndh-diaphorase complex in *Synechocystis*, based on the crystal structure of Complex I from the thermophilic, chemolithotrophic, $H_2$-oxidizing bacterium *Thermus thermophilus*. In the homology model three subunits of NDH-1 (NdhI, NdhJ and NdhK) interact with HoxU of the diaphorase moiety. Potential locations of the [Fe-S] clusters in the Ndh-diaphorase complex are very similar to their locations in Complex I. A [4Fe-4S] cluster in HoxU, located too far from the rest of the [Fe-S] clusters to participate in the electron transfer chain from the NAD(P)H-binding domain to the PQ-binding site may be involved in transferring electrons from $H_2$ to NDH-1.


## 4.1 Introduction

In the previous chapter evidence was provided for electron channeling from $H_2$ to the cytochrome $b_6f$ complex located in the thylakoid membrane of *Synechocystis*, thus providing an explanation for $H_2$ oxidation in the light (Figure 3.8). Since there is no evidence of a direct association of NiFe-hydrogenase with the cytochrome $b_6f$ complex, electrons need to first enter the thylakoid membrane either directly from hydrogenase or

via another protein complex, from where they can be transported to the cytochrome $b_6f$ complex by PQ, the electron transporter in the thylakoid membrane. Cyanobacterial NiFe-hydrogenases do not have a membrane-binding subunit. Therefore, a direct transfer of electrons from hydrogenase to the membrane is unlikely. On the other hand, among the other proteins located in the thylakoid membrane, the hydrophilic domain of the NDH-1 protein complex offers a potential anchoring site for three of the hydrogenase subunits.

As mentioned in Chapter 1, NDH-1 is involved in the respiratory electron transport chain in bacteria, chloroplasts and mitochondria and contains a cytosolic (hydrophilic) module and a membrane-embedded (hydrophobic) module (Zickermann et al., 2009). The universal function of this enzyme is to accept electrons, derived from the cell's stored metabolites via NADH or NADPH, and to transfer them to the quinone pool in the membrane, while at the same time transporting protons across the membrane, creating a proton-motive force required for ATP synthesis (Sato et al., 2014; Efremov et al., 2010; Friedrich et al., 1995; Yagi et al, 1998). While subunit compositions of NDH-1 vary significantly among different species, fourteen subunits homologous to the ones found in *E. coli* comprise a minimal set of proteins that carry all the redox centers required to perform all bioenergitic functions (Brandt, 2006). However, only 11 of these 14 subunits are found in cyanobacteria (Zhao et al., 2014a; Battchikova and Aro, 2007; Kaneko et al., 2003). In *Synechocystis* these 11 subunits are NdhH through NdhK, comprising the hydrophilic module, and NdhA through NdhG, comprising the membrane-embedded module of the complex (Figure 4.1). The three subunits in *E. coli* (NuoE, NuoF and NuoG) whose homologs are missing in cyanobacteria assemble into a single complex with four other complementary subunits, whose homologs are present in *Synechocystis*.

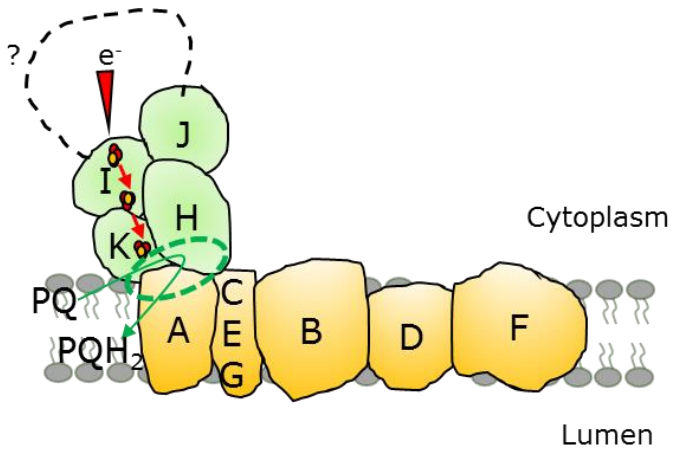


Figure 4.1
Hypothetical model of cyanobacterial NDH-1 with the minimal subunits of the hydrophobic (yellow) and hydrophilic (green) domains, modified from Battchikova et al. (2011b). The potential [Fe-S] clusters are shown in red-yellow spheres, and the electron transfer pathway from an unknown donor (dotted line with question mark) to the PQ-binding site (green dashed circle), located at the interface of NdhH, NdhK, NdhA, NdhC, NdhE and NdhG, is shown by red arrows.

Hydrogenase in *Synechocystis*, apart from its large and small subunits, contains three protein subunits HoxE, HoxF and HoxU that constitute a diaphorase moiety. These three subunits have significant sequence similarities with NuoE, NuoF and NuoG proteins, respectively, in *E. coli.* Since no other homologs of these three Nuo subunits are present in *Synechocystis,* the diaphorase module offers the potential to be able to bind with the available Ndh subunits in *Synechocystis*.

Other than the overall sequence similarities, the total number of redox-active centers ([Fe-S] clusters) in the two proteins are the same as well. The hydrophilic domain of NDH-1 usually contains a NADH-binding site, a FMN-binding site and nine [Fe-S] clusters. These clusters form a pathway for electron transport from the NADH-binding site, located furthest from the membrane to the quinone binding site, located at the

interface with the membrane domain (Efremov et al., 2010). In *Synechocystis*, NdhI and NdhK contain consensus sequences for two and one [Fe-S] clusters, respectively (Figure 4.1). Together, these three clusters could potentially carry electrons from another [Fe-S] cluster to the PQ-binding site. On the other hand, HoxE and HoxF contain consensus sequences for coordinating a single [Fe-S] cluster each, while the HoxU subunit contains four potential [Fe-S] clusters (Appel and Schulz, 1996). These clusters are suggested to be involved in electron transfer from the HoxY subunit to the redox partner of hydrogenase (Appel and Schulz, 1996; Vignais and Billoud, 2007; Eckert et al., 2012).

Even though bioinformatic evidence points towards an association of hydrogenase with the NDH-1 complex, it is to be noted that experimental evidence is still lacking for such an association. In fact, Burroughs et al. (2014) showed that in the *Synechocystis* NDH-1 mutant M55 hydrogenase was still attached to the thylakoid membrane, like in wild type. However, the mutant also showed a ~50% decrease in hydrogenase abundance (Burroughs et al., 2014; Gutthann et al., 2007). Therefore, there may be more than one way of associating hydrogenase with the membrane: one depending on NDH-1 and another depending on other protein complex(es).

In this chapter a homology model of a proposed Ndh-diaphorase complex in *Synechocystis* is presented that contains four hydrophilic subunits out of the total 11 minimal subunits of NDH-1, and three hydrogenase subunits that have sequence homologies with the remaining three NDH-1 subunits in *E. coli*. The homology model is based on the template structure of the hydrophilic domain of NDH-1 in a thermophilic, chemolithotrophic, $H_2$-oxidizing bacterium, *Thermus thermophilus*.

## 4.2 Materials and Methods

### 4.2.1 Selection of Template

The amino acid sequences of HoxE, HoxF and HoxU subunits of *Synechocystis* were obtained from the NCBI database. NCBI BLAST searches were performed with these sequences against the protein databank (PDB) database to identify similar sequences whose crystal structures are already available. The hydrophilic arm of NDH-1 in *T. thermophilus* (PDB ID: 2FUG) was identified as the only complex, whose three subunits (Nqo1, Nqo2 and Nqo3) showed significant sequence identities with HoxF, HoxE and HoxU, respectively. The amino acid sequences of the three Nqo-subunits were obtained from the NCBI database.

### 4.2.2 Sequence Alignments

The amino acid sequences of NdhH, NdhI, NdhJ and NdhK of *Synechocystis* and Nqo4, Nqo5, Nqo6 and Nqo9 of *T. thermophilus* were obtained from the NCBI database. The sequences of the *Synechocystis* proteins were aligned individually with their corresponding homologs in *T. thermophilus* (HoxF-Nqo1, HoxE-Nqo2, HoxU-Nqo3, NdhH-Nqo4, NdhJ-Nqo5, NdhK-Nqo6 and NdhI-Nqo9) using CLUSTALW.

The three-dimensional structure file of the hydrophilic arm of NDH-1 from *T. thermophilus* was obtained from the PDB database (PDB ID: 2FUG) and was used as the template structure for modeling. A structure-based alignment was then created by appending the individual alignments together to create a template sequence to be used for alignment with hydrogenase targets.

### 4.2.3 **Protein Modeling**

The PDB structure file of NDH-1 (2FUG) was truncated to remove subunit Nqo15 to create a template structure file. The alignment file containing the template sequence and the structure file containing the template structure were used as inputs for protein homology modelling software MODELLER (Webb and Sali, 2014). 100 independent output models of the *Synechocystis* Ndh-diaphorase complex were built that varied mainly in the structural arrangements of the loop regions of the polypeptide chains. From those 100 models the best-fit model was chosen based on its lowest combined energy determined by their DOPE (Discrete Optimized Protein Energy) scores. The distribution of the DOPE scores of the 100 output models is shown Figure 4.2.

The native structure of a protein generally has the lowest free energy under native conditions (Shen and Sali, 2006; Anfinsen, 1972). Therefore a free energy function can be used to predict and assess protein structures. DOPE is an atomic distance-dependent

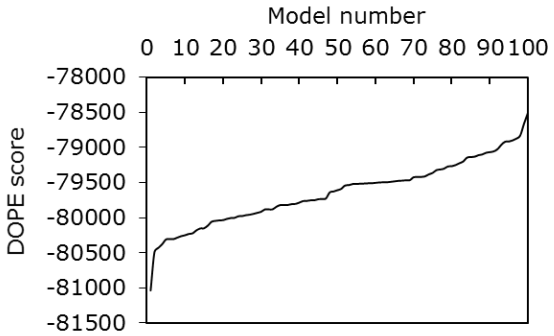


Figure 4.2
Distribution of DOPE scores of 100 output models of the *Synechocystis* Ndh-diaphorase complex that varies mainly in the structural arrangements of the loop regions of the polypeptide chians. The models were sorted from the lowest-score model (best-fit) to the highest-score model and numbered accordingly.

statistical potential that represents a scoring function whose global minimum corresponds to the native structure from a sample of native structures of different sequences deposited in the protein data bank (PDB) (Shen and Sali, 2006) and therefore is widely used for identification of the best-fit (minimum energy) model in MODELLER (Eramian et al., 2008; Kothari et al., 2013).

All the input and output three-dimensional structures were viewed using the PyMOL software (Liang et al., 2003).

## 4.3 Results and Analysis

### 4.3.1 Homology Modeling

A homology model of the Ndh-diaphorase complex in *Synechocystis* was built based on the PDB structure of the hydrophilic arm of NDH-1 in *T. thermophilus* (PDB ID: 2FUG) (Sazanov and Hinchliffe, 2006). NDH-1 from *T. thermophilus* was used as the template structure because it was the only protein that contained homologs (with available crystal structure) of all of the three diaphorase subunits of hydrogenase with significant sequence dentities. The sequence identities and coverages between the homologous subunits of the two organisms are given in Table 4.1.

### 4.3.2 Analysis of the Overall Structure

The best-fit three-dimensional homology model of the Ndh-diaphorase complex in *Synechocystis* is shown in Figure 4.3. The overall folds and lengths of HoxF, HoxE, NdhH, NdhJ, NdhK and NdhI subunits were very similar to Nqo1, Nqo2, Nqo4, Nqo5,

Table 4.1.
Amino acid sequence comparison between the subunits of NDH-1 in *T. thermophilus* and their homologs in *Synechocystis*

| **Protein subunit** | | **Identity with the target sequence in the covered sequence region** | **Target sequence coverage** | **Template sequence coverage** |
|---|---|---|---|---|
| ***Synechocystis*** **(target sequence)** | ***T. thermophilus*** **(template sequence)** | | | |
| HoxF | Nqo1 | 46% | 74% | 91% |
| HoxE | Nqo2 | 31% | 63% | 60% |
| HoxU | Nqo3 | 30% | 86% | 40% |
| NdhH | Nqo4 | 46% | 95% | 99% |
| NdhJ | Nqo5 | 56% | 29% | 39% |
| NdhI | Nqo9 | 33% | 71% | 60% |
| NdhK | Nqo6 | 50% | 83% | 60% |

Nqo6 and Nqo9, respectively. HoxU, which contained 238 amino acid residues, was a much smaller protein compared to Nqo3 (767 residues) and aligned only with its initial 307 residues, covering the N-terminal domain and initial portion of the C-terminal domain of Nqo3. No homolog of the remaining C-terminal region of Nqo3 was found in *Synechocystis*. HoxF contains a potential FMN-binding and a NAD(P)H-binding domain. Aside from the missing segment of Nqo3 in HoxU, the rest of the two units, the Ndh-diaphorase complex in *Synechocystis* and Nqo (1-6, 9) in *T. thermophilus* could be structurally superimposed.

### 4.3.3 Comparison of NdhJ and Nqo5 Structures

Because of the low template and target sequence coverages of the NdhJ-Nqo5 alignment (Table 4.1), the structures of the two subunits were examined carefully. The three-dimensional structures of the two subunits showed the same overall folds and lengths of their α-helices and β-sheets but the low sequence coverages were caused by two uneven loop regions (Figure 4.4). Nqo5 has a short (4 residues) loop region close to its N-terminus while the homolog in NdhJ is longer (23 residues). On the other hand, a second loop near the C-terminal end of Nqo5 is 72 residues long while in NdhJ the C-terminal loop spans 36 residues. While it is difficult to be certain of the precise effects of these length variations based on the homology model, both of these two loop regions in the two proteins are located near the surface of the proteins and therefore are not likely to affect the core structures of the two complexes.

### 4.3.4 Tentative Positions of the [Fe-S] Clusters

The amino acid residues coordinating the [Fe-S] clusters were compared between the two protein complexes. Consensus sequences coordinating the [Fe-S] clusters in various Hox subunits in *Synechocystis* were observed before (Appel and Schulz, 1996). The amino acid residues coordinating the [Fe-S] clusters in *T. thermophilus* were obtained from the PDB structure of the protein (PDB ID: 2FUG). Nqo1 and Nqo2 contain one [4Fe-4S] cluster each, both coordinated by four cysteine residues, and their positions are conserved in HoxF and HoxE, respectively (Figure 4.3).

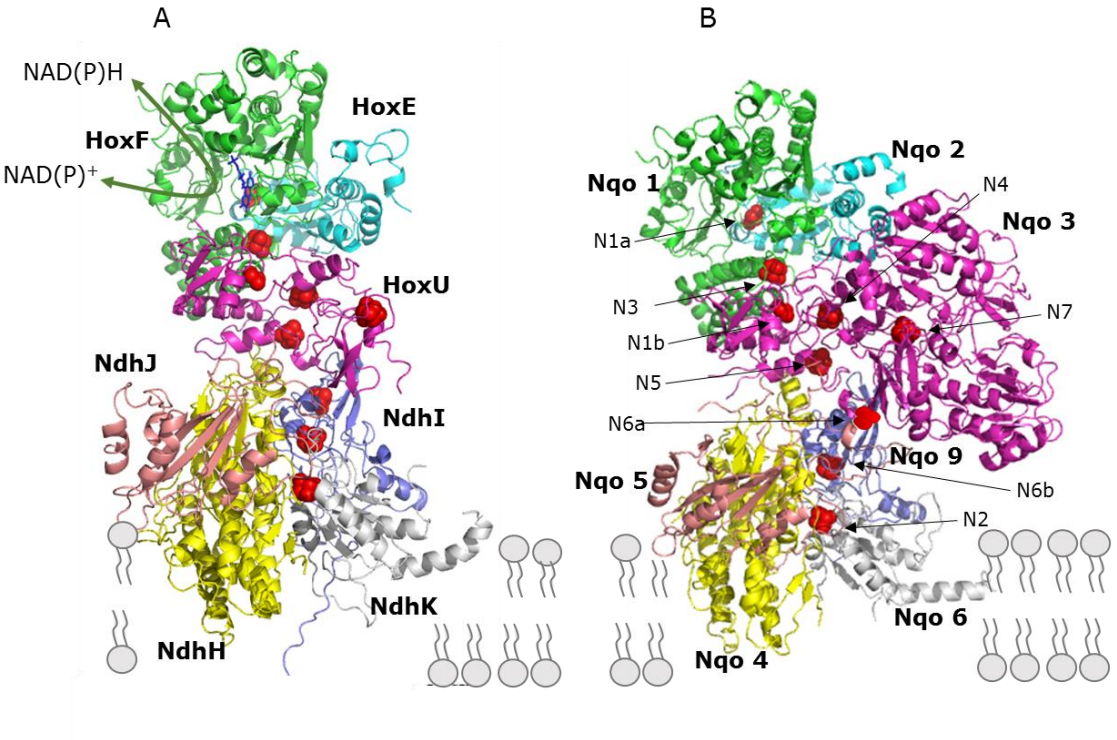


Figure 4.3
Three-dimensional homology model of the Ndh-diaphorase complex from *Synechocystis* (A) based on the PDB structure of the hydrophilic subunits of NDH-1 from *T. thermophilus* (PDB ID: 2FUG) (B). The actual positions of the [Fe-S] clusters in *T. thermophilus* and their tentative positions in the *Synechocystis* homology model are shown in red spheres. The tentative FMN-binding site (blue line) and NAD(P)H-binding site (green arrow) in HoxF are also indicated.

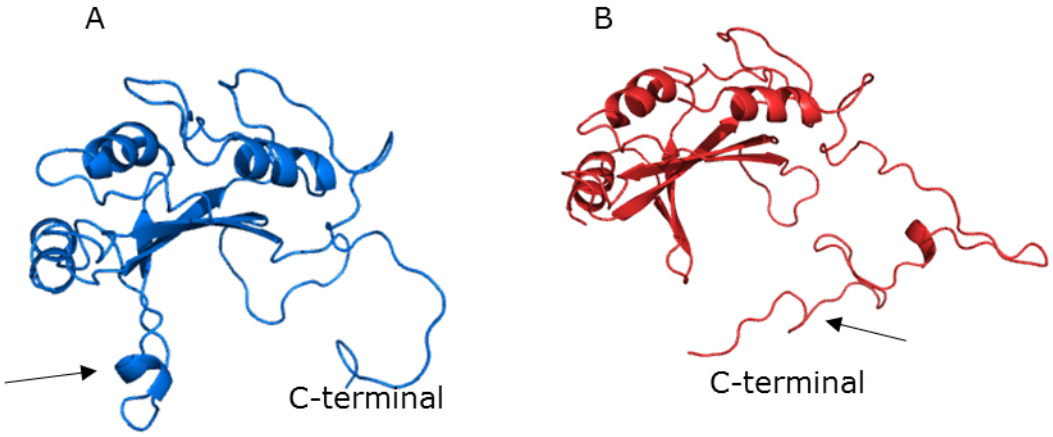


Figure 4.4
Comparison of the structures of NdhJ in *Synechocystis* (A) and Nqo5 (B) in *T. thermophilus* (PDB ID: 2FUG). The longer loop regions of NdhJ and Nqo5 are indicated by arrows.

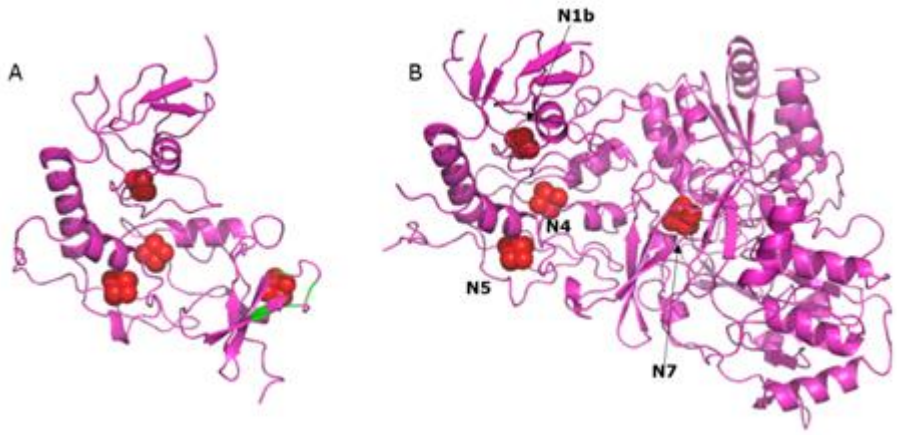


Figure 4.5
Tentative locations of the [Fe-S] clusters (red spheres) in HoxU (A) and their actual positions in Nqo3 (PDB ID:2FUG) (B). Since the position of the fourth [Fe-S] cluster in HoxU is not conserved in Nqo3, four cysteine residues that can potentially coordinate a cluster are shown in green.

The Nqo3 subunit coordinates a total of four [Fe-S] clusters: a [2Fe-2S] type binuclear cluster N1B and three [4Fe-4S] clusters N4, N5 and N7 (Figure 4.5). Clusters N1b, N4 and N5 are located in the N-terminal domain region of Nqo3 while N7 is located in its C-terminal domain. Cysteine residues coordinating cluster N1b are conserved in cyanobacterial HoxU. The N5 cluster is coordinated by residues in the motif $HX_3CX_2CX_5C$ in Nqo3 (Sazanov and Hinchliffe, 2006), while in HoxU the consensus that is present in the corresponding position is $HXCX_2CX_5C$ (Appel and Schulz, 1996) and is well conserved among cyanobacteria. This consensus was suggested to coordinate either a [4Fe-4S] cluster or a [3Fe-4S] cluster because of the position of the histidine residue. Cluster N4 is coordinated by four cysteine residues in Nqo3. The positions of three of those are conserved HoxU, and the fourth one is located at a different position. Finally, the fourth cluster N7 is located at the C-terminal domain of Nqo3, coordinated by four cysteine residues, the positions of which are not conserved in HoxU. However,

HoxU also contains a fourth consensus sequence ($CX_2CX_2CX_3C$) near its C-terminal end for potentially coordinating a [4Fe-4S] cluster (Appel and Schulz, 1996), which in the homology model points to a similar position as N7 (Figure 4.5). Because the N7 cluster is located too far away from the main redox chain from the NADH-binding site to the quinone-binding site, it was suggested that this [Fe-S] cluster does not participate in the main electron transfer chain in NDH-1 (Sazanov and Hinchliffe, 2006; Hinchliffe and Sazanov, 2005).

Cluster N6a and N6b in Nqo9 and cluster N2 in Nqo6 are coordinated by four cysteine residues each, the positions of which are conserved in NdhI and NdhK, respectively.

## 4.4 Conclusion

A homology model of the potential Ndh-diaphorase complex in *Synechocystis* is presented. The successful computational assembly of this model shows that amino acid residues of the subunits of the two proteins (hydrogenase and NDH-1) can structurally interact with each other to form a single complex. Therefore, it supports the hypothesis that subunits of hydrogenase and NDH-1 can potentially assemble into a single complex in the cell as well. Based on this model, HoxU is the only subunit of the hydrogenase enzyme that interacts with subunits of NDH-1, namely NdhI, NdhJ and NdhH, but not NdhK. Nine [Fe-S] clusters are positioned tentatively according to the positions of the conserved amino acid residues coordinating the clusters. Their positions in the Ndh-diaphorase complex are very similar to those in NDH-1. Like in NDH-1, eight out of the nine [Fe-S] clusters in the *Synechocystis* complex can potentially form a redox chain from the NAD(P)H-binding site in HoxF to the tentative PQ-binding site close to the

membrane-embedded domain, while the remaining [Fe-S] cluster (4$^{th}$ cluster in HoxU) is not likely to be a part of this redox chain.

The position of the HoxYH module relative to this complex could not be predicted with certainty because of the lack of a template structure with both the diaphorase and the hydrogenase module. However, because of the absence of the C-terminal region of Nqo3 in HoxU, and the odd position of its fourth [Fe-S] cluster, HoxU may be involved in connecting the Ndh-diaphorase complex to the HoxYH module. In that case, the participating subunits may interact in such a way that the fourth [Fe-S] cluster of HoxU can participate in transferring electrons between the [Fe-S] cluster in HoxY and the main redox chain in the Ndh-diaphorase complex (Figure 4.6).

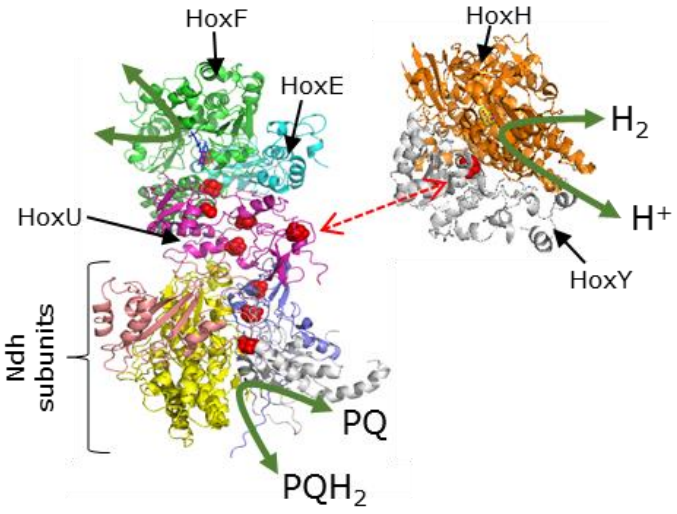


Figure 4.6
Three-dimensional homology model of the Ndh-diaphorase complex in *Synechocystis* and predicted structure of the large (HoxH) and small (HoxY) subunits from Kothari et al., 2013. A tentative route of electron transfer between the [Fe-S] cluster in the small subunit of hydrogenase and the fourth [Fe-S] cluster of HoxU is indicated by a dashed arrow in red. The [Fe-S] clusters are shown in red spheres. Electron transfer between NAD(P)H and $NADP^+$, PQ and $PQH_2$, and $H_2$ and $H^+$ are indicated by green arrows.

# CHAPTER 5

# SIGNIFICANCE OF THE DIAPHORASE MOIETY IN *SYNECHOCYSTIS* SP. PCC 6803: AN ATTEMPT TO OVEREXPRESS HYDROGENASE WITHOUT DIAPHORASE


## Summary

In the previous chapter, a homology model of a potential Ndh-diaphorase complex in *Synechocystis* containing three of the diaphorase subunits of hydrogenase (HoxEFU) and four of the peripheral subunits of NDH-1 (NdhH-K) was presented. In this chapter an existing HoxEF deletion mutant strain was assayed for potential light-induced $H_2$ uptake activity driven solely by the HoxUYH module and NDH-1. To improve the abundance of HoxUYH in the strain lacking HoxE and HoxF, the genes encoding these three subunits were overexpressed under two strong promoters. $H_2$ production was assayed to test whether in the absence of HoxEF module the partially expressed enzyme is capable of finding an alternate redox donor. The overexpression strain did not show any $H_2$ uptake or production under physiological conditions, although it displayed $H_2$ evolution with reduced methyl viologen. Altogether, these data could not provide evidence for an electron transfer pathway that is independent of the HoxE and HoxF subunits in the partially expressed hydrogenase in *Synechocystis.*


## 5.1 Introduction

Cyanobacterial NiFe-hydrogenases are multisubunit enzymes containing five protein subunits namely, HoxE, HoxF, HoxU, HoxY and HoxH. While HoxH contains the active

site of the enzyme, all of the other Hox subunits contain potential [Fe-S] cluster-binding sites. HoxH and HoxY subunits in *Synechocystis* are homologous to the large and small subunits of prototypical NiFe-hydrogenase, respectively, and form the hydrogenase moiety of the enzyme (Vignais and Billoud, 2007; Eckert et al., 2012). In the large subunit, the NiFe-containing active site catalyzes the reduction of protons or oxidation of $H_2$, while the [Fe-S] clusters in the small subunit function in electron transfer to and from the large subunit (Vignais and Billoud, 2007). On the other hand, HoxE, HoxF and HoxU subunits constitute the diaphorase moiety (Massanz et al., 1998; Boison et al., 1998) of the enzyme that catalyzes the oxidation/reduction of NAD(P)H/NAD(P)$^+$, coupling it with the reduction/oxidation reaction at the active site of the hydrogenase moiety (Long et al., 2007; Antal et al., 2006). HoxF contains NAD(P)H-binding and FMN-binding domains, making it essential for the diaphorase activity of the enzyme (Appel and Schmitz, 1996). HoxE, HoxF and HoxU contain potential [Fe-S] cluster binding sites, but their exact roles in the electron transfer to and from the active site are not known.

Due to the presence of the NAD(P)H-binding domain in HoxF, the cyanobacterial hydrogenase was classified as a NAD(P)$^+$-reducing hydrogenase, with its diaphorase moiety being essential for the NAD(P)$^+$-reducing activity. However, $H_2$ evolution depending on the electron supply from reduced methyl viologen has also been detected in *Synechocystis hoxE*, *hoxF* and *hoxU* mutants recently (Eckert et al., 2012) suggesting that the enzyme is catalytically active without these subunits. Therefore, the enzyme might be able to accept electrons from an alternate electron donor in the cell in the absence of its NAD(P)$^+$-binding diaphorase moiety.

Apart from that, in the previous chapter the homology model of a potential Ndh-diaphorase complex was presented, in which HoxU was found to be the only subunit of the hydrogenase enzyme with direct interaction with subunits of NDH-1. While it could not be predicted how the HoxY-HoxH module can potentially interact with this complex, a possible electron transfer pathway from the active site of hydrogenase to NDH-1 via the [Fe-S] clusters located in HoxY and HoxU, but not HoxE and HoxF seemed plausible (Figure 5.1).

Therefore, an existing *hoxEF*$^-$ strain (Howitt and Vermaas, 1999) was assayed for (a) potential $H_2$ production activity from an alternate electron donor, and (b) potential $H_2$ uptake activity using HoxH, HoxY, HoxU and the Ndh subunits. In the *hoxEF*$^-$ strain a portion of *hoxE* and *hoxF* was deleted and replaced with a chloramphenicol resistance cassette ($Cm^R$). The *hox* operon in *Synechocystis* spans over a ~6.5 kb DNA segment with a total of eight genes (five *hox* genes and three ORFs with unknown functions)

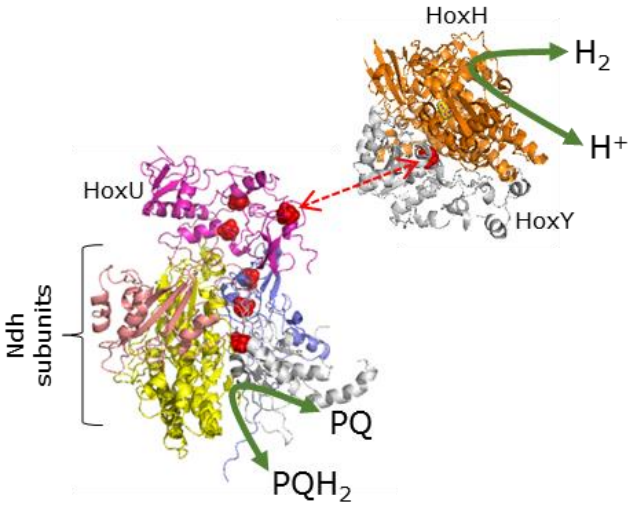


Figure 5.1
Hypothetical model of an electron transfer pathway from the active site located in HoxH to the PQ pool via the [Fe-S] clusters in HoxY and HoxU.

(Figure 1.3). Even though the known promoter of the *hox* operon is located in a ~700 nucleotide region upstream of *hoxE*, a deleterious effect of the $Cm^R$ cassette could not be ruled out. Therefore, a *hoxUYH* overexpression strain was constructed in the background of the previously constructed *hoxEF*$^-$ strain and assayed it for potential $H_2$ uptake/production activity.

## 5.2 Materials and Methods

### 5.2.1 Construction of the *hoxUYH* Overexpression Strain

A schematic diagram of the construction of the plasmid vector used to overexpress the genes is presented in Figure 5.2.

**Step 1:** The following DNA fragments were amplified from *Synechocystis* genome: a 620 bp fragment containing the region upstream of *slr0551* (bases 3250365-3250984) as the potential promoter of *slr0551* ($Pro_{0551}$), a ~2.2 kb fragment containing *hoxU*, *hoxY* and two ORFs downstream of *hoxY* (bases 1673446-1675637), a fragment containing the 490 bp region upstream of *slr0749* (bases 3415499-3415988) as the potential promoter region of *slr0749* ($Pro_{0749}$) and a ~1.4 kb fragment containing *hoxH* (bases 1673495-1672071). A SacI restriction site was engineered at the 5' end of the $Pro_{0551}$ fragment. The locations of the sequences in the *Synechocystis* genome are stated according to CyanoBase. After obtaining the individual PCR products, the amplicons were successively combined two fragments at a time, into a single DNA fragment totaling ~4.6 kb by using the overlap PCR method as described by Pogulis et al. (1996). Primers used for the amplifications are listed in Table 5.1.

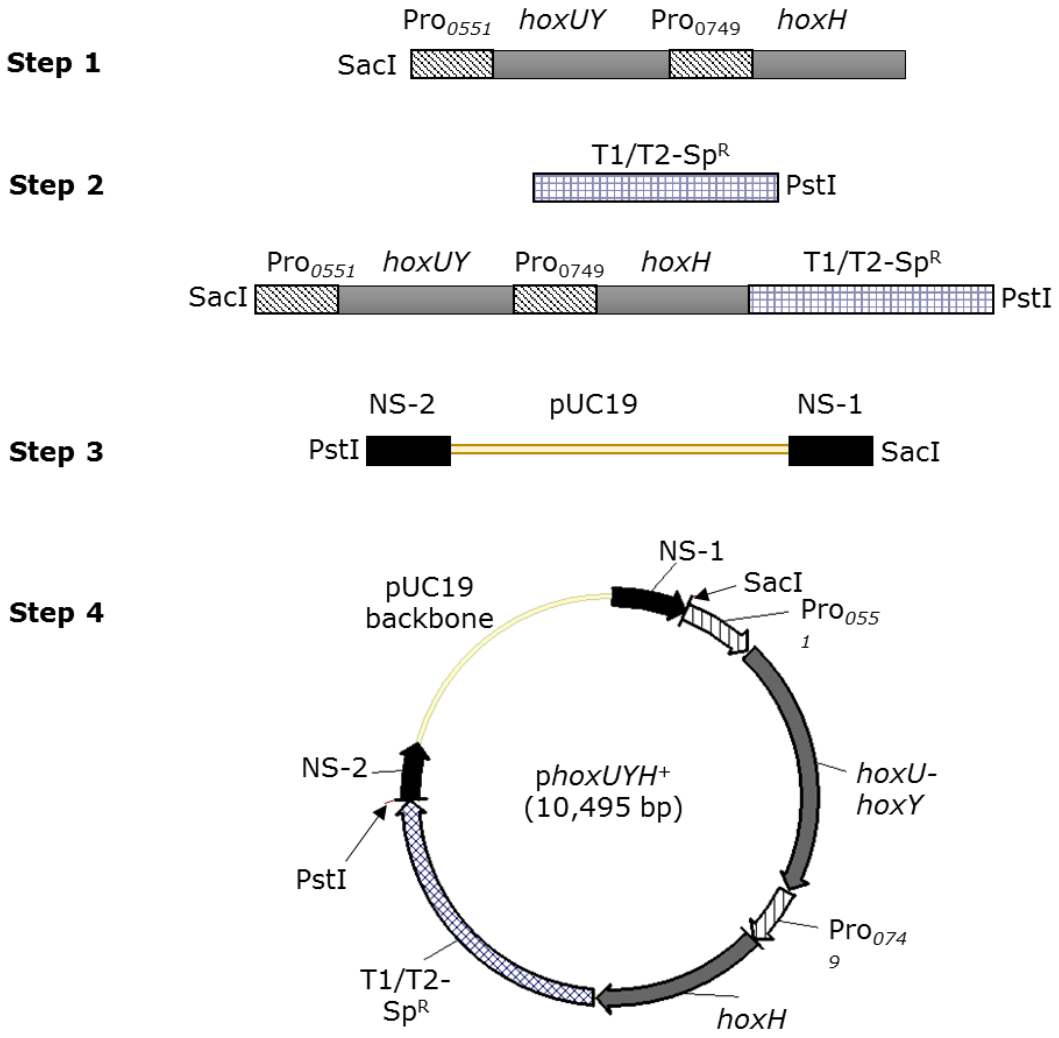


Figure 5.2

Construction of the plasmid p*hoxUYH*$^{+}$ that uses promoters from *slr0551* and *slr0749* genes to overexpress *hoxU*, *hoxY* and *hoxH* in *Synechocystis*. See text for a detailed explanation.

**Step 2:** Another DNA fragment (~2.4 kb) containing the T1/T2 terminator and spectinomycin-resistance cassette (Sp$^{R}$) was amplified from an existing plasmid vector (constructed by Dr. Hongliang Wang) and was fused to the previously obtained ~4.6 kb fragment, again by using overlap PCR method. The resultant ~7.2 kb DNA fragment

contained $Pro_{0551}$/*hoxU-hoxY*/$Pro_{0749}$/*hoxH* /(T1/T1)/$Sp^R$. A PstI restriction site was engineered at the 3' end of T1/T2-$Sp^R$ fragment.

**Step 3:** Next, a pUC19-based plasmid vector, which already included a neutral genomic DNA region (729195-730287) from the *Synechocystis* genome in two fragments, bases 729195-729805 on one side (NS-1) and bases 729820-730287 on the other (NS-2), was used as a template for another PCR. This PCR was performed to linearize this vector from NS-2 to NS-1, with the pUC19 backbone in between, and to introduce SacI and PstI restriction sites at the 3'-end of NS-1 and 5'-end of NS-2 (Figure 5.2).

**Step 4:** The previously obtained ~7.2 kb DNA fragment was then inserted in between NS-1 and NS-2 of the linearized vector with the SacI and PstI restriction sites to obtain plasmid p*hoxUYH*$^+$. The correctness of the cloned plasmid was confirmed by sequencing.

The *Synechocystis hoxEF*$^-$ strain (Howitt and Vermaas, 1999) was obtained from our laboratory and the p*hoxUYH*$^+$ plasmid was used to transform this strain following the procedure as described by Vermaas et al. (1987). Segregation analysis was performed as described in Section 2.2.3 (Chapter 2) and fully segregated transformants (*hoxEF*$^-$*/UYH*$^+$) were selected on BG-11 plates with 60 µg ml$^{-1}$ spectinomycin.

### 5.2.2 RT-PCR

RNA was extracted from cultures of *Synechocystis hoxEF*$^-$ and *hoxEF*$^-$*/UYH*$^+$ strains using Trizol reagent (Life Technologies) following the manufacturer's protocol. DNase treatment was done by Turbo DNA-free$^{TM}$ DNase (Life Technologies), followed by cDNA synthesis using the iScript Select cDNA Synthesis Kit (Bio-Rad), following the

Table 5.1.
Primer sequences used for the construction of *hoxEF*$^{-}$*/UYH*$^{+}$ strain. In the primer sequences, letters in bold indicate restriction sites for digestion and the lower case letters indicate 5' nucleotide that were added.

| **Primer** | **Sequence** | **Description** |
|---|---|---|
| NS-1-pUC19-R | aatt**GAGCTC**GTTACGGGCAAAATTGCAGACCC | Linearizes a circular pUC19-baes vector and introduces SacI and PstI restriction sites at the 3'-end of NS-1 and 5'-end of NS-2 |
| NS-2-pUC19-F | aatt**CTGCAG**TCAAGATGAAGCGGCGATCGGTAA | |
| Pro$_{0551}$-F | aatt**GAGCTC**GGCGATACCAGTCAAAGAATGG | Amplifies the region containing the promoter of *slr0551* |
| Pro$_{0551}$-R | AGTGTAAATAAAAAAACGTTGTA | |
| *hoxYH*-F | tacaacgtttttttatttacactATGTCTGTTGTTACTTTAACCATTG | Amplifies *hoxU, hoxY* and 2 ORF, located downstream of *hoxY* |
| *hoxYH*-R | TGGTTGACGGGGGATTGATTATTG | |
| Pro$_{0749}$-F | caataatcaatcccccgtcaaccaACTCCCTCTTCCCGCCGCCTTCG | Amplifies the region containing the promoter of *slr0749* |
| Pro$_{0749}$-R | TATTAACGAGGTTTGGGGTCTTGG | |
| *hoxH*-F | ccaagaccccaaacctcgttaataATGTCTAAAACCATTGTTATCG | Amplifies *hoxH* |
| *hoxH*-R | TTAATCCCGCTGGATGGACTTAAT | |
| T1/T2-Sp-F | attaagtccatccagcgggattaaGTCGACTGAGAGAAGATTTTCAG | Amplifies T1/T2 terminator and spectinomycin resistance cassette |
| T1/T2-Sp-R | **CTGCAG**GGGCCCTCTAGGGTCCCCAATTA | |

manufacturer's protocols in both cases. For RT-PCR, iTaq SYBR Green Supermix with ROX (Bio-Rad) was used with primers listed in Table 4.2 and reactions were performed using the manufacturer's protocol. An ABI Prism 7900HT Sequence Detector System was used for measuring fluorescence of SYBR green/double-stranded DNA and analysis was done using the $2^{-\Delta Ct}$ method (Schmittgen and Livak, 2008). Primers used for the RT-PCR are listed in Table 5.2.

### 5.2.3 Western Blot Analysis

Polyclonal rabbit antibodies against HoxH were kindly donated by Dr. Laurent Cournac. Western blot analysis was performed as described by Gonzalez-Esquer and Vermaas (2013). Cultures of *Synechocystis* wild type and *hoxEF*$^{-}$*/UYH*$^{+}$ (200 ml) were harvested by centrifugation while in their exponential growth phase ($OD_{730}$ 0.5-0.8) and resuspended in resuspension buffer containing 50 mM MES-NaOH (pH 6.5), 10 mM $MgCl_2$, 5 mM $CaCl_2$, 25% glycerol, and "protease inhibitor cocktail" (1 mM each of phenylmethylsulfonyl fluoride (PMSF), benzamidine, and amino caproic acid). Cells were broken by 10 x 30 s of bead beating (with 0.1 mm glass beads) in a Mini Bead Beater (BioSpec Products, Bartlesville, OK) with two minutes of intermittent cooling on ice. Cell debris was removed by centrifugation at 1600 x g for 5 min and the supernatants containing proteins were collected. The supernatants were further centrifuged at 37000 x g for 15 min to separate membrane (total membrane) fractions from soluble fractions. Both the membrane and soluble fractions were used for polyacrylamide gel electrophoresis (PAGE). Protein concentrations in the soluble fractions were determined by Bradford assay (Bradford, 1976). Proteins were separated

Table 5.2.

Primer sequences used for RT-PCR of cDNA from the wild-type, *hoxEF*$^{-}$ and *hoxEF*$^{-}$*/UYH*$^{+}$ strain. The locations of the sequences in the *Synechocystis* genome are stated according to Cyanobase.

| **Primer** | **Sequence** | **Location in *Synechocystis* genome** |
|---|---|---|
| RT-*hoxE*-F | AACCCAGTGGGAAACATACC | 1678309-1678290 |
| RT-*hoxE*-R | GGTTTCAGATGGACTTCCTGAT | 1678204-1678225 |
| RT-*hoxF*-F | ACCGCAGTGTGTTGGAAA | 1677339-1677322 |
| RT-*hoxF*-R | ATTCCGCCCGCACATAAA | 1677235-1677252 |
| RT-*hoxU*-F | CCCAAGCGAGAAGTGGATTTA | 1675273-1675253 |
| RT-*hoxU*-R | CTCCCTCAATTTCATCGCAAAC | 1675171-1675192 |
| RT-*hoxY*-F | AGCTTTGGAGTTGAGACAGAAA | 1674689-1674668 |
| RT-*hoxY*-R | GGATCGCTACCTTTGAGCATATTA | 1674585-1674608 |
| RT-*hoxH*-F | GGGTTATCCCGATGGCATTTA | 1672650-1672630 |
| RT-*hoxH*-R | CCCGTTGCCGATATTCTTCT | 1672541-1672560 |

by 12% SDS-PAGE and then transferred onto a polyvinylidene difluoride (PVDF) membrane (Immobilon-P) at 40 V and 4 °C for 4 h.

Western blotting was performed according to Millipore's "Rapid immunodetection without blocking" protocol with Phosphate-Buffered Saline (PBS; 0.1 M sodium phosphate, 0.15 M NaCl, pH 7.0) buffer and fat-free milk as blocking agent. The primary antibody was used in a 1:1000 dilution and the alkaline phosphatase (AP)-conjugated secondary antibody in a 1:3000 dilution. The immunoblot was visualized using an AP substrate kit (BioRad).

### 5.2.4 Assay for $H_2$ Production

$H_2$ production and uptake from the wild-type, *hoxEF*$^-$ and *hoxEF*$^-$*/UYH*$^+$ strains were measured using a modified Clark-type electrode, as described in Section 2.2.2 (Chapter 2). Cultures were grown photoautotropically to a final $OD_{730}$ between 0.8 and 1.0 before resuspending the pellets in fresh BG-11 medium to achieve final cell concentrations 11 µg chl *a* ml$^{-1}$. Hydrogenase activity was measured in darkness and under anaerobic conditions with the addition of glucose (10 mM), glucose oxidase (40 U ml$^{-1}$) and catalase (50 U ml$^{-1}$) as $O_2$ scavenger. To measure the potential (maximum) activity of the enzyme, methyl viologen (5 mM) and sodium dithionite (10 mM) were added to the cell suspension, and $H_2$ production was recorded in darkness.

## 5.3 Results

### 5.3.1 Overexpression of the Hydrogenase Moiety in the Absence of Diaphorase

In order to investigate the role of HoxE and HoxF, a mutant strain of *Synechocystis* was generated with overexpressed *hoxU*, *hoxY* and *hoxH*, in the absence of *hoxE* and *hoxF*. For this purpose *hoxU, hoxY* and *hoxH* genes were cloned into a pUC19-based plasmid under the control of two strong promoters from *slr0551*, encoding a hypothetical protein and *slr0449* (*chlL*), and the *hoxEF*$^-$ background strain was transformed with this plasmid (Figure 5.3). *Slr0551* and *slr0449* were selected from a microarray database because of their high and consistent level of expressions in both aerobic and anaerobic conditions (Summerfield et al., 2008).

RT-PCR was performed to check the expression levels of all five *hox* genes in *Synechocystis* wild-type, *hoxEF*$^-$ and *hoxEF*$^-$*/UYH*$^+$ strains. The relative expression levels of the *hox* genes in the mutant strains compared to the wild-type strain are shown in Figure 5.4. As expected, no transcript of *hoxE* or *hoxF* was detected in either of the mutant strains. In the *hoxEF*$^-$ strain a decrease in the expression of *hoxU, hoxY* and *hoxH*

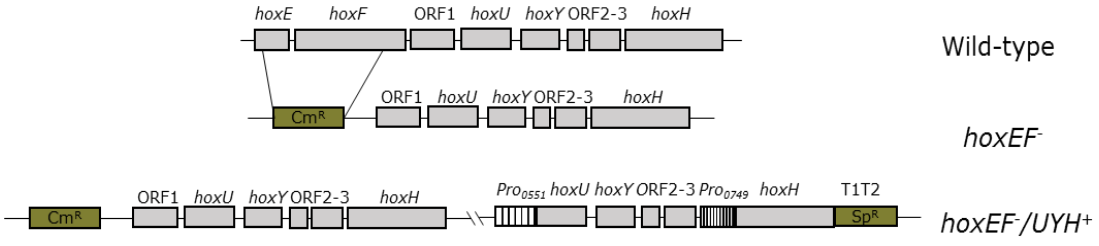


Figure 5.3
*Hox* genes in *Synechocystis* wild-type, *hoxEF*$^-$ and *hoxEF*$^-$*/UYH*$^+$ strains.

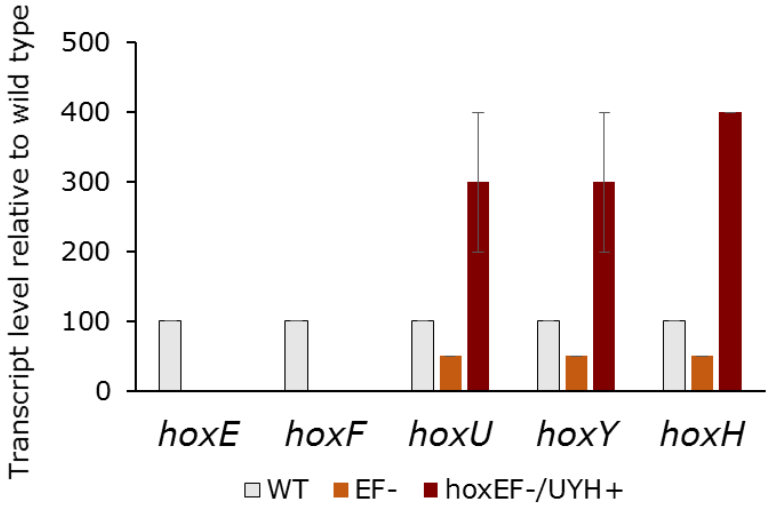


Figure 5.4

Histogram representation of the ratios of the transcript abundances (measured by RT PCR) of the five *hox* genes in *hoxEF*$^{-}$ and *hoxEF*$^{-}$*/UYH*$^{+}$ mutants relative to the wild type. Relative abundances of transcripts were normalized to *atpA* by using the $2^{\Delta Ct}$ method and then compared to the wild type.

compared to the wild type was detected. This phenomenon could be due to fact that in *hoxEF*$^{-}$ the substitution of the initial two genes of *hox* operon with a $Cm^{R}$ cassette caused a deleterious effect on the expression of the downstream genes. As expected, in the *hoxEF*$^{-}$*/UYH*$^{+}$ strain the transcript level of all three hydrogenase genes (*hoxU*, *hoxY* and *hoxH*) were increased.

In a previous study the HoxH protein abundance was found to be severely affected (10% of the wild type) by the deletion of *hoxE* and *hoxF* (Aubert-Jousset et al., 2011). Therefore, in order to check the level of HoxH abundance in the *hoxEF*$^{-}$*/UYH*$^{+}$ strain, Western blot analysis was performed with anti-HoxH antibodies using both membrane fractions and the soluble fractions from the wild-type strain and the *hoxEF*$^{-}$*/UYH*$^{+}$ strain.

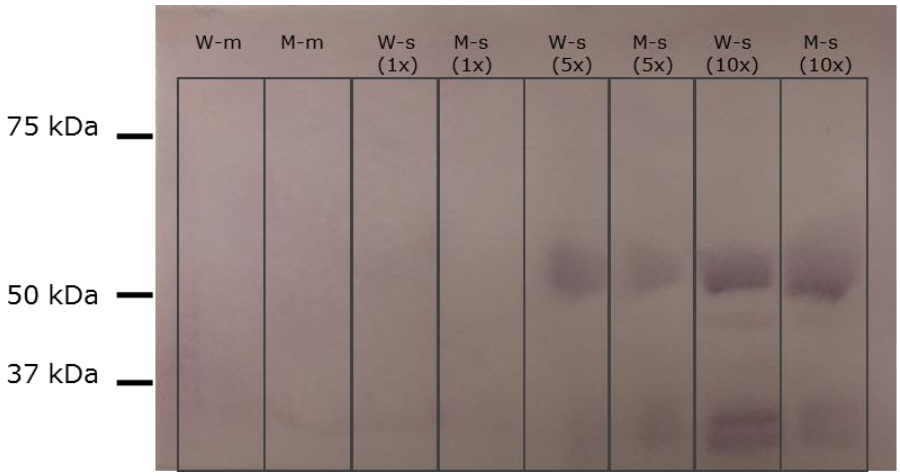


Figure 5.5
Immunoblot analysis using HoxH antibodies following SDS-PAGE (12% SDS) with isolated membrane fractions and soluble fractions from the wild-type and *hoxEF*$^{-}$*/UYH*$^{+}$ strains. W-m and M-m correspond to the wild type and *hoxEF*$^{-}$*/UYH*$^{+}$ membrane fractions, respectively (0.3 µg chl *a* each), and W-s and M-s correspond to wild type and *hoxEF*$^{-}$*/UYH*$^{+}$ soluble fraction, respectively. Minimal loading (1x) of the soluble fraction corresponds to 0.2 µg protein.

The membrane fraction of either of the two strains did not generate any cross-reactive band but the soluble fractions from both strains generated cross-reactive bands at ~50 kDa and at ~30 kDa (Figure 5.5). These additional ~30 kDa bands were observed in previous studies with HoxH antibodies and were assigned to be either non-specific bands or degradation products of HoxH (Appel et al., 2000; Aubert-Jousset et al., 2011). For the ~50 kDa HoxH-specific band no increase in the band intensities in the overexpression mutant relative to the wild type was estimated. Therefore, even though HoxH abundance in the *hoxEF*$^{-}$*/UYH*$^{+}$ mutant was higher than the previously reported 10% expression in the background strain *hoxEF*$^{-}$ (Aubert-Jousset et al., 2011), the protein abundance in the *hoxEF*$^{-}$*/UYH*$^{+}$ strain did not exceed the amount in the wild-type strain.

### 5.3.2 Hydrogenase Activity in the Mutant Strains

No $H_2$ production or uptake could be detected with the *hoxEF*$^-$ or *hoxEF*$^-$*/UYH*$^+$ strains when cultures were incubated in darkness and under anaerobic conditions indicating that in the absence of HoxE and HoxF subunits the partially expressed enzyme could not find an alternate redox partner in the cell. Trace curves of $H_2$ uptake and production measurements with the *hoxEF*$^-$*/UYH*$^+$ strain are shown in Figure 5.6 (A-B). To test if the partially overexpressed enzyme was catalytically active, a $H_2$ production assay was performed using reduced methyl viologen as the electron donor. In this assay $H_2$ production was detected from the wild-type as well as mutant strains (Figure 5.6 (C-D)). The rate of $H_2$ production in the *hoxEF*$^-$*/UYH*$^+$ strain was ~25% of the wild type (Table 5.3).

## 5.4 Discussion

Cyanobacterial bidirectional hydrogenases are known to couple $H_2$ production/oxidation with NAD(P)H/NAD(P)$^+$ oxidation/reduction, mainly due to the presence of a NAD(P)$^+$ binding site in the HoxF subunit of the enzyme. On the other hand, $H_2$ uptake in the presence of light follows a different electron transport pathway than $H_2$ production. According to the previously predicted model of the Ndh-diaphorase complex, electron transfer during light-induced $H_2$ uptake may not be mediated though HoxE and HoxF at all. Therefore, a partially expressed hydrogenase (without HoxE and HoxF) could potentially oxidize $H_2$ using this electron transfer pathway. However, in this chapter it was shown that in the absence of the diaphorase moiety (HoxE and HoxF), the partially

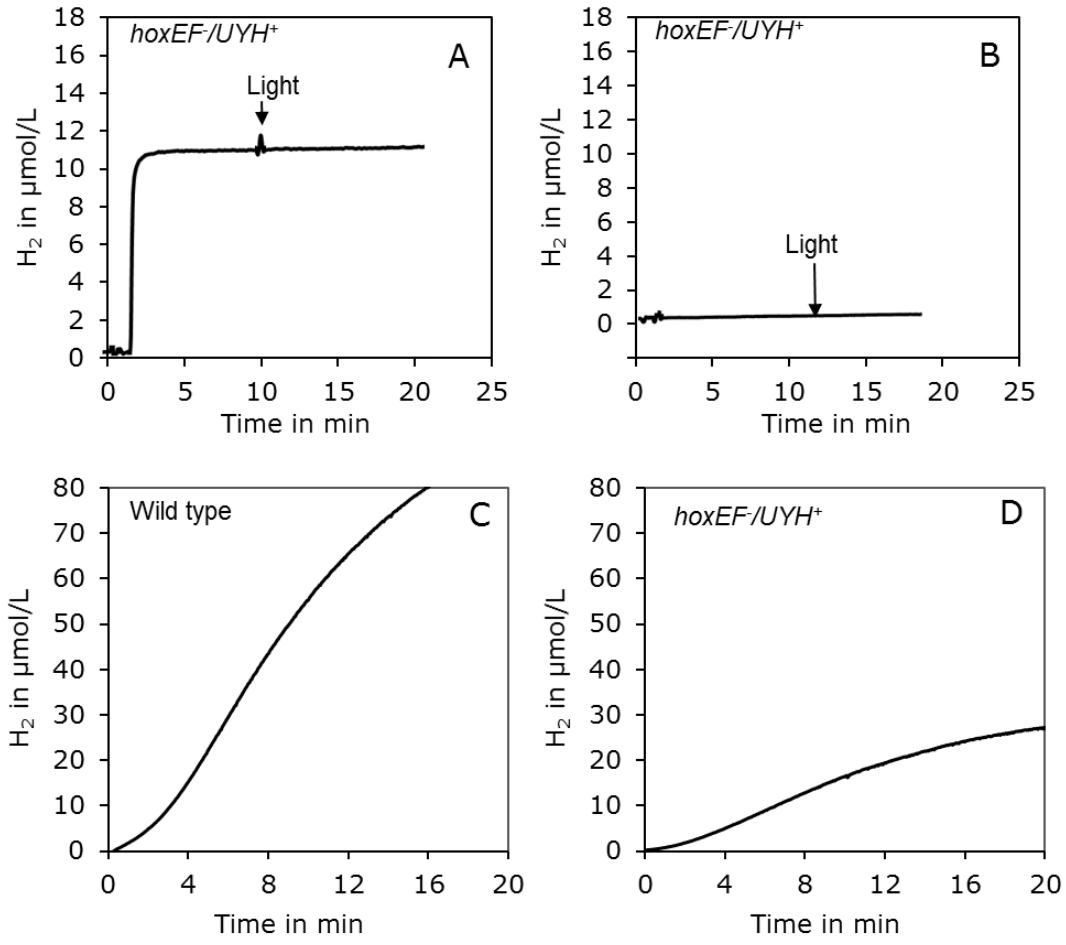


Figure 5.6
$H_2$ uptake (A) and production (B) measurements in *Synechocystis hoxEF$^-$/UYH$^+$* strain. Cell suspensions of 11 µg chl *a* ml$^{-1}$ were initially incubated in darkness and after ~10 min light was switched on (indicated by the arrows). The initial steep rise of the trace curve in graph A indicates the addition of $H_2$-saturated BG-11. $H_2$ production measurements with excess reductant in wild-type (C), *hoxEF$^-$/UYH$^+$* (D) are also shown. Prior to these two measurements methyl viologen (5 mM), reduced with sodium dithionite (10 mM) was added to the cell suspensions.

Table 5.3.
$H_2$ production rates with reduced methyl viologen (MV) in *Synechocystis* wild-type and mutant strains. Average rates were calculated from three independent measurements.

| **Strain** | **MV-dependent $H_2$ production, µmol (mg chl *a*)$^{-1}$ h$^{-1}$** |
|---|---|
| Wild-type | 36.0 ± 1.2 |
| *hoxEF*$^-$ | 7.4 ± 0.7 |
| *hoxEF*$^-$*/UYH*$^+$ | 8.7 ± 0.5 |

expressed hydrogenase did not show any hydrogenase activity (uptake or production) under physiological conditions (with no external redox donor).

Even though no hydrogenase activity could be detected in the *hoxEF*$^-$*/UYH*$^+$ strain under physiological conditions, $H_2$ production was found when reduced methyl viologen was used as the electron donor. This result supported previous reports of methyl viologen dependent $H_2$ production in the HoxYH module, which was suggested to be the minimal catalytic unit of hydrogenase (Eckert et al., 2012; Aubert-Jousset et al., 2011).

Eckert et al. (2012) showed that in the absence of HoxF or HoxU the rest of the Hox subunits in *Synechocystis* do not form a subcomplex of hydrogenase indicating that HoxF and HoxU subunits are essential for the assembly of a functional Hox subcomplex. In contrast, Hox subcomplexes can be formed in the absence of HoxY, HoxH or HoxE. A summary of the detected subcomplexes in various *hox* mutants and a representative

Table 5.4.
Presence of Hox subcomplexes in *Synechocystis hox* mutants as reported by Eckert et al. (2012).

| ***Hox* Mutants** | **Subcomplex Detected** |
|---|---|
| *hoxE*$^-$ | HoxFUYH, HoxFU |
| *hoxF*$^-$ | None |
| *hoxU*$^-$ | None |
| *hoxY*$^-$ | HoxEFU, HoxFU |
| *hoxH*$^-$ | HoxEFU, HoxFU |

diagram of the Hox subunits are given in Table 5.4 and Figure 5.7, respectively. Therefore, the absence of hydrogenase activity without an external donor in our *hoxEF*$^-$*/UYH*$^+$ strain does not necessarily indicate that the HoxE and HoxF subunits are required for the electron transfer between hydrogenase and the PQ pool. Since the *hoxEF*$^-$*/UYH*$^+$ strain does not have HoxF, according to the results reported by Eckert et al. (2012), it is likely that the remaining subunits do not form a functional subcomplex. On the other hand, the strain displayed methyl viologen dependent $H_2$ evolution, a phenomenon for which minimally HoxY and HoxH subunits are required (Eckert et al., 2012). Therefore, in the *hoxEF*$^-$*/UYH*$^+$ strain the HoxYH subcomplex is expected to be present. Either way, HoxU is not likely to be a part of the Hox subcomplex due to the absence of HoxF. Since according to the homology model HoxU plays a crucial role in the electron transfer process to/from the HoxYH module, its absence in the subcomplex may be a reason why no $H_2$ uptake could be detected in the *hoxEF*$^-$*/UYH*$^+$ strain.

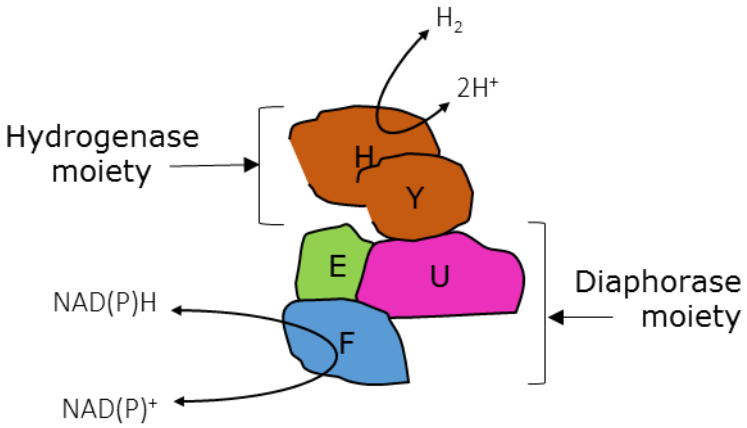


Figure 5.7
Representative diagram of the subunits of hydrogenase in *Synechocystis*.

# CHAPTER 6

# OVERALL CONCLUSION AND FUTURE DIRECTIONS

The research presented in this dissertation provides insight into the $H_2$ metabolism in the model cyanobacterium *Synechocystis*. The principal contribution of this work is to identify and characterize two distinct types of $H_2$ metabolism in *Synechocystis*, one in the presence and the other in the absence of light. In cyanobacteria NAD(P) and/or oxidized/reduced Fd/Flv are known as the redox partners of hydrogenase. All of these redox partners are reduced by the photosynthetic light reactions and can potentially be reoxidized by hydrogenase during $H_2$ production. Because the cyanobacterial enzyme catalyzes a reversible reaction, it is generally assumed that during $H_2$ oxidation electrons follow the same pathway as for $H_2$ production, but in the reverse direction. In this work the existence of a novel, NAD(P)- or ferredoxin-independent electron transfer pathway during $H_2$ oxidation in the presence of light is elucidated (Figure 3.8). In this pathway the PQ pool works as the electron acceptor of hydrogenase. From the PQ pool electrons are subsequently channeled through the cytochrome $b_6f$ complex and photosystem I in the thylakoid membrane, ultimately contributing to the production of NADPH.

$H_2$ photoevolution is an attractive mode of production of $H_2$ by using the light energy captured by the photosystems without involving a carbohydrate intermediate. However, in reality $H_2$ production in *Synechocystis* occurs only for few seconds. Results in this dissertation provide an explanation, for the first time, for the transient nature of $H_2$ photoevolution in *Synechocystis*.

Also, NDH-1 is identified as the most likely component of the thylakoid membrane for mediating this electron-transfer between hydrogenase and the PQ pool. A three-dimensional homology model of the subunits of hydrogenase and NDH-1 participating in the electron-transfer process is presented. The successful assembly of this model (the Ndh-diaphorase complex) provides support for a potential assembly of the two complexes in *Synechocystis*. Since electrons during $H_2$ production and oxidation do not follow the same pathway, the predicted model provides targets for engineering alterations in order to sever the connection between hydrogenase and NDH-1 so that $H_2$ photoevolution can continue without any light-induced $H_2$ uptake. Sustained $H_2$ photoevolution by bidirectional hydrogenase was observed before in the NDH-1 mutant M55 (Cournac et al., 2004), a phenomenon that can now be explained by the absence of $H_2$ uptake in the mutant strain. However, since NDH-1 also participates in a variety of other cellular functions, the M55 strain has other significant side-effects such as impaired $CO_2$ uptake and cyclic electron transport around PS I. Hydrogenase, on the other hand, is not known to participate in any other cellular function and therefore provides a more suitable platform for genetic alterations. Since the PQ-mediated electron transfer can only occur during $H_2$ oxidation but not during $H_2$ production, the aim of the alteration should be to do so without disrupting $H_2$ production. Based on the homology model, HoxU offers several potential target amino acid residues for such alterations.

Finally, hydrogenase from the marine cyanobacterial strain *Lyngbya aestuarii* BL J was heterologously expressed in *Synechocystis*. Hydrogenase in *Lyngbya* BL J offers great potential as a powerful $H_2$ producer (Kothari et al., 2012). However, because of its filamentous nature and slow growth rate, it is not a suitable strain for genetic

manipulation or large-scale production. Expression of the *Lyngbya* hydrogenase in *Synechocystis* provides a platform for further research on this enzyme. However, challenges must be overcome to achieve a desirable rate of fermentative $H_2$ production from the heterologously expressed enzyme in *Synechocystis*. The current version of the enzyme in *Synechocystis*, even though catalytically active, is incapable of producing $H_2$ without the addition of external reductants such as reduced methyl viologen. While expressing the maturase proteins from *Lyngbya* BL J in *Synechocystis* can potentially be an easy solution, it is also possible that hydrogenase in *Lyngbya* BL J uses a different protein/cofactor as the redox partner that is not expressed in *Synechocystis*. In that case, identification of the protein/cofactor and its subsequent expression will be required.

# REFERENCES


Abdel-Basset R, Bader KP (1998) Physiological analysis of the hydrogen gas exchange in cyanobacteria. J Photochem Photobiol B: Biol 43:146–151

Allahverdiyeva Y, Mustila H, Ermakova M, Bersanini L, Richaud P, Ajlani G, Battchikova N, Cournac L, Aro EM (2013) Flavodiiron proteins Flv1 and Flv3 enable cyanobacterial growth and photosynthesis under fluctuating light. Proc Natl Acad Sci USA 110:4111-4116

Anfinsen CB (1972) The formation and stabilization of protein structure. Biochem J 128: 37–749

Angermayr SA, Hellingwerf KJ, Lindblad P, de Mattos MJT (2009) Energy biotechnology with cyanobacteria. Curr Opin Biotechnol 20:257-263

Antal TK, Lindblad P (2005) Production of $H_2$ by sulphur-deprived cells of the unicellular cyanobacteria *Gloeocapsa alpicola* and *Synechocystis* sp. PCC 6803 during dark incubation with methane or at various extracellular pH. J Appl Microbiol 98:114-120

Antal TK, Oliveira P, Lindblad P (2006) The bidirectional hydrogenase in the cyanobacterium *Synechocystis* sp. strain PCC 6803. Int J Hydrogen Energy 31:1439–1444

Antal TK, Matorin DN, Kukarskikh GP, Lambreva MD, Tyystjarvi E, Krendeleva TE, Tsygankov AA, Rubin AB (2014) Pathways of hydrogen photoproduction by immobilized *Chlamydomonas reinhardtii* cells deprived of sulfur. Int J Hydrogen Energy 39:18194-18203

Appel J, Schulz R (1996) Sequence analysis of an operon of a NAD (P)-reducing nickel hydrogenase from the cyanobacterium *Synechocystis* sp. PCC 6803 gives additional evidence for direct coupling of the enzyme to NAD(P)H-dehydrogenase (complex I). Biochim Biophys Acta 1298:141-147

Appel J, Phunpruch S, Steinmüller K, Schulz R (2000) The bidirectional hydrogenase of *Synechocystis* sp. PCC 6803 works as an electron valve during photosynthesis. Arch Microbiol 173:333-338

Aubert-Jousset E, Cano M, Guedeney G, Richaud P, Cournac L (2011) Role of HoxE subunit in *Synechocystis* PCC6803 hydrogenase. FEBS J 278:4035-4043

Azwar MY, Hussain MA, Abdul-Wahab AK (2014) Development of biohydrogen production by photobiological, fermentation and electrochemical processes: A review. Renew Sustain Energy Rev 31:158-173

Baebprasert W, Lindblad P, Incharoensakdi A (2010) Response of $H_2$ production and Hox-hydrogenase activity to external factors in the unicellular cyanobacterium *Synechocystis* sp. strain PCC 6803. Int J Hydrogen Energy 35:6611-6616

Barz M, Beimgraben C, Staller T, Germer F, Opitz F, Marquardt C, Schwarz C, Gutekunst K, Vanselow KH, Schmitz R, LaRoche J, Schulz R, Appel J (2010) Distribution analysis of hydrogenases in surface waters of marine and freshwater environments. PLoS ONE 5:e13846

Basak N, Das D (2007) The prospect of purple non-sulfur (PNS) photosynthetic bacteria for hydrogen production: the present state of the art. World J Microbiol Biotechnol 23:31-42

Basak N, Jana AK, Das D, Saikia D (2014) Photofermentative molecular biohydrogen production by purple-non-sulfur (PNS) bacteria in various modes: The present progress and future perspective. Int J Hydrogen Energy 39:6853-6871

Battchikova N, Aro E (2007) Cyanobacterial NDH-1 complexes: multiplicity in function and subunit composition. Physiol Plant 131:22-32

Battchikova N, Zhang P, Rudd S, Ogawa T, Aro EM (2005) Identification of NdhL and Ssl1690 (NdhO) in NDH-1L and NDH-1M complexes of *Synechocystis* sp. PCC 6803. J Biol Chem 280:2587-2595

Battchikova N, Eisenhut M, Aro E (2011a) Cyanobacterial NDH-1 complexes: novel insights and remaining puzzles. Biochim Biophys Acta 1807:935-944

Battchikova N, Wei L, Du L, Bersanini L, Aro E, Ma W (2011b) Identification of novel *ssl0352* Protein (NdhS), essential for efficient operation of cyclic electron transport around photosystem I, in NADPH: plastoquinone oxidoreductase (NDH-1) complexes of *Synechocystis* sp. PCC 6803. J Biol Chem 286:36992-37001

Batyrova KA, Tsygankov AA, Kosourov SN (2012) Sustained hydrogen photoproduction by phosphorus-deprived *Chlamydomonas reinhardtii* cultures. Int J Hydrogen Energy 37:8834-8839

Benemann JR (2000) Hydrogen production by microalgae. J Appl Phycol 12:291-300

Berger S, Ellersiek U, Westhoff P, Steinmüller K (1993) Studies on the expression of NDH-H, a subunit of the NAD(P)H-plastoquinone-oxidoreductase of higher-plant chloroplasts. Planta 190:25-31

Bleijlevens B, Faber BW, Albracht SP (2001) The [NiFe] hydrogenase from *Allochromatium vinosum* studied in EPR-detectable states: H/D exchange experiments that yield new information about the structure of the active site. J Biol Inorg Chem 6:763-769

Böhm R, Sauter M, Böck A (1990) Nucleotide sequence and expression of an operon in *Escherichia coli* coding for formate hydrogenylase components. Mol Microbiol 4:231-243

Boison G, Schmitz O, Schmitz B, Bothe H (1998) Unusual gene arrangement of the bidirectional hydrogenase and functional analysis of its diaphorase subunit HoxU in respiration of the unicellular cyanobacterium *Anacystis nidulans*. Curr Microbiol 36:253-258

Brandt U (2006) Energy converting NADH: quinone oxidoreductase (Complex I). Annu Rev Biochem 75:69-92

Bradford MM (1976) A rapid and sensitive method for the quantitation of microgram quantities of protein utilizing the principle of protein-dye binding. Anal Biochem 72:248-254

Burroughs NJ, Boehm M, Eckert C, Mastroianni G, Spence EM, Yu J, Nixon PJ, Appel J, Mullineaux CW, Bryan SJ (2014) Solar powered biohydrogen production requires specific localization of the hydrogenase. Energy and Environ Sci 7:3791-3800

Burrows EH, Chaplen FWR, Ely RL (2008) Optimization of media nutrient composition for increased photofermentative hydrogen production by *Synechocystis* sp. PCC 6803. Int J Hydrogen Energy 33:6092-6099

Burrows EH, Wong W, Fern X, Chaplen FWR, Ely RL (2009) Optimization of pH and nitrogen for enhanced hydrogen production by *Synechocystis* sp. PCC 6803 via statistical and machine learning methods. Biotechnol Prog 25:1009-1017

Cai J, Wang G (2014) Hydrogen production from glucose by a mutant strain of *Rhodovulum sulfidophilum* P5 in single-stage photofermentation. Int J Hydrogen Energy 39:20979-20986

Cano M, Volbeda A, Guedeney G, Aubert-Jousset E, Richaud P, Peltier G, Cournac L (2014) Improved oxygen tolerance of the *Synechocystis* sp. PCC 6803 bidirectional hydrogenase by site-directed mutagenesis of putative residues of the gas diffusion channel. Int J Hydrogen Energy 39:16872-16884

Carrieri D, Ananyev G, Costas AMG, Bryant DA, Dismukes GC (2008) Renewable hydrogen production by cyanobacteria: Nickel requirements for optimal hydrogenase activity. Int J Hydrogen Energy 33:2014-2022

Carrieri D, Wawrousek K, Eckert C, Yu J, Maness PC (2011) The role of the bidirectional hydrogenase in cyanobacteria. Bioresour Technol 102:8368-8377

Carroll J, Fearnley IM, Shannon RJ, Hirst J, Walker JE (2003) Analysis of the subunit composition of Complex I from bovine heart mitochondria. Mol Cell Proteomics 2:117-126

Cassier-Chauvat C, Veaudor T, Chauvat F (2014) Advances in the function and regulation of hydrogenase in the cyanobacterium *Synechocystis* PCC6803. Int J Mol Sci 15:19938-19951

Chen Z, Lemon BJ, Huang S, Swartz DJ, Peters JW, Bagley KA (2002) Infrared studies of the CO-inhibited form of the Fe-only hydrogenase from *Clostridium pasteurianum* I: examination of its light sensitivity at cryogenic temperatures. Biochemistry 41:2036-2043

Chongsuksantikul A, Asami K, Yoshikawa S, Ohtaguchi K (2014) Hydrogen production by anaerobic dark metabolism in *Synechocystis* sp. strain PCC6803-GT: effect of monosaccharide in nitrate free solution. J Biochem Tech 5:735-742

Cooley JW, Vermaas WFJ (2001) Succinate dehydrogenase and other respiratory pathways in thylakoid membranes of *Synechocystis* sp. strain PCC 6803: capacity comparisons and physiological function. J Bacteriol 183:4251-4258

Cournac L, Mus F, Bernard L, Guedeney G, Vignais PM, Peltier G (2002) Limiting steps of hydrogen production in *Chlamydomonas reinhardtii* and *Synechocystis* PCC 6803 as analysed by light-induced gas exchange transients. Int J Hydrogen Energy 27:1229-1237

Cournac L, Guedeney G, Peltier G, Vignais PM (2004) Sustained photoevolution of molecular hydrogen in a mutant of *Synechocystis* sp. strain PCC 6803 deficient in the type I NADPH-dehydrogenase complex. J Bacteriol 186:1737-1746

Das D, Veziroglu TN (2008) Advances in biological hydrogen production processes. Int J Hydrogen Energy 33:6046-6057

Dincer I (2007) Environmental and sustainability aspects of hydrogen and fuel cell systems. Int J Energy Res 31:29-55

Dupuis A, Prieur I, Lunardi J (2001) Toward a characterization of the connecting module of complex I. J Bioenerg Biomembr 33:159-168

Dutheil J, Saenkham P, Sakr S, Leplat C, Ortega-Ramos M, Bottin H, Cournac L, Cassier-Chauvat C, Chauvat F (2012) The AbrB2 autorepressor, expressed from an atypical promoter, represses the hydrogenase operon to regulate hydrogen production in *Synechocystis* strain PCC 6803. J Bacteriol 194:5423-5433

Eaton-Rye JJ and Vermaas WFJ (1991) Oligonucleotide-directed mutagenesis of *psbB*, the gene encoding CP47, employing a deletion mutant strain of the cyanobacterium *Synechocystis* sp. PCC 6803. Plant Mol Biol 17:1165-1177

Eckert C, Boehm M, Carrieri D, Yu J, Dubini A, Nixon PJ, Maness PC (2012) Genetic analysis of the Hox hydrogenase in the cyanobacterium *Synechocystis* sp PCC 6803 reveals subunit roles in association, assembly, maturation, and function. J Biol Chem 287:43502-43515

Efremov RG, Sazanov LA (2012) The coupling mechanism of respiratory complex I - A structural and evolutionary perspective. Biochim Biophys Acta 1817:1785-1795

Efremov RG, Baradaran R, Sazanov LA (2010) The architecture of respiratory complex I. Nature 465:441-445

Eppley RW (1968) An incubation method for estimating the carbon content of phytoplankton in natural samples. Limnol Oceanogr 13:574-582

Eramian D, Shen M, Devos D, Melo F, Sali A, Marti-Renom, MA (2006) A composite score for predicting errors in protein structure models. Protein Sci 15:1653-1666

Folea IM, Zhang P, Nowaczyk MM, Ogawa T, Aro EM, Boekema EJ (2008) Single particle analysis of thylakoid proteins from *Thermosynechococcus elongatus* and *Synechocystis* 6803: Localization of the CupA subunit of NDH-1. FEBS Lett 582:249-254

Fontecilla-Camps JC, Volbeda A, Cavazza C, Nicolet Y (2007) Structure/function relationships of [NiFe]- and [FeFe]-hydrogenases. Chem Rev 107:4273-4303

Friedrich T (1998) The NADH: ubiquinone oxidoreductase (complex I) from *Escherichia coli*. Biochim Biophys Acta 1364:134-146

Friedrich T, Weiss H (1997) Modular evolution of the respiratory NADH: ubiquinone oxidoreductase and the origin of its modules. J Theor Biol 187:529-540

Friedrich T, Scheide D (2000) The respiratory complex I of bacteria, archaea and eukarya and its module common with membrane-bound multisubunit hydrogenases. FEBS Lett 479:1-5

Friedrich T, Weidner U, Nehls U, Fecke W, Schneider R, Weiss H (1993) Attempts to define distinct parts of NADH: ubiquinone oxidoreductase (complex I). J Bioenerg Biomembr 25:331-337

Friedrich T, Steinmüller K, Weiss H (1995) The proton-pumping respiratory complex I of bacteria and mitochondria and its homologue in chloroplasts. FEBS Lett 367:107–11

Frielingsdorf S, Fritsch J, Schmidt A, Hammer M, Löwenstein J, Siebert E, Pelmenschikov V, Jaenicke T, Kalms J, Rippers Y (2014) Reversible [4Fe-3S] cluster morphing in an $O_2$-tolerant [NiFe] hydrogenase. Nat Chem Biol 10:378-385

Fritsch J, Scheerer P, Frielingsdorf S, Kroschinsky S, Friedrich B, Lenz O, Spahn CMT (2011) The crystal structure of an oxygen-tolerant hydrogenase uncovers a novel iron-sulphur centre. Nature 479:249-252

Glass JB, Wolfe-Simon F, Elser JJ, Anbar AD (2010) Molybdenum-nitrogen co-limitation in freshwater and coastal heterocystous cyanobacteria. Limnol Oceanogr 55:667-676

Goñi G, Herguedas B, Hervás M, Peregrina JR, Miguel A, Gómez-Moreno C, Navarro JA, Hermoso JA, Martínez-Júlvez M, Medina M (2009) Flavodoxin: A compromise between efficiency and versatility in the electron transfer from Photosystem I to Ferredoxin-$NADP^+$ reductase. Biochim Biophys Acta 1787:144-154

Gonzalez-Esquer CR, Vermaas WFJ (2013) ClpB1 overproduction in *Synechocystis* sp. strain PCC 6803 increases tolerance to rapid heat shock. Appl Environ Microbiol 79:6220-6227

Greenbaum E, Lee JW, Tevault CW, Blankinship SL and Mets LJ (1995) $CO_2$ fixation and photoevolution of $H_2$ and $O_2$ in a mutant of *Chlamydomonus* lacking photosystem I. Nature 376, 438-441

Grundel M, Scheunemann R, Lockau W, Zilliges Y (2012) Impaired glycogen synthesis causes metabolic overflow reactions and affects stress responses in the cyanobacterium *Synechocystis* sp. PCC 6803. Microbiology 158:3032-3043

Gutekunst K, Phunpruch S, Schwarz C, Schuchardt S, Schulz-Friedrich R, Appel J (2005) LexA regulates the bidirectional hydrogenase in the cyanobacterium *Synechocystis* sp. PCC 6803 as a transcription activator. Mol Microbiol 58:810-823

Gutekunst K, Chen X, Schreiber K, Kaspar U, Makam S, Appel J (2014) The bidirectional NiFe-hydrogenase in *Synechocystis* sp. PCC 6803 is reduced by flavodoxin and ferredoxin and is essential under mixotrophic, nitrate-limiting conditions. J Biol Chem 289:1930-1937

Gutthann F, Egert M, Marques A, Appel J (2007) Inhibition of respiration and nitrate assimilation enhances photohydrogen evolution under low oxygen concentrations in *Synechocystis* sp. PCC 6803. Biochim Biophys 1767:161-169

Hallenbeck PC (2009) Fermentative hydrogen production: principles, progress, and prognosis. Int J Hydrogen Energy 34:7379-89

Hallenbeck PC, Benemann JR (2002) Biological hydrogen production; fundamentals and limiting processes. Int J Hydrogen Energy 27:1185-1193

Hanke GT, Satomi Y, Shinmura K, Takao T, Hase T (2011) A screen for potential ferredoxin electron transfer partners uncovers new, redox dependent interactions. Biochim Biophys Acta 1814:366-374

He F, Li F (2014) Hydrogen production from methane and solar energy - Process evaluations and comparison studies. Int J Hydrogen Energy 39:18092-18102

Hedderich R (2004) Energy-converting [NiFe] hydrogenases from archaea and extremophiles: ancestors of complex I. J Bioenerg Biomembr 36:65-75

Hemschemeier A, Fouchard S, Cournac L, Peltier G, Happe T (2008) Hydrogen production by *Chlamydomonas reinhardtii*: an elaborate interplay of electron sources and sinks. Planta 227:397-407

Herranen M, Battchikova N, Zhang P, Graf A, Sirpio S, Paakkarinen V, Aro EM (2004) Towards functional proteomics of membrane protein complexes in *Synechocystis* sp. PCC 6803. Plant Physiology 134:470-481

Hinchliffe P, Sazanov LA (2005) Organization of iron-sulfur clusters in respiratory complex I. Science 309:771-774

Hirst J (2013) Mitochondrial Complex I. Annu Rev Biochem 82 82:551-575

Hodkinson BP, Allen JL, Forrest L, Goffinet B, Serusiaux E, Andresson OS, Miao V, Bellenger JP, Lutzoni F (2014) Lichen-symbiotic cyanobacteria associated with *Peltigera* have an alternative vanadium-dependent nitrogen fixation system. Eur J Phycol 49:11-19

Hoffmann D, Gutekunst K, Klissenbauer M, Schulz-Friedrich R, Appel J (2006) Mutagenesis of hydrogenase accessory genes of *Synechocystis* sp. PCC 6803. FEBS J 273:4516-4527

Houchins JP, Burris RH (1981) Occurrence and localization of two distinct hydrogenases in the heterocystous cyanobacterium *Anabaena* sp. strain 7120. J Bacteriol 146:209-214

Howitt CA, Vermaas WFJ (1998) Quinol and cytochrome oxidases in the cyanobacterium *Synechocystis* sp. PCC 6803. Biochemistry 37:17944-17951

Howitt CA, Vermaas WFJ (1999) Subunits of the NAD (P)-reducing nickel-containing hydrogenase do not act as part of the type-1 NAD(P)H-dehydrogenase in the cyanobacterium *Synechocystis* sp. PCC 6803. p 595-601 In Peschek GA, Löffelhardt W, Schmetterer G (ed), The Phototrophic Prokaryotes. Kluwer Academic/Plenum Publishers, New York, NY

Howitt CA, Smith GD, Day DA (1993) Cyanide-insensitive oxygen uptake and pyridine nucleotide dehydrogenases in the cyanobacterium *Anabaena* PCC 7120. Biochim Biophys Acta 1141:313-320

Kaneko M, Hwang EI, Ohnishi Y, Horinouchi S (2003) Heterologous production of flavanones in *Escherichia coli*: potential for combinatorial biosynthesis of flavonoids in bacteria. J Ind Microbiol Biotechnol 30:456-461

Kaneko T, Sato S, Kotani H, Tanaka A, Asamizu E, Nakamura Y, Miyajima N, Hirosawa M, Sugiura M, Sasamoto S, Kimura T, Hosouchi T, Matsuno A, Muraki A, Nakazaki N, Naruo K, Okumura S, Shimpo S, Takeuchi C, Wada T, Watanabe A, Yamada M, Yasuda M, Tabata S (1996) Sequence analysis of the genome of the unicellular cyanobacterium *Synechocystis* sp. strain PCC6803. II. Sequence determination of the entire genome and assignment of potential protein-coding regions. DNA Res 3:109-136

Kapdan IK, Kargi F (2006) Bio-hydrogen production from waste materials. Enzyme Microb Technol 38:569-582

Kaplan A, Reinhold L (1999) $CO_2$ concentrating mechanisms in photosynthetic microorganisms. Annu Rev Plant Biol 50:539-570

Kasap M, Chen JS (2005) *Clostridium pasteurianum* W5 synthesizes two NifH-related polypeptides under nitrogen-fixing conditions. Microbiol 151:2353-2362

Keilty AT, Vavilin DV, Vermaas WFJ (2001) Functional analysis of combinatorial mutants with changes in the C-terminus of the CD loop of the D2 protein in photosystem II of *Synechocystis* sp. PCC 6803. Biochemistry 40:4131-4139

Kiss É, Kós PB, Vass I (2009) Transcriptional regulation of the bidirectional hydrogenase in the cyanobacterium *Synechocystis* 6803. J Biotechnol 142:31-37

Knoop H, Gründel M, Zilliges Y, Lehmann R, Hoffmann S, Lockau W, Steuer R (2013) Flux balance analysis of cyanobacterial metabolism: the metabolic network of *Synechocystis* sp. PCC 6803. PLoS Comput Biol 9: e1003081

Koku H, Eroğlu I, Gündüz U, Yücel M, Türker L (2002) Aspects of the metabolism of hydrogen production by *Rhodobacter sphaeroides*. Int J Hydrogen Energy 27:1315-1329

Korste A, Wulfhorst H, Ikegami T, Nowaczyk MM, Stoll R (2015) $^{1}H$, $^{13}C$ and $^{15}N$ chemical shift assignments of the NDH-1 complex subunit CupS. Biomol NMR Assign 9:169-171

Kosourov S, Seibert M, Ghirardi ML (2003) Effects of extracellular pH on the metabolic pathways in sulfur-deprived, $H_2$-producing *Chlamydomonas reinhardtii* cultures. Plant Cell Physiol 44:146-155

Kothari A, Potrafka R, Garcia-Pichel F (2012) Diversity in hydrogen evolution from bidirectional hydrogenases in cyanobacteria from terrestrial, freshwater and marine intertidal environments. J Biotechnol 162:105-114

Kothari A, Vaughn M, Garcia-Pichel F (2013) Comparative genomic analyses of the cyanobacterium, *Lyngbya aestuarii* BL J, a powerful hydrogen producer. Front Microbiol 4:363-378

Kothari A, Parameswaran P, Garcia-Pichel F (2014) Powerful fermentative hydrogen evolution of photosynthate in the cyanobacterium *Lyngbya aestuarii* BL J mediated by a bidirectional hydrogenase. Front Microbiol 5:680-689

Kulp TR, Hoeft SE, Asao M, Madigan MT, Hollibaugh JT, Fisher JC, Stolz JF, Culbertson CW, Miller LG, Oremland RS (2008) Arsenic(III) fuels anoxygenic photosynthesis in hot spring biofilms from Mono Lake, California. Science 321:967-970

Lea-Smith DJ, Ross N, Zori M, Bendall DS, Dennis JS, Scott SA, Smith AG, Howe CJ (2013) Thylakoid terminal oxidases are essential for the cyanobacterium *Synechocystis* sp. PCC 6803 to survive rapidly changing light intensities. Plant Physiol 162:484-495

Levin DB, Pitt L, Love M (2004) Biohydrogen production: prospects and limitations to practical application. Int J Hyfdrogen Energy 29:173-185

Liang MP, Banatao DR, Klein TE, Brutlag DL, Altman RB (2003) WebFEATURE: An interactive web tool for identifying and visualizing functional sites on macromolecular structures. Nucl Acids Res 31:3324-3327

Long M, Liu J, Chen Z, Bleijlevens B, Roseboom W, Albracht SPJ (2007) Characterization of a HoxEFUYH type of [NiFe] hydrogenase from *Allochromatium vinosum* and some EPR and IR properties of the hydrogenase module. J Biol Inorg Chem 12:62-78

López-Maury L, García-Domínguez M, Florencio FJ, Reyes JC (2002) A two-component signal transduction system involved in nickel sensing in the cyanobacterium *Synechocystis* sp. PCC 6803. Mol Microbiol 43:247-256

Lyon EJ, Shima S, Buurman G, Chowdhuri S, Batschauer A, Steinbach K, Thauer RK (2004) UV-A/blue-light inactivation of the 'metal-free' hydrogenase (Hmd) from methanogenic archaea. Eur J Biochem 271:195-204

Ma W, Ogawa T (2015) Oxygenic photosynthesis-specific subunits of cyanobacterial NADPH dehydrogenases. Int Union Biochem Mol Biol 67:3-8

Ma W, Deng Y, Ogawa T, Mi H (2006) Active NDH-1 complexes from the cyanobacterium *Synechocystis* sp. strain PCC 6803. Plant Cell Physiol 47:1432-1436

Manish S, Banerjee R (2008) Comparison of biohydrogen production processes. Int J Hydrogen Energy 33:279-286

Massanz C, Schmidt S, Friedrich B (1998) Subforms and *in vitro* reconstitution of the NAD-reducing hydrogenase of *Alcaligenes eutrophus*. J Bacteriol 180:1023-1029

Mayhew SG (1978) The redox potential of dithionite and $SO^{-}_{2}$ from equilibrium reactions with flavodoxins, methyl viologen and hydrogen plus hydrogenase. Eur J Biochem 85:535-547

McIntosh CL, Germer F, Schulz R, Appel J, Jones AK (2011) The [NiFe]-hydrogenase of the cyanobacterium *Synechocystis* sp. PCC 6803 works bidirectionally with a bias to $H_2$ production. J Am Chem Soc 133:11308-11319

Melis A, Melnicki MR (2006) Integrated biological hydrogen production. Int J Hydrogen Energy 31:1563-1573

Melis A, Zhang L, Forestier M, Ghirardi ML, Seibert M (2000) Sustained photobiological hydrogen gas production upon reversible inactivation of oxygen evolution in the green alga *Chlamydomonas reinhardtii*. Plant Physiol 122:127-136

Meyer J (2007) [FeFe] hydrogenases and their evolution: a genomic perspective. Cell Mol Life Sci 64:1063-1084

Mullineaux CW (2014) Electron transport and light-harvesting switches in cyanobacteria. Front Plant Sci 5:7

Mustila H, Allahverdiyeva Y, Isojärvi J, Aro EM, Eisenhut M (2014) The bacterial-type [4Fe–4S] ferredoxin 7 has a regulatory function under photooxidative stress conditions in the cyanobacterium *Synechocystis* sp. PCC 6803. Biochim Biophys Acta 1837:1293-1304

Nicolet Y, Piras C, Legrand P, Hatchikian CE, Fontecilla-Camps JC (1999) *Desulfovibrio desulfuricans* iron hydrogenase: the structure shows unusual coordination to an active site Fe binuclear center. Structure 7:13-23

Nowaczyk MM, Wulfhorst H, Ryan CM, Souda P, Zhang H, Cramer WA, Whitelegge JP (2011) NdhP and NdhQ: Two novel small subunits of the cyanobacterial NDH-1 complex. Biochemistry 50:1121-1124

Ogata H, Mizoguchi Y, Mizuno N, Miki K, Adachi S, Yasuoka N, Yagi T, Yamauchi O, Hirota S, Higuchi Y (2002) Structural studies of the carbon monoxide complex of [NiFe] hydrogenase from *Desulfovibrio vulgaris* Miyazaki F: suggestion for the initial activation site for dihydrogen. J Am Chem Soc 124:11628-11635

Ogata H, Hirota S, Nakahara A, Komori H, Shibata N, Kato T, Kano K, Higuchi Y (2005) Activation process of [NiFe] hydrogenase elucidated by high-resolution X-ray analyses: conversion of the ready to the unready state. Structure 13:1635-1642

Ogawa T (1992) Identification and characterization of the *ictA/ndhL* gene product essential to inorganic carbon transport of *Synechocystis* PCC6803. Plant Physiol 99:1604-1608

Ogawa T, Mi H (2007) Cyanobacterial NADPH dehydrogenase complexes. Photosynth Res 93:69-77

Ogden JM (1999) Prospects for building a hydrogen energy infrastructure. Annu Rev Energy Environ 24:227-279

Ohkawa H, Price GD, Badger MR, Ogawa T (2000) Mutation of *ndh* genes leads to inhibition of $CO_2$ uptake rather than $HCO_3^-$ uptake in *Synechocystis* sp. strain PCC 6803. J Bacteriol 182:2591-2596

Ohkawa H, Sonoda M, Hagino N, Shibata M, Pakrasi HP and Ogawa T (2002) Functionally distinct NAD(P) H dehydrogenases and their membrane localization in *Synechocystis* sp. PCC6803. Funct Plant Biol 29: 195–200

Oliveira P, Lindblad P (2005) LexA, a transcription regulator binding in the promoter region of the bidirectional hydrogenase in the cyanobacterium *Synechocystis* sp. PCC 6803. FEMS Microbiol Lett 251:59-66

Onda K, Kyakuno T, Hattori K, Ito K (2004) Prediction of production power for high-pressure hydrogen by high-pressure water electrolysis. J Power Sources 132:64-70

Peters JW, Lanzilotta WN, Lemon BJ, Seefeldt LC (1998) X-ray crystal structure of the Fe-only hydrogenase (CpI) from *Clostridium pasteurianum* to 1.8 angstrom resolution. Science 282:1853-1858

Peters JW, Schut GJ, Boyd ES, Mulder DW, Shepard EM, Broderick JB, King PW, Adams MWW (2015) [FeFe]- and [NiFe]-hydrogenase diversity, mechanism, and maturation. Biochim Biophys Acta 1853:1350-1369

Pieulle L, Guedeney G, Cassier-Chauvat C, Jeanjean R, Chauvat F, Peltier G (2000) The gene encoding the NdhH subunit of type 1 NAD(P)H dehydrogenase is essential to survival of *Synechocystis* PCC6803. FEBS Lett 487:272-276

Pogulis RJ, Vallejo AN, Pease LR (1996) *In vitro* recombination and mutagenesis by overlap extension PCR. Methods Mol Biol 57:167-176

Porra RJ, Thompson WA, Kriedemann PE (1989) Determination of accurate extinction coefficients and simultaneous equations for assaying chlorophylls a and b extracted with four different solvents: verification of the concentration of chlorophyll standards by atomic absorption spectroscopy. Biochim Biophys Acta 975:384-394

Price GD, Badger MR, Woodger FJ, Long BM (2008) Advances in understanding the cyanobacterial $CO_2$-concentrating-mechanism (CCM): functional components, $C_i$ transporters, diversity, genetic regulation and prospects for engineering into plants. J Exp Bot 59:1441-1461

Prommeenate P, Lennon AM, Markert C, Hippler M, Nixon PJ (2004) Subunit composition of NDH-1 complexes of *Synechocystis* sp. PCC 6803: Identification of two new *ndh* gene products with nuclear-encoded homologues in the chloroplast Ndh complex. J Biol Chem 279:28165-28173

Rees DC, Tezcan FA, Haynes CA, Walton MY, Andrade S, Einsle O, Howard JB (2005) Structural basis of biological nitrogen fixation. Phil Trans R Soc A 363:971-984

Rippka R, Deruelles J, Waterbury JB, Herdman M, Stanier RY (1979) Generic assignments, strain histories and properties of pure cultures of cyanobacteria. J Gen Microbiol 111:1-61

Rousset M, Montet Y, Guigliarelli B, Forget N, Asso M, Bertrand P, Fontecilla-Camps JC, Hatchikian EC (1998) [3Fe-4S] to [4Fe-4S] cluster conversion in *Desulfovibrio fructosovorans* [NiFe] hydrogenase by site-directed mutagenesis. Proc Natl Acad Sci USA 95:11625-11630

Rumeau D, Becuwe-Linka N, Beyly A, Louwagie M, Garin J, Peltier G (2005) New subunits NDH-M, -N, and -O, encoded by nuclear genes, are essential for plastid Ndh complex functioning in higher plants. Plant Cell 17:219

Sato M, Torres-Bacete J, Sinha PK, Matsuno-Yagi A, Yagi T (2014) Essential regions in the membrane domain of bacterial complex I (NDH-1): the machinery for proton translocation. J Bioenerg Biomembr 46:279-287

Sauter M, Böhm R, Böck A (1992) Mutational analysis of the operon (*hyc*) determining hydrogenase 3 formation in *Escherichia coli*. Mol Microbiol 6:1523-1532

Sazanov LA, Hinchliffe P (2006) Structure of the hydrophilic domain of respiratory complex I from *Thermus thermophilus*. Science 311:1430-1436

Schmittgen TD, Livak KJ (2008) Analyzing real-time PCR data by the comparative CT method. Nat Protoc 3:1101-1108

Schmitz O, Bothe H (1996) $NAD(P)^+$-dependent hydrogenase activity in extracts from the cyanobacterium *Anacystis nidulans.* FEMS Microbiol Lett 135:97-101

Schmitz O, Boison G, Hilscher R, Hundeshagen B, Zimmer W, Lottspeich F, Bothe H (1995) Molecular biological analysis of a bidirectional hydrogenase from cyanobacteria. Eur J Biochem 233:266-276

Schmitz O, Gurke J, Bothe H (2001) Molecular evidence for the aerobic expression of *nifJ*, encoding pyruvate: ferredoxin oxidoreductase, in cyanobacteria. FEMS Microbiol Lett 195:97-102

Schmitz O, Boison G, Salzmann H, Bothe H, Schütz K, Wang S, Happe T (2002) HoxE-a subunit specific for the pentameric bidirectional hydrogenase complex (HoxEFUYH) of cyanobacteria. Biochim Biophys Acta 1554:66-74

Schütz K, Happe T, Troshina O, Lindblad P, Leitão E, Oliveira P, Tamagnini P (2004) Cyanobacterial $H_2$ production - a comparative analysis. Planta 218:350-359

Seabra R, Santos A, Pereira S, Moradas-Ferreira P, Tamagnini P (2009) Immunolocalization of the uptake hydrogenase in the marine cyanobacterium *Lyngbya majuscula* CCAP 1446/4 and two *Nostoc* strains. FEMS Microbiol Lett 292:57-62

Serebriakova L, Zorin NA, Lindblad P (1994) Reversible hydrogenase in *Anabaena variabilis* ATCC 29413. Arch Microbiol 161:140-144

Serebryakova LT, Sheremetieva ME (2006) Characterization of catalytic properties of hydrogenase isolated from the unicellular cyanobacterium *Gloeocapsa alpicola* CALU 743. Biochemistry 71:1370-1376

Shastri AA, Morgan JA (2005) Flux balance analysis of photoautotrophic metabolism. Biotechnol Prog 21:1617-1626

Shen G, Vermaas WFJ (1994) Mutation of chlorophyll ligands in the chlorophyll-binding CP47 protein as studied in a *Synechocystis* sp. PCC 6803 photosystem I-less background. Biochemistry 33:7379-7388

Shen G, Boussiba S, Vermaas WFJ (1993) *Synechocystis* sp PCC 6803 strains lacking photosystem I and phycobilisome function. Plant Cell 5:1853-1863

Shen MY, Sali A (2006) Statistical potential for assessment and prediction of protein structures. Protein Sci 15:2507-2524

Shibata M, Ohkawa H, Katoh H, Shimoyama M, Ogawa T (2002) Two $CO_2$ uptake systems in cyanobacteria: four systems for inorganic carbon acquisition in *Synechocystis* sp. strain PCC 6803. Funct Plant Biol 29:123-129

Shimizu H, Peng L, Myouga F, Motohashi R, Shinozaki K, Shikanai T (2008) CRR23/NdhL is a subunit of the chloroplast NAD(P)H dehydrogenase complex in *Arabidopsis*. Plant Cell Physiol 49: 835–842

Smith SE, Gianinazzi-Pearson V (1990) Phosphate uptake and arbuscular activity in *Mycorrhizal Allium cepa* L.: effects of photon irradiance and phosphate nutrition. Funct Plant Biol 17:177-188

Stal LJ, Moezelaar R (1997) Fermentation in cyanobacteria. FEMS Microbiol Rev 21:179-211

Summerfield TC, Toepel J, Sherman LA (2008) Low-oxygen induction of normally cryptic *psbA* genes in cyanobacteria. Biochemistry 47:12939-12941

Tamagnini P, Axelsson R, Lindberg P, Oxelfelt F, Wunschiers R, Lindblad P (2002) Hydrogenases and hydrogen metabolism of cyanobacteria. Microbiol Mol Biol Rev 66:1-20

Tamagnini P, Leitão E, Oliveira P, Ferreira D, Pinto F, Harris DJ, Heidorn T, Lindblad P (2007) Cyanobacterial hydrogenases: diversity, regulation and applications. FEMS Microbiol Rev 31:692-720

Tamoi M, Murakami A, Takeda T, Shigeoka S (1998) Lack of light/dark regulation of enzymes involved in the photosynthetic carbon reduction cycle in cyanobacteria,

*Synechococcus* PCC 7942 and *Synechocystis* PCC 6803. Biosci Biotechnol Biochem 62:374-376

Tichy M, Vermaas WFJ (1999) *In vivo* role of catalase-peroxidase in *Synechocystis* sp. strain PCC 6803. J Bacteriol 181:1875-1882

Tikhonov AN (2014) The cytochrome $b_6f$ complex at the crossroad of photosynthetic electron transport pathways. Plant Physiol Biochem 81:163–183

Tiwari A, Pandey A (2012) Cyanobacterial hydrogen production–a step towards clean environment. Int J Hydrogen Energy 37:139-150

Tourova TP, Slobodova NV, Bumazhkin BK, Sukhacheva MV, Sorokin DY (2014) Diversity of diazotrophs in the sediments of saline and soda lakes analyzed with the use of the *nifH* gene as a molecular marker. Microbiology 83:634-647

Vavilin D, Yao D, Vermaas WFJ (2007) Small Cab-like proteins retard degradation of photosystem II-associated chlorophyll in *Synechocystis* sp. PCC 6803 - kinetic analysis of pigment labeling with $^{15}N$ and $^{13C}$. J Biol Chem 282:37660-37668

Vermaas, WFJ (2001) Photosynthesis and respiration in cyanobacteria. p 245-251 In: Encyclopedia of Life Sciences Nature Publishing Group, London

Vermaas WFJ, Williams JGK, Arntzen CJ (1987) Sequencing and modification of *psbB*, the gene encoding the CP-47 protein of photosystem II, in the cyanobacterium *Synechocystis* 6803. Plant Mol Biol 8:317-326

Vignais PM (2008) Hydrogenases and $H^+$ reduction in primary energy conservation. Results Probl Cell Differ 45:223-252

Vignais PM, Billoud B (2007) Occurrence, classification, and biological function of hydrogenases: an overview. Chem Rev 107:4206-4272

Vignais PM, Billoud B, Meyer J (2001) Classification and phylogeny of hydrogenases. FEMS Microbiol Rev 25:455-501

Volbeda A, Charon M, Piras C, Hatchikian EC, Frey M, Fontecilla-Camps JC (1995) Crystal structure of the nickel–iron hydrogenase from *Desulfovibrio gigas.* Nature 373:580-587

Volgusheva A, Kukarskikh G, Krendeleva T, Rubin A, Mamedov F (2015) Hydrogen photoproduction in green algae *Chlamydomonas reinhardtii* under magnesium deprivation. RSC Adv 5:5633-5637

Wang P, Best RB, Blumberger J (2011) A microscopic model for gas diffusion dynamics in a [NiFe]-hydrogenase. Phys Chem Chem Phys 13:7708-7719

Webb B, Sali A (2014) Protein structure modeling with MODELLER. Methods Mol Biol 1137:1‑15

Weber J, Krujatz F, Hilpmann G, Gruetzner S, Herrmann J, Thierfelder S, Bienert G, Illing R, Helbig K, Hurtado A, Cuniberti G, Mertig M, Lange R, Guenther E, Opitz J, Lippmann W, Bley T, Haufe N (2014) Biotechnological hydrogen production by photosynthesis. Eng Life Sci 14:592-606

Williams CR, Bees MA (2014) Mechanistic modeling of sulfur-deprived photosynthesis and hydrogen production in suspensions of *Chlamydomonas reinhardtii*. Biotechnol Bioeng 111:320-335

Xu M, Ogawa T, Pakrasi HB, Mi H (2008) Identification and localization of the CupB protein involved in constitutive $CO_2$ uptake in the cyanobacterium, *Synechocystis* sp strain PCC 6803. Plant Cell Physiol 49:994-997

Yagi T, Yano T, Di Bernardo S, Matsuno-Yagi A (1998) Procaryotic complex I (NDH-1), an overview. Biochim Biophys Acta 1364:125-133

Yamamoto H, Peng L, Fukao Y, Shikanai T (2011) An Src homology 3 domain-like fold protein forms a ferredoxin binding site for the chloroplast NADH dehydrogenase-like complex in *Arabidopsis*. Plant Cell 23:1480-1493

Yamashita E, Zhang H, Cramer WA (2007) Structure of the cytochrome $b_6f$ complex: quinone analogue inhibitors as ligands of heme $c_n$. J Mol Biol 370:39–52

Yang C, Hua Q, Shimizu K (2002) Metabolic flux analysis in *Synechocystis* using isotope distribution from $^{13}C$-labeled glucose. Metab Eng 4:202-216

Young JD, Shastri AA, Stephanopoulos G, Morgan JA (2011) Mapping photoautotrophic metabolism with isotopically nonstationary $^{13}C$ flux analysis. Metab Eng 13:656-665

Yu Y, You L, Liu D, Hollinshead W, Tang YJ, Zhang F (2013) Development of *Synechocystis* sp. PCC 6803 as a phototrophic cell factory. Mar Drugs 11:2894-2916

Zhang L, Happe T, Melis A (2002) Biochemical and morphological characterization of sulfur-deprived and $H_2$-producing *Chlamydomonas reinhardtii* (green alga). Planta 214:552-561

Zhang P, Battchikova N, Jansen T, Appel J, Ogawa T, Aro EM (2004) Expression and functional roles of the two distinct NDH-1 complexes and the carbon acquisition complex NdhD3/NdhF3/CupA/Sll1735 in *Synechocystis* sp PCC 6803. Plant Cell 16:3326-3340

Zhang P, Battchikova N, Paakkarinen V, Katoh H, Iwai M, Ikeuchi M, Pakrasi HB, Ogawa T, Aro EM (2005) Isolation, subunit composition and interaction of the NDH-1 complexes from *Thermosynechococcus elongatus* BP-1. Biochem J 390:513-520

Zhang C, Zhu X, Liao Q, Wang Y, Li J, Ding Y, Wang H (2010) Performance of a groove-type photobioreactor for hydrogen production by immobilized photosynthetic bacteria. Int J Hydrogen Energy 35:5284-5292

Zhang J, Gao F, Zhao J, Ogawa T, Wang Q, Ma W (2014) NdhP Is an exclusive subunit of large complex of NADPH dehydrogenase essential to stabilize the complex in *Synechocystis* sp strain PCC 6803. J Biol Chem 289:18770-18781

Zhao J, Gao F, Qiu Z, Wang Q, Ma W (2014a) Deletion of an electron donor-binding subunit of the NDH-1 complex, NdhS, results in a heat-sensitive growth phenotype in *Synechocystis* sp PCC 6803. Chin Sci Bull 59:4484-4490

Zhao J, Gao F, Zhang J, Ogawa T, Ma W (2014b) NdhO, a subunit of NADPH dehydrogenase, destabilizes medium size complex of the enzyme in *Synechocystis* sp strain PCC 6803. J Biol Chem 289:26669-26676

Zickermann V, Kerscher S, Zwicker K, Tocilescu MA, Radermacher M, Brandt U (2009) Architecture of complex I and its implications for electron transfer and proton pumping. Biochim Biophys Acta 1787:574-583